Zeolite nanocrystals for biomedical applications

Kamila Goldyn

▶ **To cite this version:**

Normandie Université

THÈSE

Pour obtenir le diplôme de doctorat

Spécialité CHIMIE

Préparée au sein de l'Université de Caen Normandie

Zeolite nanocrystals for biomedical applications

Présentée et soutenue par
Kamila MATYSIAK GOLDYN

Thèse soutenue publiquement le 16/11/2018 devant le jury composé de		
M. FRANCESCO DI RENZO	Directeur de recherche, UNIVERSITE MONTPELLIER 2 SCIENCES ET TEC	Rapporteur du jury
Mme CHARLOTTE MARTINEAU-CORCOS	Maître de conférences HDR, UNIVERSITE VERSAILLES ST QUENT	Rapporteur du jury
Mme MAGUY JABER	Professeur des universités, UNIVERSITE PARIS 6 PIERRE ET MARIE CURIE	Président du jury
M. SAMUEL VALABLE	Chargé de recherche HDR, UNIVERSITE CAEN NORMANDIE	Membre du jury
M. VALENTIN VALTCHEV	Directeur de recherche au CNRS, 14 ENSI de Caen	Directeur de thèse
Mme SVETLANA MINTOVA	Directeur de recherche au CNRS, UNIVERSITE CAEN NORMANDIE	Co-directeur de thèse

Thèse dirigée par VALENTIN VALTCHEV et SVETLANA MINTOVA, Laboratoire catalyse et spectrochimie (Caen)

UNIVERSITÉ CAEN NORMANDIE

NC

Normande de Chimie

"Try not to become a person of success, but rather try to become a person of value"

- Albert Einstein

Acknowledgements

I would like to dedicate this section to express my gratitude to all the people who helped me to complete my PhD journey.

First of all, I would like to thank my supervisors, Svetlana and Valentin, for giving me the opportunity to do my PhD under their wings. Thank you for your guidance and time, for allowing me to make mistakes and learn from them, all of which contributed to make me a better scientist. I really appreciate the knowledge that you have passed to me and the possibility to work with the best experts in the field of zeolites. Svetlana, your endless, innovative ideas and enthusiasm in regards to the new applications of nanozeolites are utterly inspirational. Valentin, your way of thinking about zeolite modifications is incredible, you are a true genius when it comes to turning commercial zeolites to a superior materials with enhanced properties. Thank you both for everything that you have done for me, it has been a genuinely enjoyable journey. Additionally, I would like to thank the jury members: Charlotte Martineau-Corcos, Francesco Di Renzo, Maguy Jaber and Samuel Valable for accepting to read the manuscript and providing helpful indications to make this PhD thesis better.

Further, I would like to thank Jean-Pierre and Louwanda for sharing their knowledge in regards to catalysis. I did learn a lot from you both. I would also like to express my appreciation to Sarah and Moussa for a lot of scientific discussions and help provided during my PhD. Additionally, I want to acknowledge the much needed help provided by Marie, Benjamin, Valerie, Aurelie, Jaafar, Pascal, Blandine, Nathalie and Sophie. You made my life in the lab much easier by dedicating your time, effort and expertise.

I want to say thank you to all the people that I have met during those three years at LCS. A special gratitude to my retarded friends: Eli, Eddu, Shashino, Sandra, Dudu and Julin. Thank you for welcoming me in Caen with the strongest beer provided by Trappist, you made it very easy for me to adapt to a new place. Thanks for making me laugh, and for lots of memories that I would never forget. Thank you for your support and always being there for me no matter what. I love you all. A special thanks to my Stinchus (pi pa pa para po), Luz (perreo!), Maxime (Pretty Boy) and Rafa (Gypsy queen) for accepting my dark humour jokes and the banter in the lab. You guys made my days at LSC so much fun, and they would not be the same without you.

Furthermore, I would like to thank my mum and my grandma for the motivation and support provided over the years of education. I love you for believing in me, for being a great example of how to fight for what you want in life and most importantly for teaching me how to be a good person. Everything that you have done for me contributed to who I am today, which I am forever grateful for.

Lastly, I would like to express the deepest appreciation to my dearest husband and best friend, Patryk. Thank you for challenging me to break the barriers and try something different in life. Thanks for always being there for me, even during my grumpy and stressed days. I really appreciate all the sacrifices that you have made form me in order to peruse my career. I could not ask for a better life companion, I love you with all my heart!

Table of Contents

Chapter 1- Introduction

1   Introduction

The employment of zeolites in conventional applications such as catalysis, ion exchange and gas separation have proved their potency over the years.[1–3] The zeolite nanocrystals have also been used for more advanced applications, namely in biomedicine (sensors, drug and gas delivery) and microbiology (antibacterial agents) thanks to their high surface area, non-toxic nature and high chemical/thermal stability.[4] However, the full potential of nanozeolite utilisation for forward-looking applications concerning biomedical science has not yet been fully discovered.

The resistance towards conventional treatments, namely antibiotics and radiotherapy in microbiology and medicine, respectively, is a matter of concern in terms of increasing numbers of deaths caused by infectious diseases and cancers. Moreover, the antibiotic resistant bacteria are the main cause of severe infections, inflammations and food poisoning in hospital environments. During the past three decades the bacterial resistance rises much faster than total number of approved new antibiotics as presented in Figure 1.[5] In addition, the intense use of antibiotics is not largely applicable because of side effects. Therefore, the development of new, antimicrobial strategies to kill bacteria and prevent a vast number of diseases is of great interest.
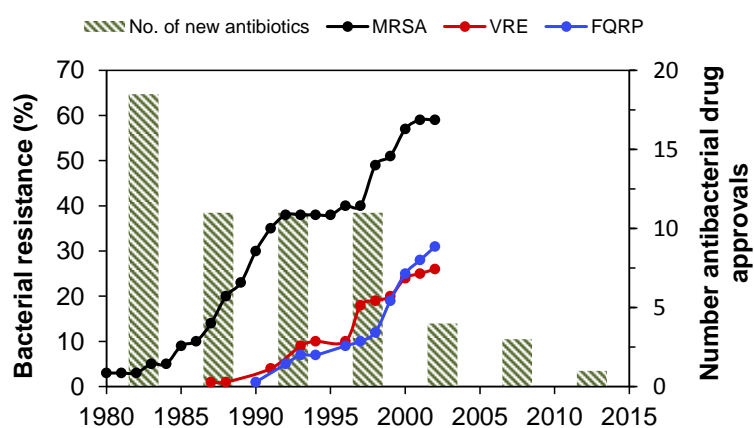
Figure 1. Number of new antibacterial drugs authorised by New Drug Application Approvals and resistance rates for three types of bacteria: methicillin–resistant *S. aureus* (MRSA), vancomycin-resistant Enterococci (VRE), and fluoroquinolone-resistant *P. aeruginosa* (FQRP). Modified from: Centers of Disease Control and Prevention.[6]

Another important problem is the treatment of brain tumours. It has been recognised that the main cause of resistance to radiotherapy treatments of tumours, especially glioblastoma (primary brain tumour) is caused by the insufficient oxygen supply to its tissues, called hypoxia.[6] Previously, several paths were taken to reduce hypoxia in tumours, namely by O_2 and carbogen (mixture of 5% CO_2+ 95% O_2) breathing. The results of this method were poor in terms of selectivity and response to radiotherapy. Further, the extrinsic delivery of nitric oxide (NO) to prevent blood clots formation at the surface of artificial blood vessels and medical devices is an important matter. Nowadays, heparin is employed as anticoagulant to prevent thrombosis, however, its use can lead to an unexpected bleeding in other parts of the body, leading to loss of platelets.

A possible solution to prevent, bacterial infections, radiotherapy resistance and thrombosis is to employ metal exchanged nanozeolites to act as antimicrobial agents and gas carriers. The sizes of zeolite crystals play a very important role when used in *in vivo* studies. Micronsized zeolites have well-defined pore structure and high sorption capacity, however they are not stable in solutions, tending to aggregate which influence their activity and transport, leading to toxic effects. On the other hand, nanozeolites with sizes <100 nm possess all important textural properties and most importantly they are stable in colloidal suspensions. Moreover, they show the absence of acute and chronic toxicity in living animals which makes them perfect candidates to be considered for biomedical use.

Despite the fact that a lot of studies have been devoted to explore the use of zeolites in microbiology and medicine, the full potential of such materials still remains to be developed mostly in regards to their biocompatibility and selectivity. The goal of this PhD research is to synthesise and post-synthetically modify template-free FAU-X nanozeolite for biomedical applications. The post-synthesis alterations mainly involve the optimisation of ion-exchange procedure for different cations introduction and thus functionalisation for desired application. The gained information throughout this study will enable to understand the effect of cation exchange in the zeolite structure and its properties linked to wanted applications.

2 Background

2.1 Zeolites- literature review

2.1.1 History and general information of zeolites

Zeolites by definition are crystalline porous aluminosilicates build-up of four connected tetrahedra.[7] The framework cations (TO_4) can be isomorphously substituted by other elements with appropriate size and valency (T= Ge, Ga, P, Ti, B, Fe…). The framework cations arrange around templating species, alkali metal cations with their hydration spheres or positively charged organic species, during the crystallization process, which takes place under hydrothermal conditions. This specific interconnection forms a three-dimensional network structure, resulting in microporous space, channels and/or cavities, giving them molecular-sieve characteristics. There are more than 239 types of synthetic zeolites, all of them listed on the International Zeolite Association website (IZA).[8] Their structure is defined by framework topology established by arrangement of primary, secondary and polyhedral building units.[9] These crystalline materials are grouped into three types of categories based on the framework largest pore dimension: (i) small-pore zeolites, 8-membered ring (8-MR) (RHO and CHA),[10] (ii) medium-pore zeolites, 10-MR (FER and TON)[11] and (iii) large-pore zeolites, 12-MR (FAU, IWW).[12] There are a few extra-large- pore zeolites (>12-MR), but the quest for such materials is very intense during last decade.[13,14]

The IZA database consists of detailed information about all synthetic zeolites, starting from framework type, dimensions, synthesis conditions etc. Nevertheless, the final properties of a zeolite are controlled by a lot of variables, starting from synthesis conditions, post-synthetic modifications to activation for a specific reaction. The number of Al^{3+} atoms in the zeolite framework is an important parameter that governs the main properties of aluminosilicates. If the zeolite matrix is composed only of Si^{4+} atoms, the corresponding silica (SiO_2) in tetrahedral framework has a neutral charge. Any substitution of Si^{4+} with Al^{3+} atoms (AlO_2^-) results in a negative framework charge, which has to be balanced out with counter cation (Na^+, K^+, NH_4 or H^+). Upon the change of the cation type (located in the framework channels and cages) the physical properties of zeolites are being modified, which influence their ultimate applications. The Al^{3+} content in the framework also control the hydrophilic properties of zeolites, hence its negative charge attract the polar water molecules (H_2O). Therefore, zeolites with high alumina content are considered to be hydrophilic, whereas the

ones with high silica content occur to be hydrophobic. Consequently, the acidity of zeolites increases with increasing Al^{3+} content. Its strength is influenced by density of acid sites and thus the Si/Al ratio, which is an important point when taking into account the use of zeolites as solid acid catalysts.[15] However, the degree of Si^{4+} to Al^{3+} substitution is restricted to 50% as stated in by Löewenstein's rule (Al avoidance rule); two Al tetrahedral species (O-Al-O) cannot share one neighbouring O atom due to electrostatic repulsion of the negative charge, as a result of which the O-Al-O must be separated by a minimum one O-Si-O site.

The first zeolite that opened the door for commercial applications of aluminosilicates was employed in 1960's by Mobil Oil Corporation. They have used synthetic faujasite (FAU) zeolite, both X and Y-type, as a catalyst for Fluid Catalytic Cracking process (FCC).[16] Nowadays, the family of FAU zeolites along with many others, namely MFI, Beta, FER, MOR and TON are being employed in various catalytic and separation processes found in oil refining and petro-chemistry.[17] The utilisation of zeolites as catalysts is encountered to be around 27% of the total zeolite market worldwide from which 95% is used as FCC catalysts. The entire, worldwide zeolite consumption is estimated roughly to be 350 thousand tonnes per year, where the North America is being assigned as the primary consumer (Figure 2).[18]
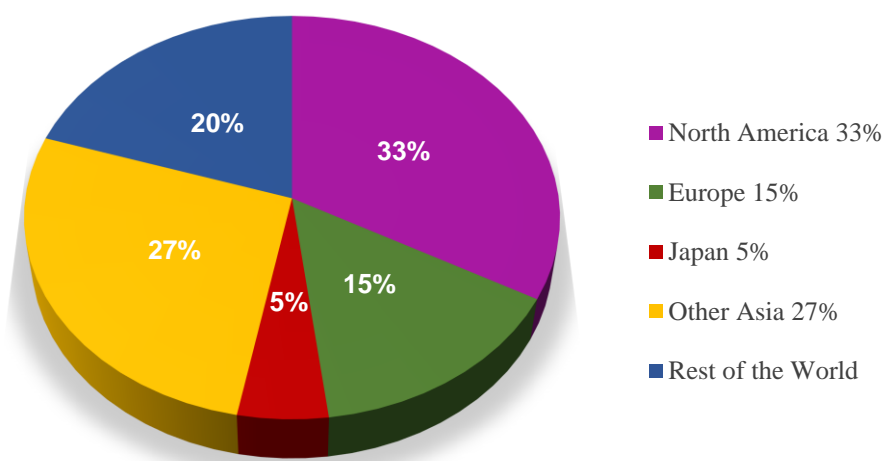
Figure 2. Annual zeolite consumption by area. Modified from[18]

The general attraction caused by zeolites in industrial and environmental applications can be justified by their distinctive properties such as: (i) well-defined pore structure, which makes them shape-selective, (ii) high thermal and chemical stability, which is important for harsh operation conditions, (iii) strong Brønsted acidity (essential for catalytic

transformations) and (iv) ability to exchange cations, vital for environmental usage e.g. water softening, wastewater treatment.[19,20] Consequently, all of those engaging properties of zeolites made them widely used in previously mentioned FCC but also in paraffin's isomerisation, aromatic processing and gas sorption/separation.[21,22] Moreover, the zeolite properties, namely crystal size, porosity (micro-mesoporous hierarchical zeolites) and active acid accessibility can be further altered using various post-synthetic modifications depending on the required application. The general review of all possible post-synthetic modifications and their outcome is well presented by Valtchev *et al.*[23]

Considering all the important morphological transformations of zeolites, in where the main goal is to enhance their properties and thus activity have already been well investigated. The one that attracted the most attention was the zeolite crystal size reduction to nanometre scale. The main advantages of nanozeolites are tuneable crystal sizes, high external surface area, better micropore accessibility and decreased diffusion constrains (Figure 3).[24] These properties enabled nanocrystals to be tested in enhanced reactions with bulky molecules as well as membranes and films in gas separation and sensing.[25,26] Furthermore, the template-free synthesis of nanosized aluminosilicates, associated with them controlled crystal engineering and biocompatibility opened the door for novel biology and medicine related applications e.g. biosensing, gas/drug delivery and antibacterial.[27–29]
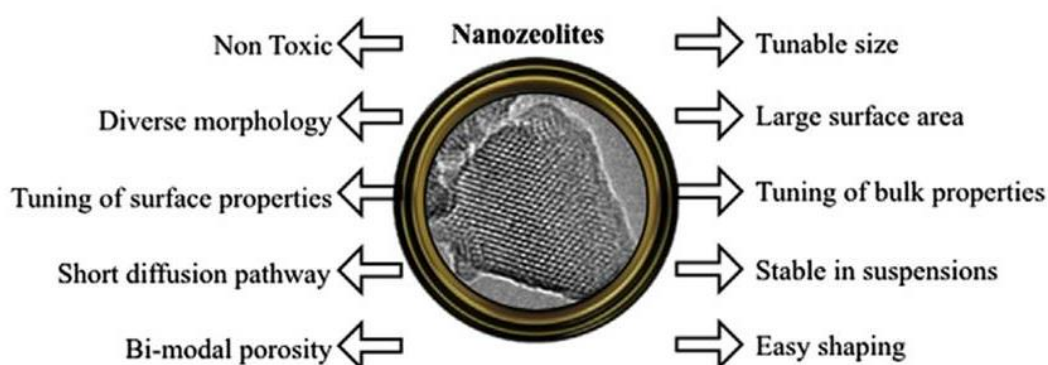
Figure 3. Advanced properties of nanozeolites.[24]

2.1.2 Synthesis of nanozeolites

The knowledge advancement about growing conditions of natural zeolites has made an important contribution in understanding the synthesis process for laboratory made zeolites.

The laboratory preparation process of aluminosilicates took on broad variety of conditions that implement the natural growth of zeolites, such as temperature, pH, pressure and time. The general synthesis of nanozeolites involves hydrothermal treatment (HT) of mixed aluminate and silicate solution in a closed system, under alkali conditions (pH≥11), at raised temperatures (RT-180 °C) and pressures over the period of minutes to days. The zeolite synthesis requires preparation of starting solution/gel precursor from a mixture of raw materials, which then could be subjected to homogenisation, aging and finally HT resulting in crystalline material. The molar ratio formula has been employed in order to describe the general, chemical composition of particular zeolite, where M symbolise counter cation or organic structure directing agent (OSDA), x/n stands for the number of cations and x represents the number of alumina species.[30]

$$M_{x/n}[(AlO_2)_x(SiO_2)_y].mH_2O$$

There are several variable components that have to be controlled when synthesising the desired zeolite, one of the important ones being Si/Al ratio, followed by the source of starting materials, metal cations, OSDA's and H_2O quantities. The latter two play vital role in size/morphology determination and as catalyst in chemical reactions within the synthetic system. A few details have to be taken into consideration when starting a new synthesis. Particularities like the purity/source of reagents, order of mixing, speed of agitation and temperature/time of aging are essential things to bear in mind.

As mentioned above the synthesis of nanozeolites is always executed in the closed system. The reaction between the starting components within the initial gel leads to nucleation of particles and crystal growth. Nucleation and crystal growth are two very complex processes, which occur simultaneously and for that reasons the separation between them is impossible. Hence, the correlation between them is crucial when it comes to crystal size design. The increase in viable nuclei number results in the formation of smaller crystals, as demonstrated in Figure 4a. The zeolite crystal growth manner is typically described based on classical S-shaped crystallization curve (Figure 4b). Therefore, in order to obtain smaller crystals the synthesis conditions have to be adjusted in the way to favour nucleation over crystal growth e.g. lower synthesis temperature/time[31] The control of initial precursor's homogeneity as well as the uniformity of the nucleation process is crucial when the main aim is to synthesise nanosized zeolite crystals with monomodal particle size distribution.

The appearance of zeolite yielding systems is diverse in nature, due to the type of starting precursors employed as well as the mixing conditions (stirring, shaking) used for homogenisation. Its form can differ starting from very dense, almost paste-like gels to water clear suspensions.[32] Usually, hydrogels (separated into the mother liquor and solid part) are applied when it comes to zeolites preparation. However, the outcome of such approach results in the formation of micron-sized zeolite crystals. Therefore, a better understanding of zeolite nucleation process, along with the identification of the key elements that govern the formation and number of viable nuclei in the system is needed. The zeolite formation process is still not well understood due to convolution of many actions that are happening within the system at relatively short space of time. Besides the control of crystal size the future research in this topic will also considerably improve the ability to control the zeolite crystal morphology.
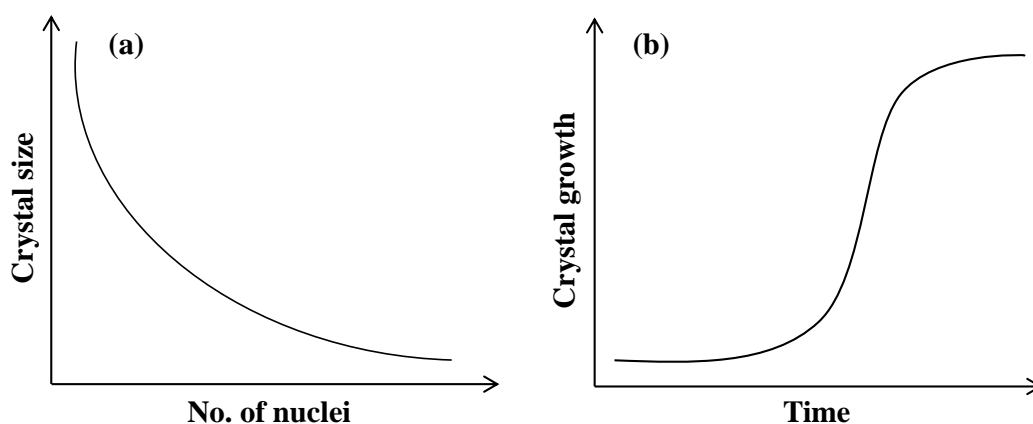
Figure 4. (a) Correlation between the number of nuclei per unit gel and ultimate crystals size, (b) Typical S-shaped curve representing the crystal growth with time.

2.1.2.1 Conventional synthesis of nanozeolites

The term, conventional synthesis refers to preparation of nanocrystals from hydrogels in a closed system under hydrothermal treatment. The first reports on syntheses of zeolite nanocrystals with narrow particle size distribution was documented in the beginning of 90's by the group of Swedish researchers, led by Schoeman *et al.*[33–35] They have reported the synthesis of industrially important zeolites, such as ZSM-5, sodalite, Y and A with particle sizes ranging from 100-300 nm. The nanozeolites were synthesised from so-called 'clear homogenous solutions' at rather low temperatures (~100 °C), purified, redispersed in water and kept in form of stable colloidal suspension. They have shown that although the starting

colloidal mixture was visually clear, it contained discrete particles from which the zeolite nanocrystals were formed (crystallisation). Those studies provided an excellent starting point for the understanding and further development of nanocrystal synthesis.

The homogeneity of the initial system is the key factor for nanozeolite formation, among carefully selected reactants (mainly silica source) and conditions. Generally speaking, in order to acquire the homogenous system the quantity of alkali cations must be kept as low as possible (which will limit the particle aggregation), whereas the high amounts of tetraalkylammonium hydroxides are vital to stimulate alkalinity of reaction (basic pH). The high water content keeps the system diluted, which is necessary for preventing crystal aggregation and the crystallisation temperature is typically bellow 100 °C, to encourage nucleation rather than crystal growth. The product recovery plays equally a principal part in the final particle size as well as the synthesis itself. The nanocrystals are retrieved, and purified from the excess of unreacted reagents by high-speed centrifugation (>20000 rpm) for times longer than 15 min (depending on the crystal size). Usually, nanocrystals are then washed with distilled (dd) H_2O and kept in stabilised suspension at pH around 9. The appropriate pH of zeolite suspension maintains the negative charge on zeolite crystals (keeping them stable), avoiding agglomeration (even when stored for a long period). The transformation of zeolite suspension into solid is preferably performed using freeze drier, rather than conventional, oven drying, to minimise the level of agglomeration. Indeed, the synthesis from clear suspensions enables the study of zeolite crystallisation process and profits highly crystalline nanozeolites with well-defined morphology, however it compromises on the total reaction yield due to synthesis conditions.

Lately, EMT zeolite nanocrystals were synthesised from colloidal solution, free from organic template.[36] This synthesis breakthrough was critical, as until 2013 this potentially active zeolite in separation and ion-exchange processes was prepared with the presence of very expensive organic structure directing agents and thus its commercialisation was impossible for obvious financial reasons. This successful approach was carried out in Na-rich starting precursor mixture and conditions specially selected to avoid impurities with competing phases of FAU and SOD zeolites. Initially, the amorphous colloidal particles were formed (as expected from the crystallisation process reported for zeolites X, Y and A), and during hydrothermal treatment at very low temperature (around 30 °C), these amorphous particles were converted to ultrasmall, hexagonal crystals with sizes 6-15 nm. Upon extended

crystallisation time these ultrasmall particles grew to 50-70 nm nanocrystals. Besides the employment of green synthesis methods which resulted in the formation of ultrasmall crystals with narrow particle size distribution, the great achievement was obtained by the elimination of OSDA's, bringing the EMT nanozeolite production cost down, ultimately making them commercially accessible.

Another example of industrially important aluminosilicate is zeolite A. This small pore (4.2 Å) zeolite has a superior ion-exchange capacity and thus is broadly used as a key component of washing powders to act as water softener. The preparation of zeolite A nanocrystals from clear suspension was firstly acquired in the presence of tetramethylammonium hydroxide (TMAOH) structure directing agent.[37] The synthesis was performed at room temperature (RT) for 7 days which resulted in the formation of particles with sizes 40-80 nm. Latter was heated at 80 °C for 1-2 hours, the hydrothermal treatment produced larger crystals (up to 400 nm) with well-developed faces. Few years later, the "green" synthesis approach in the preparation of template-free LTA nanozeolite was employed.[38] Zeolite A was prepared under very mild conditions (40 °C) in order to favour the nucleation and consequently delay the crystallisation process, allowing the fundamental study of crystal birth. After 18 hours of hydrothermal treatment the fully crystalline zeolite A with crystal sizes between 40-300 nm was acquired.

Overall, the template-free, low temperature material preparation enabled to study the crystallogenesis of zeolite formation. The nanocrystals preparation in the absence of OSDA's made nanozeolites biocompatible and empowered their use in on-demand, biomedical applications which are discussed in detail in sections 2.1.3.2 and 3.4

2.1.2.2 Non-conventional synthesis of nanozeolites

The non-conventional synthesis methods were developed to conquer the problematic crystal size control linked to the conventional approach. A technique that can be used to control the crystal growth is the confined-space synthesis. This method applies physical barriers to control crystal growth and thus the final crystal size is determined by the available free-space. The first case of such synthesis was reported by the group of Jacobsen *et al.* where they used carbon nanotubes (impregnated into initial precursor mixture) for the preparation of ZSM-5 zeolite. After crystallization the zeolite with average crystals sizes of 15 nm was

obtained and carbon removal was accomplished by pyrolysis.[39,40] Next, various polymers and surfactants were introduced to zeolite precursor suspensions (instead of carbon nanotubes) to act as a space limiting agent.

In the past decade, several studies proposed the employment of multivalent surfactants for the synthesis of nanozeolites. The function of surfactants was to manage the mesopore formation (micelle) during which microporosity was created from the surfactant head groups, effectively limiting the crystal growth.[41,42] Through this approach zeolites with the following framework structures have been synthesised; FAU, CHA, MFI and MOR. The main drawback of such procedure was that the resulting nanocrystals were very much aggregated creating a thick layer of particles.

Moreover, the organosilanes have been used as surface functionalising agents of nanozeolite precursors, which could rather be viewed as confined-space synthesis. The idea of introducing silane coupling agents is to interrupt the zeolite crystal growth.[43] Lately, the work of Hu *et al.* stated a one-step synthesis route, using amino-, mercapto- and allyl-surface groups to control the crystal growth of ZSM-5 nanozeolite.[44] The consequent zeolite crystals were homogenous and highly crystalline with sizes around 100 nm. Furthermore, the silanes addition not only influenced the crystal size but also induced changes to Si/Al ratio and hydrophilicity.

Correspondingly, ultra-sonication has also been used for the synthesis of zeolite nanocrystals. Recently, nanosized NaP zeolite was prepared by sonochemical method followed by either traditional hydrothermal treatment.[45] By the use of this method a noticeable decrease in particle size was noted when compared to synthesis without sonication. In this study the sonication energy was held at 150 W and the zeolite starting solution aged in the ultrasonic batch 2 h. This issued a formation of small zeolite P nanocrystals (50 nm).

Another sort of non-conventional zeolite synthesis applies the use of Microwave (MW) radiation instead of traditional oven heating. The main advantages of this method are fast, uniform and direct heating in the reaction holder, which generally produce more homogeneous systems and smaller crystals. In 1998, a great review on MW techniques for zeolite synthesis and modification has been produced by Cundy *et al.*[46] Subsequently, followed by a lot of reports on MW synthesis, its applications and future developments. For

example, the publication by Heyden *et al.* describes the successful preparation of AlPO-18 nanocrystals by MW route.[46] The MW synthesis was performed at 130 °C for 30 min, which resulted in the formation of nanocrystals (300 nm) with well-developed faces.

2.1.3 Properties and applications of nanozeolites

The main properties of nanozeolites have been well documented in the past. The decrease of zeolite particles size to nanometre scale made a huge impact on their performance in well-established applications, namely, catalysis, ion-exchange and separation. By decreasing the crystal size the number of external atoms increase, and thus the external areas, as well as surface activity. The large surface area and acidity of nanozeolites are essential to maintain their activation for catalytic applications, especially where the zeolite is involved in the systems with bulky molecules. Moreover, smaller zeolite crystals have shorter diffusion path lengths and therefore reduce the mass transfer limitations, which is crucial for catalysis to ensure rapid reactions and avoid coke formation. In addition, nanocrystals possess high chemical and thermal stability due to their well crystalline structures, enabling their utilisation in harsh conditions. The improved preparation and post-synthetic modifications of nanomaterials facilitate their use in advanced applications illustrated in Figure 5. This section will provide an overall summary regarding on-demand nanozeolite applications including optical/sensing, biological and medicinal uses.
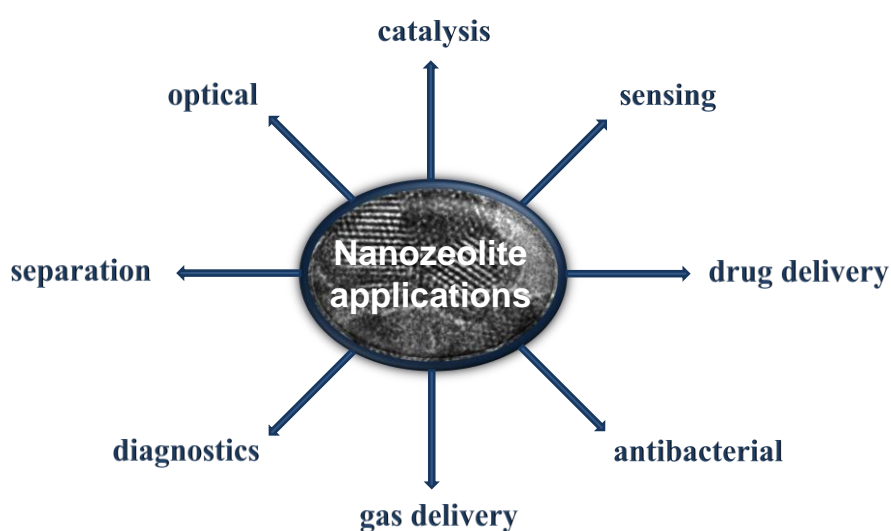
Figure 5. Novel applications of nanosized zeolites.

2.1.3.1   Optical and sensing applications of nanosized zeolites

Nanozeolites are model materials for the preparation of optical devices, thanks to their high thermal stability, diverse and rigid structures. They are introduced to optical devices in form of zeolite films, with a thickness of 200-10 000 nm, made by spin (dip) coating, hydrothermal growth of zeolite layers and screen printing.[47,48] The thin film preparation method as well as zeolite and binder type influence the final optical properties such as thickness, hardness and related to those extinction coefficient and reflective index.

The first example of zeolite based photovoltaic cells has been reported by Calzaferri *at al.* where the one dimensional, LTL nanozeolite was used for the incorporation of organic dyes for light harvesting and energy storage.[49–51] In all three cases the 30 nm sized zeolites L were used. It has been demonstrated the dye incorporation into the zeolite micropores did not affect its optical properties. Further functionalisation of hybrid films was necessary to efficiently catch and inject electronic energy from/to the nanocrystals. In order to do so, a coupling acceptor or donor stopcocks fluorophore molecules were positioned at the ends of LTL nanozeolite channels. The final stage of organisation involved the coupling to an external device through stopcock molecules. The versatility and easy adjustability of those organised systems showed a great potential in excitation energy trapping and transfer, which provide a platform for development of future photonic devices.

Recently, a great attention was drawn to the preparation of new photovoltaic solar cells based on 3D CdS, PbS and PbSe quantum dots (QD) arrays loaded into FAU-Y zeolite voids.[52,53] Their results indicated that the performance of the devices greatly depends on the type of QD used. The best efficiency was obtained for Y zeolite encapsulated with multi QD arrays, in this case CdS and PbS.

Nanozeolites are excellent candidates for chemical sensing/detection owning to the presence of exhalable cations, adsorption capacity, high surface areas and porosity, providing a fast response required especially in sensing appliances. Latterly, a very detailed review about the use zeolites for sensing devices in automotive and biomedical industries was presented.[25] The authors demonstrated several instances where zeolites can be utilised for NO_x, NH_3, H_2O and hydrocarbons detection. They can also be employed as base for CO_2, O_2 and alcohol detection in air control and biosensors.[54–56]

The size and shape selectivity of zeolites towards different analytes is refined by the introduction of various framework topologies, which are characterised by specific pore dimensions, shapes and volumes, which permit segregation between heterogeneous molecules. The chemical composition of nanosized zeolites can be modified which will affect the sensor sensitivity and response, e.g. by increasing Si/Al ratio (hydrophobic) and ion-exchange (adsorption capacity). In general, nanozeolites have several important benefits to offer when it comes to sensors manufacture; (i) stability in suspensions, (ii) relatively simple deposition (thin films), (iii) faster response (zeolite films thickness reduction), (iv) selectivity and accessibility (use of different types of zeolites, desired crystals positioning in the films). All of these advantages make nanozeolites potential candidates for conductive, selective, active and most importantly stable sensing devices.

2.1.3.2   Biomedical applications of nanozeolites

Nanozeolites have been widely examined for different biomedical applications, namely, antibacterial, drug delivery and gas storage. However, the main question in regards to their toxicity still remains uncertain, as nanoparticles can cause unwanted effects in human health. This issue is of great importance as zeolites are used in industry and commercial products, and thus the exposure to environment and eventually humans will highly increase. Therefore, the nano-safety regulations must be applied due to easy adsorption of nanoparticles, through breathing/skin and distribution via blood to vital organs.

The toxicity tests were performed mostly on FAU, EMT, LTA, and MFI zeolites.[57–60] The results demonstrated that nanosized zeolite have very low or non-toxic effects. The review on biological toxicity of LTL nanozeolites showed very low toxicity towards HeLa cancerous cells. Although, at high concentrations a toxic response was observed, this was assigned to positively charged crystalline surface.[61] They stated that nanosized zeolites toxicity strongly rely on their size, shape and metal functionalisation.

The implementation of green synthesis techniques, without the use of template, performed at low temperatures, open the door for nanomaterials to be used as potential gas carriers for biomedical applications. For this kind of application the nanosized zeolite has to be able to adsorb, store and deliver gasses essential for biological functions. The gas adsorption capacity

and cytotoxicity of iron-exchanged, EMT nanozeolite was assessed.[62] The results indicated that particles with sizes 10-30 nm are non-toxic towards human glioblastoma (U87-MG) and kidney cells (HEK-293T). The greater gas adsorption capacity towards CO_2 and NO was noted after iron introduction in comparison to as synthesised sodium containing nanozeolite. Additionally, the ability of metal-exchanged LTA nanozeolite to release NO has expanded their use for medical purposes, in particular as coating of artificial blood vessels to prevent thrombosis during and after surgery.[63] Moreover, the Zn- and Co- containing LTA nanozeolite proved to have higher NO adsorption affinity than Na-form. The amount of gas released strongly depended on the type of cation, its concentration and charge.[63,64]

The drug delivery applications of nanozeolites have been previously reported. The attention was drawn mostly to LTA, FAU and MFI zeolites for anti-cancer drug delivery.[28,65] Conventional cancer therapies with traditional drugs such as 5-fluorouracil (5-FU) often result in adverse toxic effects. Therefore, the encapsulation of these anticancer drugs is not only needed for simpler administration but also to avoid harmful properties. The 5-FU anticancer drug was encapsulated into FAU, MFI and LTA zeolites to test them in drug delivery systems. The drug loading was found to be the highest in FAU nanozeolite followed by MFI and LTA, which clearly follows the size of pore openings of individual frameworks, and thus adsorption capacities. *In vitro* drug delivery report showed a fast drug release from nanozeolites, 75% of 5-FU drug was released within 5 min. Besides fast drug delivery, the parent nanozeolites showed nontoxic behaviour towards RKO and HCT-15 colon and breast cancer cells respectively. However, after 5-FU introduction into nanozeolites, the cell viability drastically decreased even when compared to the anti-cancer drug itself. On that basis it can be concluded that drug delivery systems involving nanozeolites are effective in anticancer therapy.

Finally, it is worth mentioning that nanozeolites also possess antifungal and antibacterial activity. These inorganic aluminosilicates have well-defined porous systems and provide chemical and thermal stability as well as easy functionalisation needed for antimicrobial properties. The antibacterial efficiency of colloidally stable EMT zeolite loaded with silver was recently reported by Dong and co-workers.[66] The study demonstrated that nanozeolite containing high silver amounts effectively inhibited the growth of *E. coli*, no viable bacterial cells were observed after two min of exposure.

3   Faujasite (FAU)

3.1   Framework characteristics

Faujasite is a rare, natural zeolite found only in several locations over the world. The crystal structure of FAU was first resolved in 1956 by Bergerhoff *et al.*,[67,68] latter in early 60's the first synthetic zeolite X was discovered by Milton *et al.*[69]

Zeolite X and Y are large pore zeolites which belong to FAU framework topology. The only contrast between them comes from the small change in Si/Al ratio, being 1-1.5 and above 1.5 for zeolite X and Y, respectively. Their three-dimensional structure is constructed of sodalite cages consisting of 24 T atoms (Figure 6a) interconnected by hexagonal prisms (double 6-rings). The sodalite cages assemble together to from large supercage with diameter of 1.2 nm and opening of 0.73 nm. As presented in Figure 6b, the single unit cell contains 8 sodalite cages and 16 double 6-rings. Those single units are connected together along [001] through hexagonal prism to create the FAU-type framework (Figure 6). FAU-type zeolite has an open structure, which is indicated by the low number of tetrahedrally coordinated T atoms per 1000 Å^3, giving a framework density of about 13.3 T/1000 Å^3.
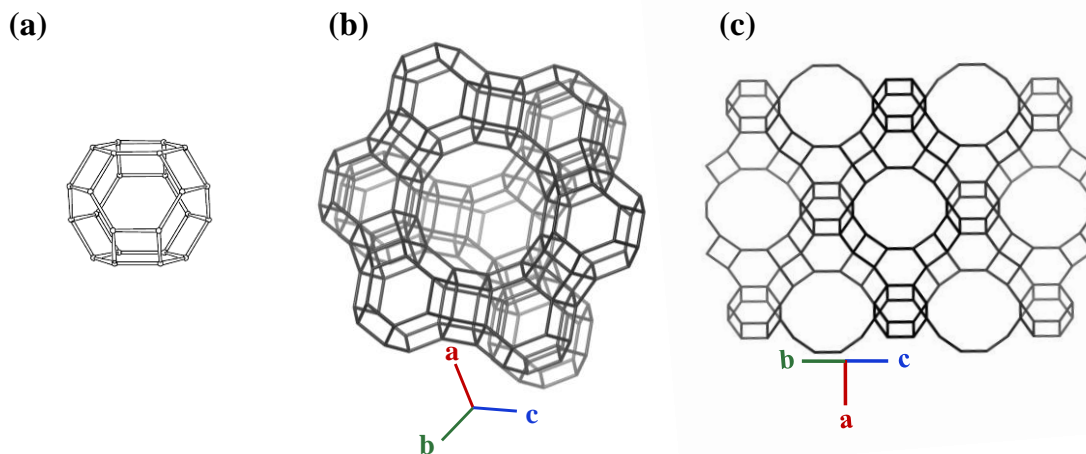
Figure 6. (a) Sodalite cage - a basic structural unit, (b) single unit cell of FAU framework consisting of super cage, sodalite cages and hexagonal prisms, (c) Connected unit cells of FAU zeolite.

3.2   Cation distribution in Na-X zeolite

As mentioned in the previous section, the introduction of aluminium atoms into zeolite brings a negative charge to the framework, which is compensated by the presence of extra framework cations. The properties of zeolites are closely associated with the type, position and accessibility of those cations to interact with other molecules. Therefore, the determination of different locations of those metals is essential to understand their behaviour in adsorption and ion-exchange processes. Since the primary study of Mortier *et al.* who devoted his research to understand the location of extra framework sites in the zeolite,[70] a lot of studies have been reported to study Na$^+$ distribution in X zeolite.

Na-X from of FAU zeolite acts as a predecessor for almost all ion-exchanged FAU type aluminosilicates. The main characterisation methods used for determination of cation locations include: powder or single-crystal X-ray diffraction, NMR (magic angle spinning and double rotation), powder neutron diffraction and computational predictions.[71]
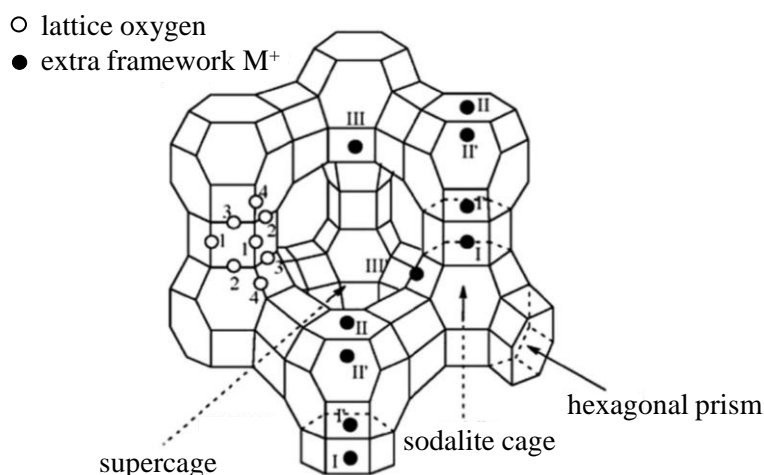
Figure 7. Single unit cell of FAU framework with possible cation site locations.[72]

Na$^+$ cations occupy different crystallographic sites in the framework for two main reasons: (i) to increase their interactions with oxygen atoms, and (ii) to reduce cation-cation repulsion. Sodium cations can be located inside of hexagonal prisms - sites I, within sodalite cages - site I′, in the interior of supercages, in front of 6-rings - sites II, and in the supercage close to 4-rings of the sodalite cages - sites III. For the schematic representation of all sites within FAU-X please refer to Figure 7.[72]

The site multiplicity per unit cell varies depending on the site type, e.g. site I has a multiplicity of 16, sites I′ and II have 32 and site III possess 48. It has been reported that if there is less than 32 cations per unit cell the first site to be occupied by is site II due to reduced cation-cation electrostatic repulsions. However, if the number of extra framework metals increases from 33 to 48 per unit cell, site I will be the most populated one.[73] It is worth mentioning that sites I and I′ cannot be inhabited by metal ions at the same time in the same hexagonal prism due to strong repulsions caused by a short distance between them. When the cation number increases from 49- 64 per unit cell, site I occupation is reduced in the advantage of site I′ (more favourable). Sites III and III′ are the last one to be occupied with growing numbers of metals.[74]

3.3 Functionalisation of Na-X with metal ions

Faujasite Na-X zeolite exchanged with various metal ions, such as Li^+, K^+, Rb^+, Cs^+, Cu^{2+}, Zn^{2+}, Fe^{3+}, and many others, have been thoroughly investigated over the past half-century in regards to their employment in crystal engineering, separation, biomedical science and catalysis. The post-synthetic metal introduction allows the preparation of zeolite with properties suitable for particular application. The cation exchange can be achieved via two different methods, ion-exchange or impregnation depending on the loading, size and charge of the metal ions.

3.3.1   Ion exchange

Ion-exchange is a relatively simple process that can be executed in solid, liquid and gas phases. Usually, the exchange is performed in nitrate or chloride solutions with specific concentration of metal ions and zeolite in form of solid or colloidal suspension. The ion mobility is not significantly affected by the temperature, thus in most cases exchange is executed in the range of 25-80 °C. Although, this procedure needs numerous treatment steps such as filtration, washing, purification etc., it can be employed to different kinds of zeolites without affecting their stability.

Ion-exchange has been extensively used in a zeolitic systems used in applications regarding water purification, gas separation and catalysis.[75–77] The interactions between different ions and zeolite lattice changes the material activity and accessibility towards

various type of molecules. As a consequence it creates new possibilities for exchanged-zeolites to be used in environmental and biomedical sectors.

3.3.2   Impregnation

When ion-exchange is not effective enough e.g. due to cation size and charge, impregnation can be applied as an alternative method for metal introduction into zeolite materials. The amount of impregnated ion species is controlled by the concentration and pH ionic solutions. In case of nanozeolites, their physical properties, namely high surface areas and open structures, increase their capability of metal introduction making impregnation very efficient.

3.4 Biomedical applications of metal exchanged zeolite X

The development of "green" synthesis methods combined with metal ion functionalisation of nanozeolites opened the door for them to be considered in microbiology, biomedicine and gas adsorption applications.

3.4.1   Microbiology

Nowadays, the number of infections and inflammations caused by the pathogens is rising due to their increasing resistance towards antibiotics.[78,79] Antimicrobial resistance (AMR) is naturally developing process where microorganisms are able to resist the treatments by antimicrobial agents. If the antimicrobial resistance (AMR) continues to grow at the current rate, the estimated number of deaths caused by AMR per year will exceed 10 million by 2050 as illustrated in Figure 8. This prediction is very much warring as it will surpass the number of life losses caused by cancer.[80] Therefore, the necessity for development of new antibacterial agents, which are not based on antibiotics, is of great demand.

In the past, zeolites functionalised with antibacterial metals such as Zn^{2+}, Co^{2+}, Cu^{2+} and Ag^+ have been employed to fight bacteria.[81–84] Those inorganic aluminosilicates own several benefits in contrast to generally used organic agents, mainly chemical/thermal stability allowing easier preparation of nanocomposites and other elaborated structures.[85] Silver exchanged zeolites, have been by far the most studied system. The main reason for it is that silver contains rather wide spectrum of antimicrobial properties, where zeolites hold well-

defined microporosity and high-surface area, providing slow release of silver cations in solution and effectively long-term antibacterial activity.[86] The antibacterial mode of silver can be divided into four parts: (i) release of metal ions in solution, (ii) provoking loss of water from cells, (iii) entering the bacteria cell and (iv) inhibiting the bacterial DNA replication.
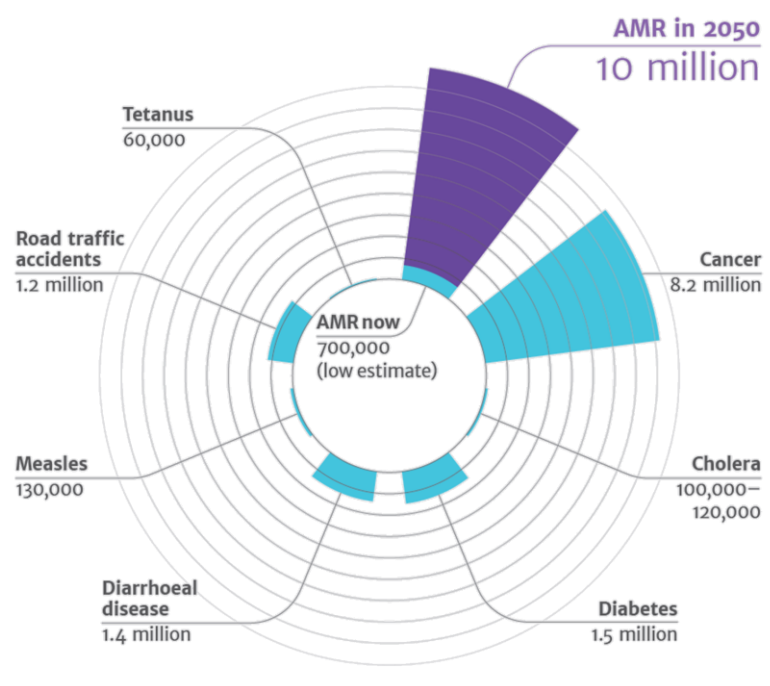
Figure 8. Estimated number of deaths caused by AMR in comparison to other causes life loss.[80]

The final antimicrobial properties of silver containing aluminosilicates strongly depend on zeolite pore size (micro-meso porous), physical appearance (powder, pellets) and silver form (cationic, metal).[87] Moreover, the research by Sabbani *et al.* demonstrated the use of FAU zeolite films with stabilised silver nanoparticles, to be efficient against *E. coli* with the complete bacteria elimination within 120 min.[88] Despite the fact that silver has proven its activity against a broad spectrum of bacteria and pathogens, there are major concerns regarding the use of silver nanoparticles in commercial products (textiles, cosmetics) which can lead to silver accumulation in the environment.[89]

Additional example of zeolites used in microbiology was documented by the research group of Fox *et al.*, where they used NO loaded zinc exchanged zeolite for bifunctional antibacterial strategy. This study showed the material potency in treatment against Gram-negative and Gram-positive bacteria.[90]

To conclude, the use of nanozeolites in microbiology can potentially grow due to offered flexibility in terms of preparation and modification. Besides, they can be stabilised in suspensions, deposited in membranes and thin films, which give the possibility for versatile use in different settings.

3.4.2 Drug delivery

The importance of using nanozeolites in biotechnology and biomedicine comes from their ability to adsorb different molecules, depending on their pore size and hydrophilic/hydrophobic nature, without compromising on their high stability and structure. Pharmaceutical substances, like drugs, can be introduced to zeolites via different ways: (i) by loading into channels and cages of zeolites, and (ii) immobilisation to the external surface. As a consequence, the synthesis of zeolites with high external surface areas became substantial, especially when large biomolecules are immobilised to them.

The FAU type zeolite was used for adsorption and *in vitro* delivery of anti-inflammatory drugs.[91,92] The study revealed that the amount of drug adsorbed corresponded to the zeolite pore volume and delivery rate was affected by Al content. The drug delivery rate was dependent on Al amount due to the fact that Ibuprofenate boned more strongly to the active sites of zeolite . The ibuprofen loaded FAU demonstrated an improved drug release manner than inspected for mesoporous silica (MCM-41). Apart from anti-inflammatory substances, the FAU zeolite was also employed as a carrier of anthelmintic drugs.[93] Dichlorvos is a relatively small molecule which has been introduced to FAU in order to decrease the number of worms in pigs and rats. The results indicated that dichlorvos immobilised zeolite showed earlier removal of worms than the drug itself, due to slow release of the substance in the regions more populated by worms. Besides its efficiency, the drug-zeolite matrix remained stable and active at different temperatures for over 6 months. This brought the benefit of using zeolites as a stabilising agent for drugs to extend their shelf life, instead of highly-priced plastic beads, which role is to hinder excessive release.

As mentioned earlier, the nanozeolites have both micropores and textural mesopores which provide them with the ability to adsorb a broad spectrum of different size molecules. The FAU zeolite milled with magnetite was used to adsorb anticancer drug doxorubicin. The milling process enabled to obtain small, ferromagnetic crystals with average sizes of 400 nm.

The nanoparticles were competent to store and release 77 % of the loaded drug in over 12 h. Another study of anticancer drug loading into FAU zeolite was performed by Amorim and co-workers. They encapsulated the anticancer drug, cyano-4-hydroxycinnamic acid (CHC) into zeolite porosity and evaluated the host-drug delivery effect on human colon carcinoma cells (HCT-15).[28] This research revealed that zeolite structure can be used for sustained drug release, increasing CHC bioavailability and thus its efficiency, which is related to enhanced drug solubility when loaded into the pores of zeolite. More importantly, FAU zeolite alone showed no toxicity to cancer cells, whereas when encapsulated with anticancer drug it led to inhibition of cell viability. The loaded drug showed an increase in potency up to 585-fold in comparison to CHC drug alone. These findings pointed out the capability of zeolites to act as a host for anticancer drugs, boosting their delivery and performance.

3.4.3   Gas storage and delivery

Additional application of nanosized zeolites involved the adsorption, storage and controlled delivery of gases, such as O_2, CO_2 and NO for biomedical applications. The challenge is to control the gas release kinetics as they are often toxic when introduced in large amounts, whereas inefficient when delivered in petite quantities.[94] In case of oxygen delivery, materials such as ceramic oxides were mostly considered; however, lately zeolites with reduced size became appealing for oxygen delivery regarding medical applications.[95]

Very recently, a simple route towards increasing oxygen adsorption capacity in nanozeolite FAU was reported.[96] The nanosized zeolite X was functionalised with bromoperfluoro-n-octane (perfluorinated compound) or cerium cation to increase its oxygen capacity which can be used for storage and delivery. These relatively simple modifications resulted in significant increase in oxygen affinity by 33% in both fluorinated and cerium exchanged materials when compared to as prepared Na-X. The functionalisation process did not compromise on the zeolite morphology, as the crystallinity and size remained the same. Additionally, the as prepared and modified nanozeolites displayed no toxicity towards human cells, *E. coli* and mice astrocytes, providing greatly required biocompatibility for biomedical testing.

Nitric oxide (NO) is an example of another biologically important gas molecule that is involved in many biological processes, namely regulation of the blood flow, neurotransmission and immune response.[97,98] The external delivery of this very active

molecule can contribute to treatment of major diseases such as thrombosis. Consequently, materials with the ability to release NO can be applied for production of artificial blood vessels and medical devices. So far, the significant research, done by the group of Morris and co-workers, described the use of LTA zeolite exchanged with various cations to act as effective gas depot and carrier in biological conditions.[63,99] The amount of NO released from zeolite in the water suspension was measured electrochemically, showing that between all metal-exchanges samples Co-exchanged zeolite released the most NO, whereas the as prepared Na form of LTA zeolite released the least NO. It was concluded that the amount of NO liberated from the zeolite was influenced not only by the type of transition metal introduced but also on the amounts of metal ions present. They have also showed that NO-releasing zeolite can inhibit platelets aggregation, which opened the door for them to be used in medical applications, not only during bypass surgery (catheters) but also as antimicrobial adjuncts for infection hindrance.

3.4.4   MRI imaging

The recent development of magnetic resonance imaging (MRI), which is used as a diagnostic tool for discrimination between pathological and normal tissue, caused a huge interest in employment of lanthanide metal complexes to act as a contrast agents. In order to be an effective contrast agent the material has to fulfil several criteria's: (i) it must have a strong local effect on the proton relaxation rated of water, by which the MRI signal intensity is provided, (ii) it has to present adequate pharmacokinetic in terms of specification, distribution and metabolism, and (iii) most importantly it has to be nontoxic. Nowadays, Dotarem is one of the commercially used MRI contrast agents, however its use, rise a debate about the stability of gadolinium chelates complex, which is linked to adverse effects as well as accumulation of Gd^{+3} in tissues.[100] Therefore, the development of new gadolinium containing contrast agents is of great demand.

In the past decade, gadolinium containing FAU zeolites were used as MRI contrast agents for the gastrointestinal tract and the intravascular system imaging, which proved their efficiency in biological systems.[101–103] Moreover, the zeolite crystals were subjected to surface modifications with trialkoxysilane monomers, which aim was to add biological activity and selectivity to the zeolite surface, resulting in crystals accumulation in particular parts of the body.

Besides the capability of iron oxide nanoparticles to repair tissues and deliver drugs, they can also be used as imaging contrast promotor for MRI applications. Additionally, it was demonstrated that iron-exchanged EMT nanozeolite showed better adsorption capacity towards CO_2 and NO, with the absence of toxicity towards various cells.[62] Therefore, the combination of excellent properties of nanozeolites with MRI active particles can lead to development of stimuli-responsive systems for novel therapies, namely, tumour treatment.

4   Literature review- Conclusion

The aim of the literature review was to understand the zeolite-cation exchange mechanism which led to material functionalisation towards potential biomedical applications. The collected information about the use of different types of nanozeolites in advanced biochemical applications and the possibilities of employing functionalised, FAU nanozeolite as antimicrobial agent as well as drug and gas carrier, provided a base for new zeolite utilisation ideas for this research study.

Taking into consideration that a lot of studies have already been dedicated towards finding on-demand zeolite applications in biologically active systems, more research is needed to optimise nanozeolite functionalities. Nowadays, there are a lot of controversies and debates in nanoscience society, about the safety and biocompatibility of nanozeolites to be applied to *in vivo* systems. Therefore, in order to prove their harmless nature, a lot of research still has to be performed, mainly in regards to nanozeolite accumulation and degradation within the body.

5 References

[1]   A. Corma, J. Catal. 216 (2003) 298–312.

[2]   M.W. Ackley, S.U. Rege, H. Saxena, Microporous Mesoporous Mater. 61 (2003) 25–42.

[3]   S. Wang, Y. Peng, Chem. Eng. J. 156 (2010) 11–24.

[4]   S. Mintova, J.P. Gilson, V. Valtchev, Nanoscale 5 (2013) 6693–6703.

[5]   Cent. Dis. Control Prev. Antibiot. Resist. Threat. United States, 2013 (2013) 114.

[6]   A. Monteiro, R. Hill, G. Pilkington, P. Madureira, Cells 6 (2017) 45.

[7]   R.M. Barrer, Hydrothermal Chemistry of Zeolites, Academic Press, London, 1982.

[8]   Int. Zeolite Assoc. Database Zeolite Struct. (n.d.).

[9]   K. Byrappa, M. Yashimura, Handb. Hydrothermal Technol. (2013) 315–413.

[10]   M. Dusselier, M.E. Davis, Chem. Rev. 118 (2018) 5265–5329.

[11]   J.A.Z. Pieterse, S. Veefkind-Reyes, K. Seshan, J.A. Lercher, J. Phys. Chem. B 104 (2000) 5715–5723.

[12]   A. Corma, M.J. Diaz-Cabañas, J. Martínez-Triguero, F. Rey, J. Rius, Nature 418 (2002) 514–517.

[13]   J. Jiang, J. Yu, A. Corma, Angew. Chemie - Int. Ed. 49 (2010) 3120–3145.

[14]   J. Jiang, Y. Yun, X. Zou, J.L. Jorda, A. Corma, Chem. Sci. 6 (2015) 480–485.

[15]   A. Corma, Curr. Opin. Solid State Mater. Sci. 2 (1997) 63–75.

[16]   A.G. Pelmenschikov, E.A. Paukshtis, M.O. Edisherashvili, G.M. Zhidomirov, J. Phys. Chem. 96 (1992) 7051–7055.

[17]   A. Primo, H. Garcia, Chem. Soc. Rev. 43 (2014) 7548–7561.

[18]   B. Yilmaz, U. Müller, Top. Catal. 52 (2009) 888–895.

[19]   G. Busca, Microporous Mesoporous Mater. 254 (2017) 3–16.

[20]   S. Wang, H. Li, S. Xie, S. Liu, L. Xu, Chemosphere 65 (2006) 82–87.

[21]   N. Kosinov, J. Gascon, F. Kapteijn, E.J.M. Hensen, J. Memb. Sci. 499 (2016) 65–79.

[22]   J.A. Martens, D. Verboekend, K. Thomas, G. Vanbutsele, J.P. Gilson, J. Pérez-Ramírez, ChemSusChem 6 (2013) 421–425.

[23]   V. Valtchev, G. Majano, S. Mintova, J. Pérez-Ramírez, Chem. Soc. Rev. 42 (2013) 263–290.

[24]   S. Mintova, J. Grand, V. Valtchev, Comptes Rendus Chim. 19 (2016) 183–191.

[25]   D.J. Wales, J. Grand, V.P. Ting, R.D. Burke, K.J. Edler, C.R. Bowen, S. Mintova, A.D. Burrows, Chem. Soc. Rev. 44 (2015) 4290–4321.

[26]   S. e. Gul, D. Cody, A. Kharchenko, S. Martin, S. Mintova, J. Cassidy, I. Naydenova, Microporous Mesoporous Mater. 261 (2018) 268–274.

[27]   B. Ozansoy Kasap, S. V. Marchenko, O.O. Soldatkin, S. V. Dzyadevych, B. Akata Kurc, Nanoscale Res. Lett. 12 (2017).

[28]   R. Amorim, N. Vilaça, O. Martinho, R.M. Reis, M. Sardo, J. Rocha, A.M. Fonseca, F. Baltazar, I.C. Neves, J. Phys. Chem. C 116 (2012) 25642–25650.

[29]   S. Belkhair, M. Kinninmonth, L. Fisher, B. Gasharova, C.M. Liauw, J. Verran, B. Mihailova, L. Tosheva, RSC Adv. 5 (2015) 40932–40939.

[30]   P.A. Jacobs, E.M. Flanigen, J.C. Jansen, H. van Bekkum, Introduction to Zeolite Science and Practice, Elsevier B.V., 2001.

[31]   R.M. Barrer, Zeolite Synth. 398 (1989) 11–27.

[32]   J. Grand, H. Awala, S. Mintova, CrystEngComm 18 (2016) 650–664.

[33]   B.J. Schoeman, J. Sterte, J.E. Otterstedt, J. Porous Mater. 1 (1995) 185–198.

[34]   B.J. Schoeman, J. Sterte, J.E. Otterstedt, Zeolites 14 (1994) 110–116.

[35]   A.E. Persson, B.J. Schoeman, J. Sterte, J.E. Otterstedt, Zeolites 15 (1995) 611–619.

[36]   E.P. Ng, D. Chateigner, T. Bein, V. Valtchev, S. Mintova, Science (80-.). 335 (2012) 70–73.

[37]   S. Mintova, N.H. Olson, V. Valtchev, T. Bein, Science 283 (1999) 958–960.

[38]   M. Smaihi, O. Barida, V. Valtchev, Eur. J. Inorg. Chem. (2003) 4370–4377.

[39]   C. Madsen, C. Madsen, C.J.H. Jacobsen, Chem. Commun. (1999) 673–674.

[40]   A.S. Nmr, C.J.H. Jacobsen, C. Madsen, T.V.W. Janssens, H.J. Jakobsen, 39 (2000).

[41]   M. Choi, K. Na, J. Kim, Y. Sakamoto, O. Terasaki, R. Ryoo, Nature 461 (2009) 246–249.

[42]   C. Jo, J. Jung, H.S. Shin, J. Kim, R. Ryoo, Angew. Chemie - Int. Ed. 52 (2013) 10014–10017.

[43]   D.P. Serrano, M. Escola, M. Rodrı, R. Juan, C. Uni, Chem. Mater. 18 (2006) 2462–2464.

[44]   Y. Hu, Y. Zhang, Y. Tang, Chem. Commun. 46 (2010) 3875–3877.

[45]   P. Pal, J.K. Das, N. Das, S. Bandyopadhyay, Ultrason. Sonochem. 20 (2013) 314–321.

[46]   C.S. Cundy, Collect. Czechoslov. Chem. Commun. 63 (1998) 1699–1723.

[47]   Z. Wang, Y. Yan, Zeolites in Sustainable Chemistry, 2016.

[48]   K.Y. Huang, H.Y. Chi, P.K. Kao, F.H. Huang, Q.M. Jian, I.C. Cheng, W.Y. Lee, C.C. Hsu, D.Y. Kang, ACS Appl. Mater. Interfaces 10 (2018) 900–908.

[49]   S. Huber, A.Z. Ruiz, H. Li, G. Patrinoiu, C. Botta, G. Calzaferri, Inorganica Chim. Acta 360 (2007) 869–875.

[50]   V. Vohra, A. Bolognesi, G. Calzaferri, C. Botta, Langmuir 25 (2009) 12019–12023.

[51]   G. Calzaferri, S. Huber, H. Maas, C. Minkowski, Angew. Chemie - Int. Ed. 42 (2003) 3732–3758.

[52]   D.-K. Ko, A. Maurano, S.K. Suh, D. Kim, G.W. Hwang, J.C. Grossman, V. Bulović, M.G. Bawendi, ACS Nano 10 (2016) 3382–3388.

[53]   H.S. Kim, N.C. Jeong, K.B. Yoon, Langmuir 27 (2011) 14678–14688.

[54]   X. Xu, J. Wang, Y. Long, Sensors 6 (2006) 1751–1764.

[55] K. Kaneyasu, K. Otsuka, Y. Setoguchi, S. Sonoda, T. Nakahara, I. Aso, N. Nakagaichi, Sensors Actuators B Chem. 66 (2000) 56–58.

[56] G.A. Urban, Anal. Bioanal. Chem. 405 (2013) 5365–5366.

[57] A. Petushkov, J. Intra, J.B. Graham, S.C. Larsen, A.K. Salem, Chem. Res. Toxicol. 22 (2009) 1359–1368.

[58] L.C.J. Thomassen, D. Napierska, D. Dinsdale, N. Lievens, J. Jammaer, D. Lison, C.E.A. Kirschhock, P.H. Hoet, J.A. Martens, Nanotoxicology 6 (2012) 472–485.

[59] S. Męczyńska-Wielgosz, A. Piotrowska, A. Majkowska-Pilip, A. Bilewicz, M. Kruszewski, Nanoscale Res. Lett. 11 (2016) 1–14.

[60] R.S. Bedi, D.E. Beving, L.P. Zanello, Y. Yan, Acta Biomater. 5 (2009) 3265–3271.

[61] S.E. Lehman, S.C. Larsen, Environ. Sci. Nano 1 (2014) 200–213.

[62] V. Georgieva, C. Anfray, R. Retoux, V. Valtchev, S. Valable, S. Mintova, Microporous Mesoporous Mater. 232 (2016) 256–263.

[63] P.S. Wheatley, A.R. Butler, M.S. Crane, S. Fox, B. Xiao, A.G. Rossi, I.L. Megson, R.E. Morris, J. Am. Chem. Soc. 128 (2006) 502–509.

[64] C. Pal, P.S. Wheatley, H. El Mkami, D.J. Keeble, R.E. Morris, O. Schiemann, Appl. Magn. Reson. 37 (2010) 619–627.

[65] N. Vilaça, A.F. Machado, F. Morais-Santos, R. Amorim, A. Patrícia Neto, E. Logodin, M.F.R. Pereira, M. Sardo, J. Rocha, P. Parpot, A.M. Fonseca, F. Baltazar, I.C. Neves, RSC Adv. 7 (2017) 13104–13111.

[66] B. Dong, S. Belkhair, M. Zaarour, L. Fisher, J. Verran, L. Tosheva, R. Retoux, J.-P. Gilson, S. Mintova, Nanoscale 6 (2014).

[67] G. Bergerhoff, W.H. Baur, W. Nowacki, Neues Jahrb, Miner. Monatsh 193–200 (1958).

[68] G. Bargerhoff, H. Koyama, W. Nowacki, Experimenta 12 (1956) 418–419.

[69] R.M. Milton, N.Y. Buffalo, U.S. Patent, 2882243, 1959.

[70] W.J. Mortier, Compilation of Extra Framework Sites in Zeolites, Butterworth Scientific Ltd., Guildford, 1982.

[71] C. Beauvais, X. Guerrault, F.-X. Coudert, A. Boutin, A.H. Fuchs, J. Phys. Chem. B 108 (2004) 399–404.

[72] Y. Yang, N. Burke, J. Zhang, S. Huang, S. Lim, Y. Zhu, RSC Adv. 4 (2014) 7279–7287.

[73] C. Beauvais, A. Boutin, A.H. Fuchs, Comptes Rendus Chim. 8 (2005) 485–490.

[74] T. Frising, P. Leflaive, Microporous Mesoporous Mater. 114 (2008) 27–63.

[75] R.T. Yang, Y.D. Chen, J.D. Peck, N. Chen, Ind. Eng. Chem. Res. 35 (1996) 3093–3099.

[76] O. Kikhtyanin, Y. Ganjkhanlou, D. Kubička, R. Bulánek, J. Čejka, Appl. Catal. A Gen. 549 (2018) 8–18.

[77] N. Jiang, R. Shang, S.G.J. Heijman, L.C. Rietveld, Water Res. 144 (2018) 145–161.

[78] R.J.L. Willems, W.P. Hanage, D.E. Bessen, E.J. Feil, FEMS Microbiol. Rev. 35 (2011)

872–900.

[79] G.M. Rossolini, F. Arena, P. Pecile, S. Pollini, Curr. Opin. Pharmacol. 18 (2014) 56–60.

[80] J. O'Neill, Review on Antimicrobial Resistance, Wellcome Trust, London, 2014.

[81] K.A. Rieger, H.J. Cho, H.F. Yeung, W. Fan, J.D. Schiffman, ACS Appl. Mater. Interfaces 8 (2016) 3032–3040.

[82] S. Demirci, Z. Ustaoğlu, G.A. Yilmazer, F. Sahin, N. Baç, Appl. Biochem. Biotechnol. 172 (2014) 1652–1662.

[83] S. Chen, J. Popovich, N. Iannuzo, S.E. Haydel, D.K. Seo, ACS Appl. Mater. Interfaces 9 (2017) 39271–39282.

[84] B. Kwakye-Awuah, C. Williams, M.A. Kenward, I. Radecka, J. Appl. Microbiol. 104 (2008) 1516–1524.

[85] A. Muñoz-Bonilla, M. Fernández-García, Prog. Polym. Sci. 37 (2012) 281–339.

[86] Y. Matsumura, K. Yoshikata, S. Kunisaki, T. Tsuchido, Appl. Environ. Microbiol. 69 (2003) 4278–4281.

[87] B. Dong, S. Belkhair, M. Zaarour, L. Fisher, J. Verran, L. Tosheva, R. Retoux, J.P. Gilson, S. Mintova, Nanoscale 6 (2014) 10859–10864.

[88] S. Sabbani, D. Gallego-Perez, A. Nagy, W. James Waldman, D. Hansford, P.K. Dutta, Microporous Mesoporous Mater. 135 (2010) 131–136.

[89] D.K. Tripathi, A. Tripathi, Shweta, S. Singh, Y. Singh, K. Vishwakarma, G. Yadav, S. Sharma, V.K. Singh, R.K. Mishra, R.G. Upadhyay, N.K. Dubey, Y. Lee, D.K. Chauhan, Front. Microbiol. 8 (2017) 1–16.

[90] S. Fox, T.S. Wilkinson, P.S. Wheatley, B. Xiao, R.E. Morris, A. Sutherland, A.J. Simpson, P.G. Barlow, A.R. Butler, I.L. Megson, A.G. Rossi, Acta Biomater. 6 (2010) 1515–1521.

[91] P. Horcajada, C. Márquez-Alvarez, A. Rámila, J. Pérez-Pariente, M. Vallet-Regí, Solid State Sci. 8 (2006) 1459–1465.

[92] M.G. Rimoli, M.R. Rabaioli, D. Melisi, A. Curcio, S. Mondello, R. Mirabelli, E. Abignente, J. Biomed. Mater. Res. - Part A 87 (2008) 156–164.

[93] A. Dyer, S. Morgan, P. Wells, C. Williams, J. Helminthol. 74 (2000) 137–141.

[94] R.E. Morris, P.S. Wheatley, Angew. Chemie - Int. Ed. 47 (2008) 4966–4981.

[95] V. Rama Rao, S. Farooq, and W.B. Krantz, AIChE J. 56 (2010) 354–370.

[96] S. Komaty, C. Anfray, M. Zaarour, H. Awala, V. Ruaux, S. Valable, S. Mintova, Molecules 23 (2018) 37.

[97] J. Bachmann, Pascale A., Luisi, Pier L., Lang, Nature 357 (1992) 57–59.

[98] V. Calabrese, C. Mancuso, M. Calvani, E. Rizzarelli, D.A. Butterfield, A.M. Giuffrida Stella, Nat. Rev. Neurosci. 8 (2007) 766–775.

[99] P.S. Wheatley, A.R. Butler, M.S. Crane, A.G. Rossi, I.L. Megson, R.E. Morris, Stud. Surf. Sci. Catal. 158 B (2005) 2033–2040.

[100] M. Rogosnitzky, S. Branch, BioMetals 29 (2016) 365–376.

[101] I. Bresinska, K.J. Balkus, J. Phys. Chem. 98 (1994) 12989–12994.

[102] C.H. Reynolds, N. Annan, K. Beshah, J.H. Huber, S.H. Shaber, R.E. Lenkinski, J.A. Wortman, J. Am. Chem. Soc. 122 (2000) 8940–8945.

[103] C. Platas-Iglesias, L. Vander Elst, W. Zhou, R.N. Muller, C.F.G.C. Geraldes, T. Maschmeyer, J.A. Peters, Chem. - A Eur. J. 8 (2002) 5121–5131.

Chapter 2- Experimental

1 FAU-X zeolite

1.1 Synthesis

The template-free, nanosized FAU zeolite was prepared from a precursor mixture with the molar composition: 9 Na2O: 1.1 Al2O3: 10 SiO2: 77 H2O.[1] Solution A was made by dissolving 2.5 g of sodium hydroxide (NaOH, 97%, Sigma-Aldrich) in 3.0 g of double distilled water (ddH$_2$O), followed by gradual addition of 0.297 g aluminum powder (325 mesh, 99.5%, Alfa Aesar). The mixture was stirred until a clear solution was obtained. Solution B was prepared by dissolving 1.1 g of NaOH in 1.0 g of ddH$_2$O, followed by the addition of 10 g colloidal silica (Ludox-HS 30, 30 wt % SiO2, Aldrich). The resultant turbid suspension was placed in an oven at 100 °C for 5 min in order to obtain a clear suspension. After, Solution A was added dropwise to solution Bin an ice-bath, under vigorous stirring. The resulting clear suspension was aged at room temperature for 24 h under stirring followed by dehydration using freeze-drying in order to adjust the desired water content. The hydrothermal treatment was performed at 50 °C for 26 h. The crystalline product was diluted with 80 °C double distilled water ddH$_2$O, purified by centrifugation (20,000 rpm, 25 min) and finally redispersed in ddH$_2$O. Part of this nanosized Na-FAU suspension was freeze-dried for further characterization and the rest was kept as suspension for post-synthetic modifications.

1.2 Post-synthetic modifications

1.2.1 Ion-exchange

The as synthesised, Na-X zeolite suspension was ion-exchanged with copper (II) nitrate trihydrate Cu(NO$_3$)$_2$.3H$_2$O, iron nitrate nonahydrate Fe(NO$_3$)$_3$.9H$_2$O and gadolinium (III) nitrate hexahydrate (Gd(NO$_3$)$_3$.6H$_2$O. The ion-exchange procedure involved vigorous mixing of metal ion solution with zeolite suspension at room temperature for 1 h, with the ratio of 5:1. This was followed by purification via centrifugation (at 20,000 rpm for 25 min) and redispersion in ddH$_2$O. The final pH of all prepared suspension was equal to 7.0. The detailed information concerning ion-exchange processes with different metal solutions is described within each chapter under experimental methods.

2   Characterisation

It is crucial to understand the physical and chemical properties of synthesized zeolite material in order to properly functionalise them for certain application. Therefore, the importance of selecting appropriate, highly sensitive and accurate characterisation techniques is highly recognized as they provide fundamental information about the prepared nanozeolite systems. The toolbox of different characterisation methods was used since a solitary technique is not fully representative for zeolites. The detailed information about employed characterization techniques are provided in this chapter.

2.1 X-ray diffraction

Principle

This characterisation method employs X-rays, which are classified as electromagnetic waves with energies varying from 100 eV- 10MeV to determine the crystal structure and phase purity of crystalline materials.[2–4] A monochromatic, X-ray beam is pointed on the crystalline sample at an angle (θ) and interacts with the zeolite planes of atoms. Consequently, following this beam-sample contact, the beam is being partly transmitted, absorbed, refracted, scattered and diffracted. Bragg's law is applied to determine the distance between the planes (d_{hkl}) of different atoms in the crystalline structure, basing on the relationships between the angle (θ) and the wavelength (λ) of X-rays (Figure). Depending on the type of atomic species and their arrangement the X-rays are diffracted in a diverse manner, providing a specific diffraction patterns for a particular crystalline material.

$$n\lambda = 2d \sin \theta$$
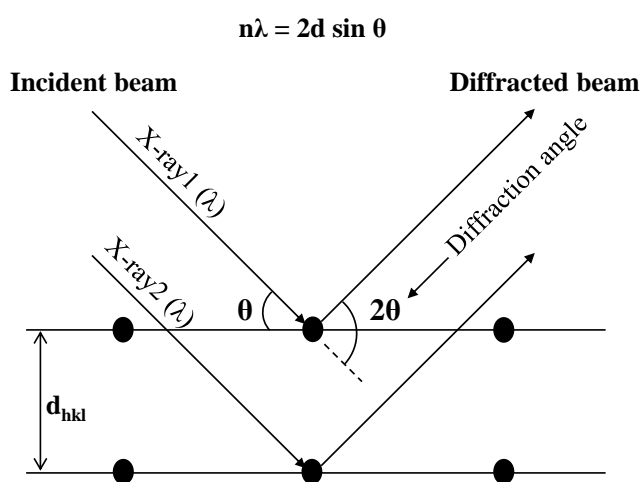
Figure 9. Bragg's Law, representation of a 2-dimensional crystal lattice.

Zeolites are crystalline aluminosilicates which structure is formed by a network of three-dimensional building blocks. Different kinds of zeolite have their own unique XRD pattern, so-called "fingerprint", used for phase and purity recognition. Attentive pattern interpretation is required in order to obtain detailed information about the zeolite structure, namely, peak position, intensity and width, which depend on the specific unit cell parameters, type of atoms present and crystallinity/size respectively. The peak broadening is usually associated with the presence of small nanocrystals, whereas very sharp peaks indicate high material crystallinity, representative for micron sized crystals.

Experimental approach

In the present study, powder X-ray diffraction (XRD) experiments are carried on polycrystalline materials in Debye-Scherrer geometry using a PANalytical X'Pert Pro diffractometer with CuKα radiation (λ = 1.5418 Å). The powder samples were homogenized finely and loaded in sample holders. The samples were scanned in 2θ range of 4-50º with a step size of 0.02º. Before analysis, the powders (ca. 20 mg) of the as-synthesized samples were loaded on a silicon wafer.

2.2 Dynamic light scattering and zeta potential

Principle

Dynamic light scattering (DLS) is well-established technique to determine the size and size distribution of particles in suspensions.[5,6] This method uses a monochromatic light beam, (laser), that penetrates the solution containing spherical particles and measures the Brownian motion. The latter is not only determined by the particle size, as larger particles scatter slower than the smaller ones, but also by temperature and solvent viscosity. Doppler Shift occurs when the light hits the moving particle changing the wavelength of the incoming light. This change is related to the size of the particle. The DLS measurement provides the information about the average hydrodynamic diameter of particles in a suspension using the Stokes-Einstein equation:

$$d_H = \frac{kT}{3\pi\eta D}$$

where d_H is hydrodynamic diameter, k is Boltzmann's constant, T is absolute temperature, η is viscosity and D is translational diffusion coefficient.

Additionally, using the same instrument the zeta potential of nanoparticles can be determined. This technique measures the electrostatic repulsion/attraction among particles and evaluates the stability of colloidal suspensions.[7,8] The stability depends on the size of colloidal particles, for instance small particles will have a high zeta potential and thus high stability as they are less likely to aggregate. In case of low zeta potential, the repulsion is surpassed by the attractive forces and particles tend to coagulate. The zeta potential value depends on the concentration, pH and conductivity of colloidal solution. Generally speaking, the good stability of particles is declared when the zeta potential value is greater than +30 mV and less than -30 mV.

Experimental approach

In all experiments presented in the thesis, the hydrodynamic diameters and stability of the nanoparticles in the suspensions were determined with a Malvern Zetasizer Nano. The analyses were performed on samples with original concentrations without any pre-treatments of the colloidal suspensions. The back scattering geometry (scattering angle 173°, HeNe laser with 3 mV output power at 632.8 nm wavelength) allows measurements at high sample concentration, since a complete penetration of the incident light through the sample was not required.

2.3 Gas physisorption

Principle

The gas adsorption is one of the most powerful and widely applied methods to study physical adsorption and textural characterisation of porous materials. This technique deliver information about surface area and pore volumes and sizes.[9] The fundamentals of this method are based on the adsorption of inert gases in most cases N_2, Ar and CO_2 at constant cryogenic temperatures over a range of pressures. Physisorption occurs when the adsorbate gas (adsorptive) interact with the surface of a solid (adsorbent). During such process chemical bonds are not being broken or formed as only van der Waals forces are involved.

An appropriate choice of adsorptive is very important for the purpose of obtaining reliable structural analysis. Commonly, nitrogen adsorption at 77K has been employed for the micropore size analysis of zeolites. However, it is becoming clear that nitrogen is not an ideal adsorptive for microporosity evaluation, due to the presence of quadruple moment, which influences the micropore filling. Therefore, argon at 87K should be used as a preferred gas for

micropore characterisation of zeolites, but argon's extremely high price suppress its utilisation and for that reason nitrogen is still largely employed. The physisorption begins with sample outgassing to remove physically adsorbed molecules from the material surface (mostly water) without its modification, followed by gradual increase of adsorptive pressure and finishing with pressure decrease. The information acquired is expressed in the form of adsorption/desorption isotherms, where the quantity of adsorbed gas is presented as a function of the relative pressure. The isotherms of a different shape are used to determine valuable parameters, namely, surface area and pore structure. According to updated IUPAC recommendations, the isotherms are classified into six types as presented in Figure 10.[10]
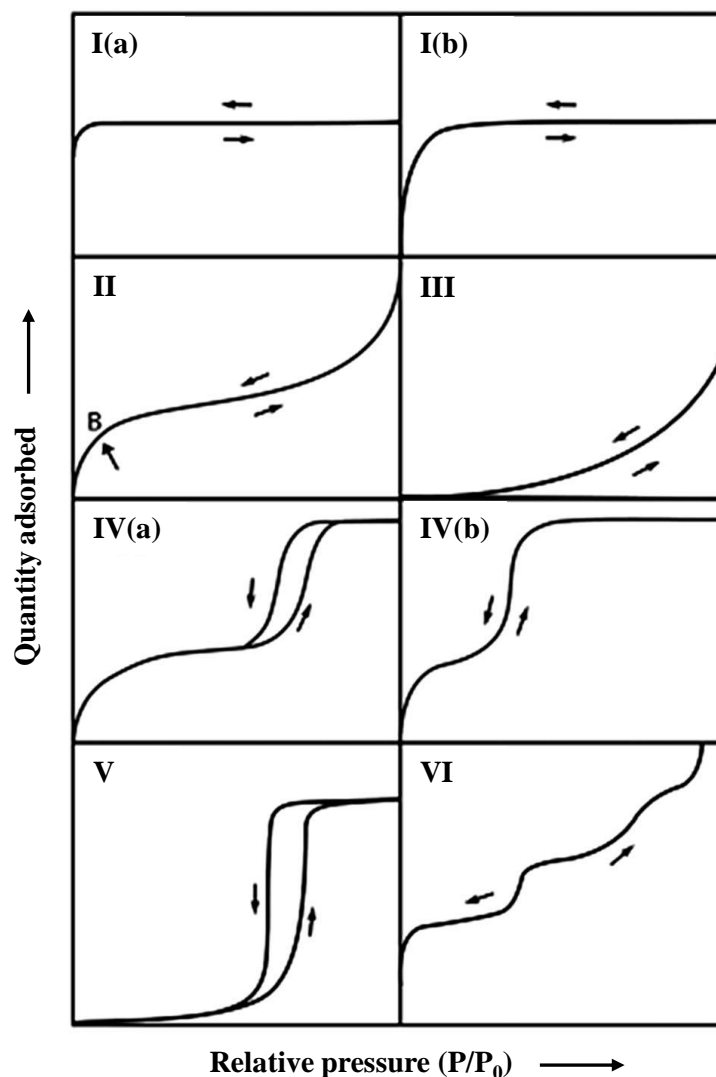

Figure 10. IUPAC classification of physisorption isotherms.[10]

The type I(a) and I(b) isotherms are characteristic for microporous materials with pore width < 0.7 nm and 0.7 − 2 nm, respectively. Type II isotherms are found in non-porous or

macroporous materials, govern by mono- and then multi-layer surface adsorption. Point B usually indicates the completion of the monolayer coverage. Type III isotherm is also typical for nonporous or macroporous solids, but in this case the lack of Point B indicates very weak adsorbent adsorbate interactions. The adsorbed species are gathered around the most favourable site on the adsorbent surface. Unlike to Type II isotherm, the amount adsorbed is restricted at p/p^0. Type IV(a) and IV(b) isotherms are representative for mesoporous materials, where as in the previous case the difference between them is associated with the size of mesopores. Regarding type IV(a) isotherm the hysteresis begins to appear for pores wider than ~4 nm, whereas in case of type IV(b) isotherm the absence of hysteresis loop indicates completely reversible process characteristic for mesopores of smaller width. Additionally, type IV(b) isotherms appear when the analysis is performed on conical and cylindrical mesopores that are closed at the tapered end. The shape of type V isotherm is comparable to type III at low P/P_0, indicating weak adsorbent-adsorbate interactions. However, with increasing relative pressure the pore filling process begins, which is usually seen in case of water adsorption on hydrophobic microporous and mesoporous solids. Type VI isotherm represents typical layer-by–layer adsorption on nonporous surface.

In order to calculate the specific surface area of zeolite, the Brunauer-Emmett-Teller (BET) method is applied.[11,12] Despite its imperfection of theoretical assumptions, this technique continues to be widely used.

Experimental approach

Nitrogen adsorption/desorption isotherms in this thesis were measured using Micrometrics ASAP 2020 volumetric adsorption analyser. About 0.1 g of sample was degassed at 300°C under vacuum overnight prior to the measurement. The external surface area (S_{ext} / m^2g^{-1}) and micropore volume (V_{mic} / cm^3g^{-1}) were estimated by t-plot method based on the Harkins-Jura equation[13] using Silica-1000 (22.1 m^2g^{-1} assumed) as a reference. The micropore and mesopore size distributions of solids were estimated by Nonlocal Density Functional Theory (NLDFT)[14] and Barret-Joyner-Halenda (BJH)[15] methods, respectively.

2.4 Thermal analysis

Principle

Thermal analysis method is employed to determine the physio-chemical changes of zeolites at elevated temperatures. The main properties of a catalyst that could be analysed by

this technique are stability, decomposition of organic molecules, dehydration, adsorption, desorption etc.[16–18] There are two different types of thermal analysis; (i) thermogravimetric analysis (TGA), which evaluates the change of sample weight as a function of temperature/time, and (ii) differential thermal analysis (DTA) that correlates the difference in temperature between the sample and inert reference material. Hence, the physio-chemical transformations of the sample are temperature dependent they are usually supplemented with the liberation or absorption of heat, which corresponds to exo- and endothermic reactions respectively. Therefore, if the difference in temperatures (sample from the reference) is plotted against time, exo- and endothermic curves appear which can be linked to particular reactions occurring at specific time and temperature.

Experimental approach

TGA/DTA measurements of different samples were carried out on a SETSYS 1750 CS evolution instrument (SETARAM). Prior measurement, the samples were placed in a desiccator at around 70% humidity and stored overnight. About 15-20 mg of each sample was introduced in an alumina crucible that was loaded in the analyser chamber. The sample was heated from 30°C to 800°C with a heating ramp of 5°C/min under air (flow rate: 40 mL/min).

2.5 Scanning electron microscopy

Principle

Scanning electron microscopy (SEM) is a very common and practical approach when examining the morphology, particle size and homogeneity of zeolite crystals.[19] The scanning electron microscope is using a high-energy beam of electrons ejected from filament and focused into a small probe that is scanning over the surface of the sample. SEM micrographs are generated as a result of transformed signal of low energy secondary electron ejection from the sample surface. Further, the interaction of the electron beam with the atoms in the sample induces atoms excitation, which results in the X-ray emission characteristic for different specimen. This method, called energy-dispersive X-ray spectroscopy (EDS) can be used to determine the general chemical composition of sample within specific area.

Experimental approach

The SEM characterization in this study was performed on small amounts of dried sample in powder form. They were mounted on a specimen holder using double stick carbon tapes.

To improve the electrical conductivity of the sample, they were coated with platinum using CRESSINGTON 108 auto evaporative coating machine. SEM micrographs were recorded with TESCAN Mira field-emission scanning electron microscope operating at 30 kV.

2.6 Transmission electron microscopy

Principle

The transmission electron microscopy (TEM) provides more detailed information about crystal morphology thanks to the employment of high energy beam. This method allows acquisition of sample monographs at very high magnification with high resolution, resulting in in-depth textural analysis. Hence, TEM gives very comprehensive information about material porosity and atoms arrangement, it can also be used to identify structural defects, such as dislocations and stacking. In TEM, the high energy beam passes through a condenser before hitting the thin layer of sample. After, the electrons penetrate the specimen giving rise to a projection of a sample mass which is magnified by projector lens to obtain bright field image. TEM instrument is usually equipped with an EDS device for determination of sample composition.

Experimental approach

The TEM imaging and electron tomography were performed using a JEOL 2100F microscope operating at 200 kV, equipped with a Cs probe corrector and a GATAN Tridiem imaging filter. The zeolite samples were dispersed in ethanol (99.9%) and then a drop of solution was deposited on a TEM nickel grid covered by a holey carbon membrane. The emission current was kept constant at ~160 μA. The chemical composition of the observed samples was determined by EDS analysis.

2.7 Inductively coupled plasma-atomic emission spectroscopy

Principle

Inductively coupled plasma atomic emission spectroscopy (ICP-AES) is considered as the most precise method for quantitative chemical analysis.[19] This technique can inspect up to 50 elements simultaneously and thanks to its sensitivity it can detect trace levels of components. The sample introduced into spectrometer is atomised with argon into hot plasma, which ensures electron excitation of elements. The excited sample emits light wavelengths

characteristic for each element in the ultraviolet or visible region. Further, spectrometer disperses the emitted light and separates the particular element emissions. The intensity of emitted light is directly proportional to the concentration of each element in the analysed sample. Special software is used in order to transform the electronic signal into concentrations.

Experimental approach

The elemental analysis of all samples was performed by inductively coupled plasma–atomic emission spectroscopy using an OPTIMA 4300 DV (Perkin–Elmer) instrument. The standard sample preparation process is illustrated in Figure 11. The procedure involved the following: (i) 50 mg of sample was dissolved in 3 ml of hydrofluoric acid (HF) (Sigma Aldrich 40-45 %), (ii) 0.5 ml of mixture (HNO_3 : HCl $\equiv$ 1:3 v/v) was added and heated at 100°C for 1 h in polytetrafluoroethylene (PTFE) bottle, and finally (iii) 10 ml of double deionized water (ddH_2O) and 1.4 g of boric acid (H_3BO_3) were added. The resulted solution was transferred to PTFE volumetric flask (100 mL), diluted with ddH_2O up to 100 ml mark and homogenised by shaking.

50 mg of solid sample + 0.5 ml aqua regia (HNO_3 : HCl = 1:3 v/v) + 3 ml HF

10 ml of ddH_2O + 1.4 g H_3BO_3

Heated at 110 °C for 1 hrs, cooled down to RT

Polytetrafluoroethylene (PTFE) bottle

Sample solution transferred to 100 ml volumetric flask

Dilution with ddH_2O up to the mark, homogenisation by shaking for 3 hrs
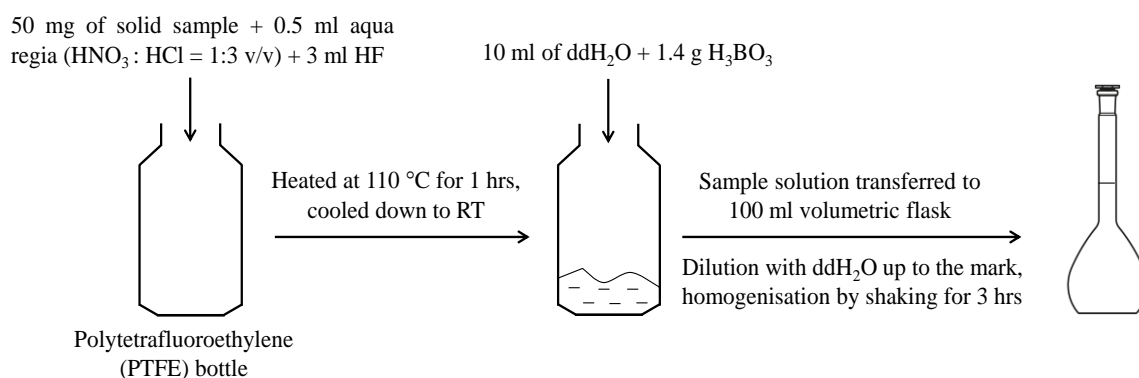
Figure 11. Sample preparation procedure for ICP-AE analysis.

2.8 Fourier transformed infrared spectroscopy

Principle

Fourier transformed infrared spectroscopy (FTIR) is a well-known characterisation tool for zeolite structure investigation as well as identification of adsorbed species. This method studies the transitions between vibrational levels due to absorption of molecules at specific frequencies (v).[20] The distinct absorption frequency is influenced by the mass of atoms in the molecule and the bond strength. The vibrational frequencies increase with increasing bong

strength and with decreasing mass of the vibrating atoms. In fact, not all the vibrations are infrared active due to the lack of change in the dipole moment. The dipole moment is generated as the result of vibrations that are produced when infrared radiation is absorbed. There are different types of infrared spectroscopy, such as diffuse reflectance (DRIFT), transmission and attenuated total reflectance (ATR). The choice of appropriate method relays on the type of material analysed and wanted structural information. In case of zeolites, the transmission infrared spectroscopy mode is usually applied. For the purpose of measurement, the sample has to be pressed into self–supporting homogeneous wafers of about 20 mg. IR enables to obtain quantitative information about the sample when the Lambert-Beer law is applied, however for zeolites the determination of molar extinction coefficient can be very problematic.

This technique also permits to acquire information about zeolite acidity and adsorption capacity. The choice of probe molecule is of great importance, since depending on the properties of the probe, diverse particularities about zeolite structure can be obtained. For the purpose of this study different, biologically important gases (CO_2, O_2, and NO) were selected as probe molecules, to assess the adsorption capacity of modified zeolites.

Experimental approach

The IR spectra of prepared porous materials were recorded on a Nicolet Impact 410 FTIR spectrometer equipped with a MCT detector in the range 400-5500 cm^{-1}. Prior to the measurement, the solid materials were grinded and pressed into self-supported, thin pellets (ca. 20 mg cm^{-2}). They were placed in a standard LCS *in-situ* FTIR set-up and activated under vacuum (approx. 10^{-6} hPa) using activation procedure presented in Figure 12 . After cooling to room temperature, a spectrum of the samples before adsorption was recorded for further use as a reference. The CO_2 and NO adsorption was performed at room temperature, whereas the analysis for O_2 at -196 °C. The probe molecules were introduced in small doses or equilibrium (depending on the experiment) and the spectra were recorded. The OMNIC version 7.3 SP1 program was used for data processing. The IR adoption details are written under experimental session in each chapter.
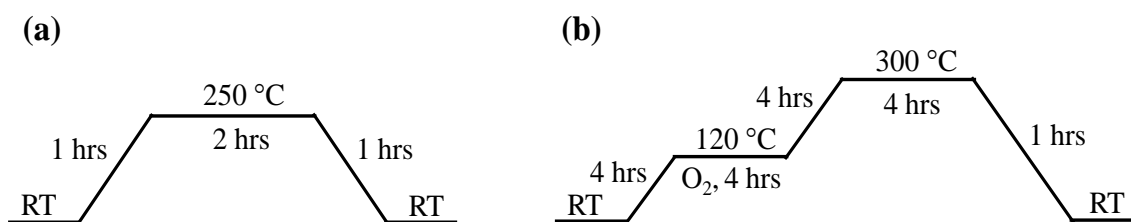
Figure 12. Activation procedure for (a) O_2 and CO_2 adsorption (Chapter 4) and (b) for NO and CO_2 adsorption (Chapter 5).

2.9 Ultraviolet-Visible Spectroscopy

Principle

Ultraviolet-Visible spectroscopy (UV-Vis) is used to measure electronic transitions between molecular orbital in the UV-Vis spectral region. During the measurement, sample is subjected to high-energy electromagnetic radiation which produces different types of electronic transitions, those are passed to the detector which measures the absorbance or reflection of light (photons) at different wavelengths.[21] UV-Vis spectroscopy is widely employed method for the qualitative or quantitative determination the optical properties of different analytes. A quantitative way to determine the optical densities of an absorbing species in solution is possible by using the Beer-Lambert law, where the amount of light absorbed is proportional to the number of absorbing species.

Experimental approach

In this study the UV-Vis was applied for cells optical density measurements of various microorganisms at 540 nm, using Jenway 6305 Spectrophotometer, UK.

2.10 Magnetic Resonance Imaging

Principle

The Magnetic Resonance Imaging (MRI) is a non-invasive diagnostic technique used for medical investigation purposes. This method is based on the use of strong magnets and low-energy radiofrequency signals that are able to provide information from certain atomic nuclei within the body.[22] The atomic nuclei often used for imagining are hydrogen, sodium, phosphorus and carbon-13. MRI is a very useful technique to examine internal body structures and it is extensively applied for detection of abnormalities in the brain.

Experimental approach

MRI studies were performed on a 7T Pharmascan® (Bruker) device available on the Cyceron biomedical imaging platform. This device dedicated to the small animal is equipped with a horizontal magnet, a cradle and two transmitting / receiving antennas adapted to the heads of rats and mice. The data was acquired with Paravision 6.0.1 software (Bruker). This method was used for glioblastoma, brain tumour detection as well as for blood volume and O_2 concentration measurements after zeolite injection. More details about MRI are included in the experimental part of chapter 5.

3 References

[1]   H. Awala, J.P. Gilson, R. Retoux, P. Boullay, J.M. Goupil, V. Valtchev, S. Mintova, Nat. Mater. 14 (2015) 447–451.

[2]   H.G. Karge, M. Hunger, H.K. Beyer, in:, J. Weitkamp, L. Puppe (Eds.), Catal. Zeolites, Springer-Verlag, Berlin, (1999) 295–326.

[3]   H. Van Koningsveld, J.M. Bennett, Mol. Sieves 2 (1999) 1–29.

[4]   Y. Waseda, E. Matsubara, K. Shinoda, in:, X-Ray Diffr. Crystallogr., Springer, New York, (2011), 1–310.

[5]   B.J. Schoeman, J. Sterte, J.E. Otterstedt, J. Porous Mater. 1 (1995) 185–198.

[6]   J. Stetefeld, S.A. McKenna, T.R. Patel, Biophys. Rev. 8 (2016) 409–427.

[7]   S. Bhattacharjee, J. Control. Release 235 (2016) 337–351.

[8]   R.J. Hunter, Zeta Potential in Colloid Science, Principles and Applications, Academic Press Limited, London, 1981.

[9]   M. Thommes, K.A. Cychosz, Adsorption 20 (2014) 233–250.

[10]   K.A. Cychosz, R. Guillet-Nicolas, J. García-Martínez, M. Thommes, Chem. Soc. Rev. 46 (2017) 389–414.

[11]   K. Sing, Colloids Surfaces A Physicochem. Eng. Asp. 187–188 (2001) 3–9.

[12]   S. Brunauer, P.H. Emmett, E. Teller, J. Am. Chem. Soc. 60 (1938) 309–319.

[13]   W.D. Harkins, G. Jura, J. Chem. Phys. 11 (1943) 431–432.

[14]   W. Kohn, L.J. Sham, Phys. Rev. 140 (1965) A1133–A1138.

[15]   E.P. Barrett, L.G. Joyner, P.P. Halenda, J. Am. Chem. Soc. 73 (1951) 373–380.

[16]   L.P. Van Reeuwijk, Meded. Landbouwhogesch. Wageningen 74 (1974) 1–88.

[17]   Z. Gabelica, J.B. Nagy, E.G. Derouane, J.-P. Gilson, Clay Miner. 19 (1984) 803–824.

[18]   A.W. Coats, J.P. Redfern, Analyst 88 (1963) 906–924.

[19]   J.I. Goldstein, D.E. Newbury, J.R. Michael, N.W.M. Ritchie, J.H.J. Scott, D.C. Joy, Scanning Electron Microscopy and X-Ray Microanalysis, 4th ed., Springer, New York, (2017).

[20]   C. Li, Z. Wu, in:, S.M. Auerbach, K.A. Carrado, P.K. Dutta (Eds.), Handb. Zeolite Sci. Technol., Marcel Dekker Inc, New York, (2003) 549–660.

[21]   H.H. Perkampus, UV-VIS Spectroscopy and Its Applications, Spinger-Verlag, Berlin, (1992).

[22]   T. Owen, Fundamentals of Modern UV-Visible Spectroscopy: Primer, Agilent Technologies, (2000).

Chapter 3- Application of Cu-FAU nanozeolites for decontamination of surfaces soiled with the ESKAPE pathogens

Abstract

Antimicrobial resistance is a global threat with catastrophic forecasts in terms of human and economic losses. The so-called ESKAPE pathogens (*Enterococcus* species, *Staphylococcus aureus*, *Klebsiella pneumoniae*, *Acinetobacter baumanii*, *Pseudomonas aeruginosa* and *Enterobacter* species) represent a range of species of particular concern because they cause many serious hospital infections, and can show resistance toward available commercial antibiotics. Copper-containing zeolite nanocrystals (10-30 nm) with FAU-type structure (Cu-FAU), in the form of stable colloidal suspensions, were prepared at high yield in the absence of organic templates and studied for their activity against ESKAPE microorganisms. The materials were active against all six ESKAPE species. The survival of *Staphylococcus aureus, Klebsiella pneumoniae* and *Pseudomonas aeruginosa* on stainless-steel coupons after direct treatment with the Cu-FAU zeolite suspensions was determined quantitatively. Complete decontamination (5-log reduction in bacterial counts) was achieved within 20 minutes for *P. aeruginosa*, and within 10 minutes for the *K. pneumoniae* and *S. aureus*. This result is significant, particularly for sanitization of surfaces in healthcare settings, with the potential to initiate a new direction of research to help address the global antimicrobial resistance threat.

1   Introduction

Colloquially known as the ESKAPE pathogens, *Enterococcus* species, *Staphylococcus aureus*, *Klebsiella pneumoniae*, *Acinetobacter baumanii*, *Pseudomonas aeruginosa* and *Enterobacter* species have been identified by the Infectious Disease Society of America as the microorganisms most commonly causing infections that can be resistant to antimicrobial agents.[1,2] Antimicrobial resistance (AMR) is a naturally occurring evolution whereby microorganisms are capable of withstanding treatment by antimicrobial agents. It is estimated that about 700,000 people die each year due to drug resistant infections, with the potential for this number to rise to 10 million deaths a year by 2050, succeeding the number of deaths by cancer, causing economic losses of 100 trillion USD.[3] In light of this global crisis, research into antimicrobial agents has begun to focus on ESKAPE pathogens as model targets. In this

work, we use copper-containing zeolite nanocrystals for the first time as antimicrobial carriers against ESKAPE pathogens. Moreover, we employ zeolites in the form of stable colloidal suspensions for direct sanitization of surfaces.

Zeolites in the form of stable colloidal suspensions with a size of 100 nm or less were developed in the early 1990s.[4] The next 10-15 years saw a tremendous academic interest in nanozeolites sparked by the opportunities to gain insights into zeolite crystallization mechanisms and to prepare novel zeolite materials such as films and membranes.[5] However, the unsustainable synthesis of nanozeolites, characterized by very low yields and abundant use of structure-directing templates, gradually shifted research efforts towards developments of other materials, for instance hierarchical zeolites.[6] A breakthrough in nanozeolite research was reported in 2012 with the synthesis of ultrasmall EMT-type zeolite from a template-free system under mild conditions at a very high yield.[7] The approach used was recently applied to prepare nanosized FAU-type zeolites, and the advantages of using these nanosized zeolites in catalysis compared to a high quality commercial micron-sized zeolite were clearly demonstrated.[8] The development of green and industrially-friendly methods for synthesis of nanosized zeolites in the form of stable colloidal suspensions is now enabling their exploration in more conventional application areas such as microbiology.

Zeolites have been used in antimicrobial applications after ion-exchange of an antimicrobial metal, most often silver.[9-16] Owing to their microporosity and high surface areas, silver-exchanged zeolites slowly release silver ions in solution, creating a material with long-term antimicrobial activity.[17] Silver-exchanged zeolites in the form of zeolite supported films or additives to polymers and polymer coatings have also shown potential for different antimicrobial applications.[18-20] Although silver has demonstrated antimicrobial activity against a broad spectrum of microorganisms, concerns exist about the widespread use of silver nanoparticles in household products, cosmetics and textiles, leading to an observed accumulation of silver in the environment.[21] In addition, silver can easily be reduced to metallic silver, which requires special treatment for use and could affect the activity of materials. Copper is a cheaper and more stable metal than silver. It has attracted considerable research interest in recent years, particularly in hospital settings.[22,23] Copper has also been hosted within zeolites for potential environmental applications.[24-26] Although the mechanism of the antibacterial effect of copper cations is still not well understood, it has been suggested that the metal cations enter the cells and damage the bacterial cell membranes through the formation of reactive oxygen species.[27]

The aims of the present study were to evaluate the potential of using Cu-nanozeolite suspensions against ESKAPE pathogens and to develop relevant microbiology methods to test the antibacterial activity of Cu-nanozeolites. EMT- and FAU-type zeolites are the only zeolites that have been prepared in the form of stable colloidal suspensions without the use of organic templates.[7,8] FAU-type zeolite was selected in this work because of its more extensive use in antibacterial studies. The activity of ultrasmall 10-30 nm Cu-containing FAU-type zeolites (Cu-FAU) materials against six ESKAPE microorganisms, *Enterococcus faecalis* (*E. faecalis*), *Staphylococcus aureus* (*S. aureus*), *Klebsiella pneumoniae* (*K. pneumoniae*), *Acinetobacter baumanii* (*A. baumannii*), *Pseudomonas aeruginosa* (*P. aeruginosa*) and *Enterobacter cloacae* (*E. cloacae*), and a standard reference microorganism, *Escherichia coli* (*E. coli*), was studied semi-quantitatively. Following this, the zeolite suspensions were applied to stainless steel coupons fouled with bacteria to quantitatively establish the survival of *S. aureus*, *K. pneumoniae* and *P. aeruginosa* and to assess the surface decontamination potential of Cu nanozeolites.

2   Experimental

2.1   Synthesis of Cu-FAU

The template-free, nanosized FAU zeolite was prepared from a precursor mixture with the molar composition: 9 Na_2O: 1.1 Al_2O_3: 10 SiO_2: 77 H_2O.[8] Firstly, solutions A and B were prepared as follows: Solution A was made by dissolving 2.5 g of sodium hydroxide (NaOH, 97 %, Sigma-Aldrich) in 3.0 g of distilled water, followed by gradual addition of 0.297 g aluminum powder (325 mesh, 99.5 %, Alfa Aesar). The mixture was stirred until a clear solution was obtained. Solution B was prepared by dissolving 1.1 g of NaOH in 1.0 g of distilled H_2O, followed by the addition of 10 g colloidal silica (Ludox-HS 30, 30 wt % SiO_2, Aldrich). The resultant turbid suspension was placed in an oven at 100 °C for 5 min in order to obtain a clear suspension.

Solution A was added dropwise to solution B under vigorous stirring; solution B was kept in ice during the addition. The resulting clear suspension was aged with stirring at room temperature for 24 h followed by dehydration by freeze-drying to adjust the desired water content. The hydrothermal treatment was performed at 50 °C for 26 h. The crystalline product was diluted with hot distilled water (80 °C) and purified by centrifugation (20000 rpm, 25 min) and redispersion in distilled H_2O. Part of this nanosized Na-FAU suspension was freeze-

dried for further characterization and the rest was kept as suspension for post-synthetic Cu ion-exchange.

The Na-FAU zeolite suspension was ion-exchanged with copper (II) nitrate trihydrate $Cu(NO_3)_2.3H_2O$ to prepare Cu-FAU. The ion-exchange procedure was carried out as follows: 50 mL of $Cu(NO_3)_2.3H_2O$ (99-104 %, Sigma-Aldrich) with a concentration of 0.008 M was added to 10 mL of Na-FAU zeolite suspension (3.6 wt % zeolite) and vigorously stirred at room temperature for 1 h. This was followed by purification via centrifugation and redispersion in distilled water. The purification process was repeated twice under the same conditions. After the second ion-exchange, the final samples were washed twice with distilled water by centrifugation at 20000 rpm for 25 min, and re-dispersed in distilled H_2O. The final pH of the Cu-FAU suspensions was 7.0.

2.2 Characterisation methods

The crystal structure of the parent Na-FAU and the ion-exchanged zeolite Cu-FAU was determined using a PANalytical X'Pert Pro diffractometer with Cu Kα. The morphology of the synthesized materials was studied by scanning electron microscope (SEM) taken on MIRA-LMH (TESCAN) supplied with a field emission gun. Further, the samples were studied by transmission electron microscopy (TEM). TEM analysis was carried out using a 200 kV JEOL 2010 FEG electron microscope. Energy dispersive spectroscopy coupled with the TEM instrument was used to study the Cu-FAU sample. The stability of the zeolite suspensions at pH = 7.0 before and after the ion-exchange was measured by zeta potential using a Malvern Zetasizer Nano instrument. The elemental analysis of the samples was determined by inductively coupled plasma-atomic emission spectroscopy (ICP-AES) using an OPTIMA 4300 DV (PerkinElmer) instrument.

2.3 Microorganisms

Pseudomonas aeruginosa NCTC 6749, *Staphylococcus aureus* NCTC 6571, *Enterobacter cloacae* NCTC 10005, *Acinetobacter baumannii* NCTC 12156, *Klebsiella pneumoniae* NCTC 9633 and *Enterococcus faecalis* NCTC 775 (ESKAPE pathogens) as well as *Escherichia coli* ATCC 8739 (reference microorganism) were maintained on Nutrient Agar (Oxoid, Basingstoke) at 5 °C and inoculated into 100 mL Nutrient Broth (Oxoid). For each experiment and each culture, 2-4 colonies were inoculated into 100 mL Nutrient Broth

(Oxoid) and grown overnight (22 ± 1 h) at 37 °C with agitation (180 rpm). Cells were harvested by centrifugation (3600 rpm, 10 min) and washed once in 0.85% NaCl (Oxoid), resuspended to optical density 1.0 at 540 nm (Jenway 6305 Spectrophotometer, UK) resulting in a suspension concentration of $3.24 \pm 0.14 \times 10^9$ CFU mL^{-1}.

2.4 Semi-quantitative testing for microbial kill

E. faecalis suspension (25 µL) was added to 5 mL of 2 mg mL^{-1} of Cu-FAU, whilst 25 µL of the remaining strains were added to 5 mL of 1 mg mL^{-1} of Cu-FAU. The Cu-free FAU was used for control experiments. The samples were incubated at 37 °C in a rotary shaker incubator set to 150 rpm and a 20 µL sample was taken every 40 min over a period from 0-280 min for *E. faecalis* and every 20 min over a period of 0-140 min for all other microorganisms. Each 20 µL sample was pipetted onto one segment of a thioglycollate agar plate and a nutrient agar plate (Oxoid) which had been divided into eight segments. The thioglycollate agar was prepared by mixing thioglycollate broth (Oxoid) with 1.2% wt technical agar (Oxoid). All tests were carried out in duplicate and the experiment was repeated. Plates were incubated at 37 °C overnight and examined for the amount of bacterial growth following exposure to the Cu-FAU samples. A decrease in colony numbers was apparent as time progressed but this was not scored. Kill was noted as the total absence of colonies.

2.5 Survival of microorganisms on stainless-steel (SS) in the presence of Cu-FAU

Following semi-quantitative analysis for microbial kill, *P. aeruginosa*, *K. pneumoniae* and *S. aureus* were selected for assessing survival on SS in the presence of Cu-FAU. SS (316 2B) 2x2 cm coupons and polyethylene (PE) sheets (SLS, Nottingham, UK) cut to 2x2 cm were soaked in ethanol for 30 minutes, washed with sterile distilled water and left to dry for 90 minutes in a class two cabinet (BH-EN 2003, Faster, Cornaredo). 50 µL of bacterial culture was placed onto a SS coupon, spread using the end of a sterile pipette tip, and left to dry on the surface for 90 minutes in a class two cabinet. Once dry, 50 µL of Cu-FAU was pipetted onto the SS, and a 2x2 cm piece of polyethylene was placed on top of the inoculum to ensure the liquid was evenly distributed over the SS coupon. At the appropriate sample time, the SS coupon with PE sheet was dropped into 10 mL of neutralizing buffer (15 g Tween80 (Sigma-Aldrich, Dorset) and 30 g Soya Lecithin (Optima Healthcare Lecithin, Holland and Barrett,

UK) dissolved in 1 L of distilled water).[28] The role of this neutralizing buffer was to halt the antibacterial action of copper at the appropriate time point. Neutralizing buffer was then vortex-mixed for 30 sec to remove the polyethylene from SS and remove any cells from the surface into the liquid. The bacterial suspension was then diluted 10-fold (1 mL into 9 mL of sterile physiological saline), seven times, to a concentration of 10^{-7} of the original suspension. 100 µL of each dilution was pipetted out in duplicate on nutrient agar and spread evenly across the agar surface. Plates were incubated for 18 h at 37 °C, after which the number of colonies was counted to calculate CFU mL^{-1}. Time points sampled were 0, 5, 10, 20, 40 and 60 minutes. All samples were duplicated and the experiment was repeated.

3   Results and discussion

FAU-type zeolite was prepared in the absence of organic template as described previously.[8] TEM images indicated that the sample was fully crystalline with crystallites in the size range 10-30 nm (Figure 13). The zeolite nanocrystals are well-shaped and most of them exhibit the typical octahedral morphology with well-developed faces. Depending on crystals orientation on the grid, they appear as bi-pyramidal, isometric or even plate-like. Cu was introduced into the FAU-type zeolite by an ion-exchange approach. Elemental analysis indicated that 75% of Na was exchanged resulting in 11 wt % Cu content in the Cu-FAU sample (Table 1). The Cu-exchange did not affect the Si/Al ratio, which was 1.2 for both Na-FAU and Cu-FAU zeolites. TEM showed that the ion-exchange did not affect the zeolite crystallinity, crystal size or shape (Figure 13b). This conclusion was further confirmed by XRD and SEM analysis. XRD patterns of the Na-FAU and Cu-FAU were typical of the FAU-type zeolite with similar intensity of the XRD peaks indicating that the zeolite structure was preserved during the Cu ion-exchange (Figure 13c).
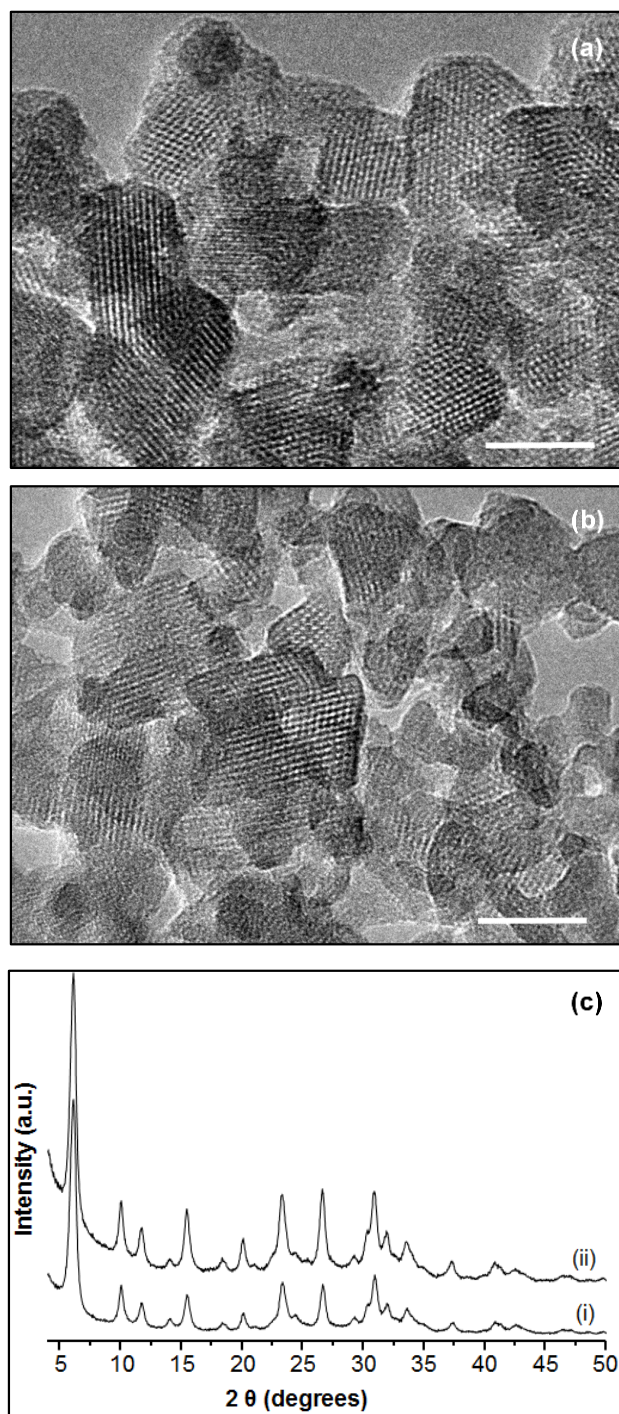
Figure 13. TEM images of (a) Na-FAU and (b) Cu-FAU (scale bar= 20 nm), and (c) XRD patterns of Na-FAU (i) and Cu-FAU (ii).

Table 1. Chemical analysis of prepared FAU zeolite samples.

Sample name	Na (wt. %)	Cu (wt. %)	Al (wt. %)	Si (wt. %)	Si/Al
Na-X	13.41	-	14.59	18.10	1.24
Cu-X	4.80	11.08	14.73	17.38	1.18

The SEM images showed that the zeolite crystallites were well-shaped with a narrow particle size distribution in both Na-FAU and Cu-FAU samples (Figure 14).
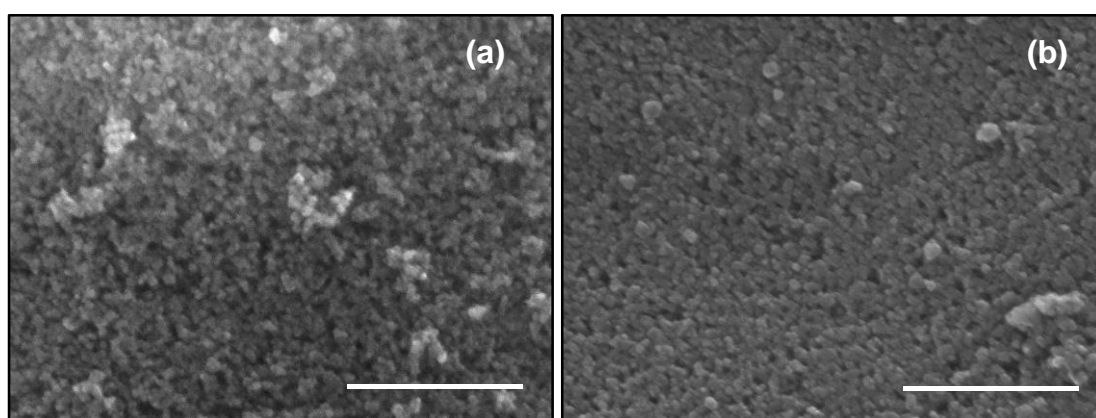
Figure 14. SEM images of (a) Na-FAU and (b) Cu-FAU samples (scale bar = 500 nm).

The Cu content in the zeolite crystals was determined based on EDS (Figure 15); with the copper signal coming only from the zeolite particles since Ni-grids were used to prepare the samples. Under prolonged exposure of the crystals to the e-beam (1 minute), the Cu nanoparticles were reduced and aggregated as shown in the Figure 16.
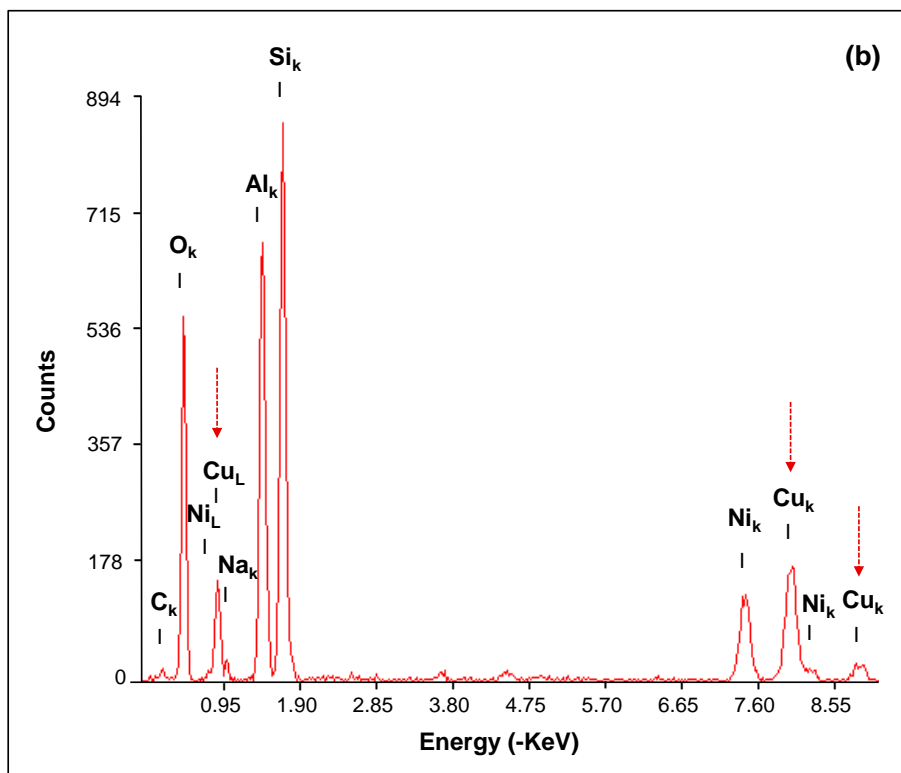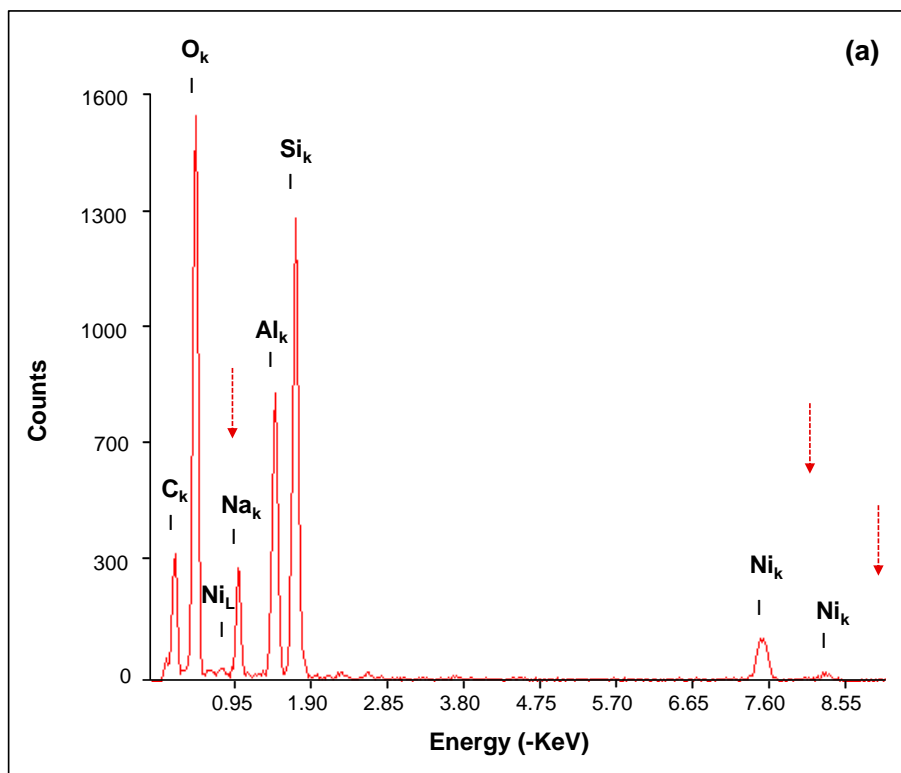
Figure 15. EDS spectra of (a) Na-FAU and (b) Cu-FAU samples measured on Ni grids. The chemical composition of the samples retrieved from the EDX is shown in **Table 2**.

Table 2. Chemical composition of FAU samples retrieved from EDX.

Sample name	Na (wt. %)	Cu (wt. %)	Al (wt. %)	Si (wt. %)	Si/Al
Na-X	11.84	-	31.36	56.8	1.81
Cu-X	2.1	11.7	34.2	52.0	1.52
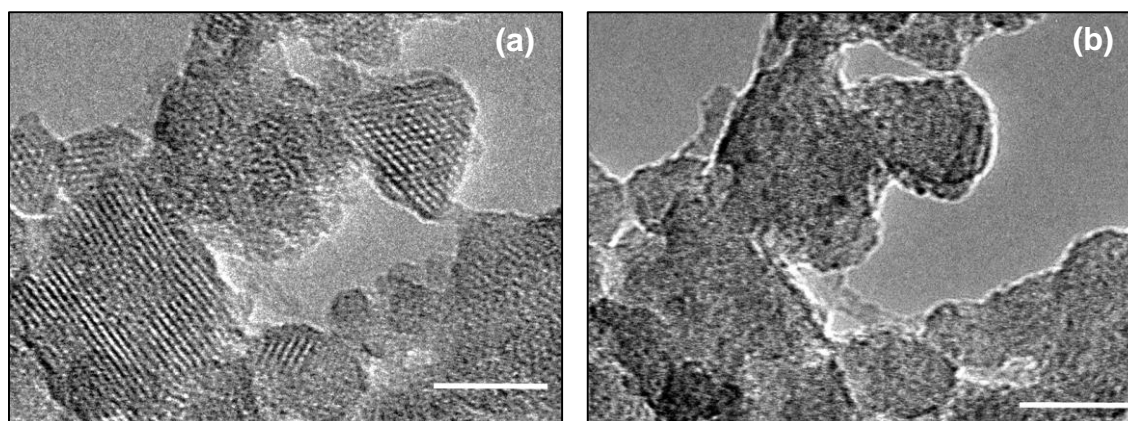
Figure 16. HRTEM images taken on same Cu-FAU zeolite crystals after (a) 20 sec and (b) 60 sec (scale bar = 20 nm)

The colloidal stability of the prepared zeolite suspensions is of paramount importance for the application of the materials to treat surfaces. The stability of the zeolite samples was studied using zeta potential measurements (Figure 17a). Usually, a zeta potential threshold value of ± 30 mV is used to measure stability; values above this threshold value indicate colloidal stability. The zeta potential of the zeolite suspensions varied between -41.5 mV and -45.6 mV for Na-FAU and Cu-FAU, respectively, indicating that both suspensions were colloidally stable. The colloidal stability of the samples can be seen clearly from the digital images in Figure 17a, inset. In addition, the samples did not aggregate upon storage for at least 3 months. After Cu ion-exchange, the suspension was a light-bluish color. DLS results (Figure 17b) indicated a monomodal particle size distribution, which was similar for the Na-FAU and Cu-FAU samples.
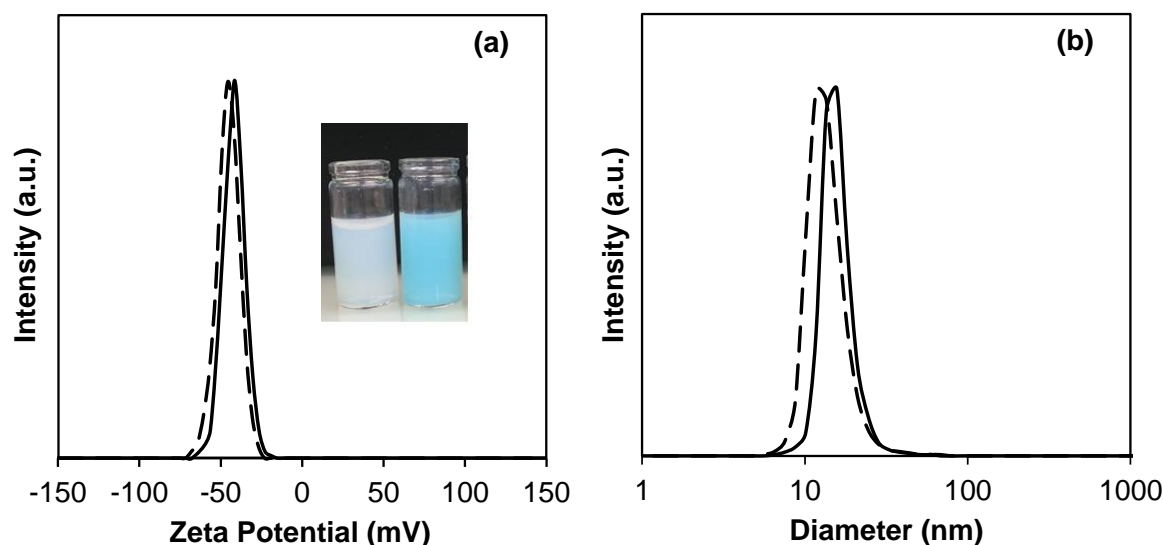
Figure 17. (a) Zeta potential and (b) DLS curves of Na-FAU (solid line) and Cu-FAU (dotted line) samples; Inset: digital images of the Na-FAU (white) and Cu-FAU (blue) zeolite suspensions.

The antibacterial properties of the Cu-FAU suspensions were firstly studied using our previously developed semi-quantitative method with *E. coli* as a reference microorganism.[14] The Cu-free samples (Na-FAU) were used as controls throughout this work and they showed no antibacterial activity in all experiments. In our previous work, we used Ag-loaded EMT zeolites with zeolite concentrations of 0.5 mg mL^{-1}.[14] Killing times were achieved within less than 10 minutes depending on the Ag content and the Ag form, metallic or ionic. Initial experiments using Cu-FAU with zeolite concentrations of 0.5 mg mL^{-1} did not kill *E. coli* quickly enough (within 15 minutes) to provide a viable testing method, for which reason the concentration in all further experiments was doubled to 1 mg mL^{-1}. Similarly to our previous results, the use of thioglycollate agar as a growth medium was important to halt the antibacterial action of Cu at the corresponding sampling time (Figure 18). *E. coli* was killed within 35 min when thioglycollate agar was used and within 20 min using nutrient agar. These experiments indicated that the Cu-exchanged ultrasmall zeolites had lower antibacterial activity compared to Ag-exchanged ultrasmall zeolites. We have reported similar trends for FAU-type zeolites prepared from fly ash after ion-exchange with Ag and Cu.[26]
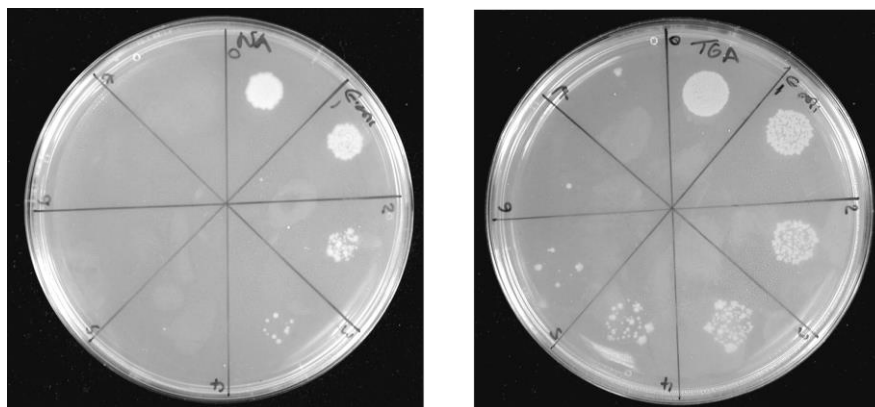
Figure 18. Spot inoculation of *E. coli* onto (left) nutrient agar and (right) thio-neutralizing agar following 5 minute interval exposure to the Cu-X suspension. Each drawn segment on the plates above corresponds to five minutes sampling time; the first sample (top) is taken directly after mixing (0 min) with clockwise inoculation over time.

After optimization of the semi-quantitative tests in terms of zeolite concentrations using the reference *E. coli*, experiments continued using ESKAPE microorganisms. Typical images of the thioglycollate plates after incubation are shown in Figure 19 with the average killing times summarized in the accompanying histogram (Figure 20). All experiments were performed in duplicates and repeated. Also, experiments were performed with Cu-FAU suspensions from different batches to test reproducibility; similar results were obtained when samples from different batches were used. *E. faecalis* showed increased time to kill compared to the other ESKAPE microorganisms. Such increased time to kill *E. faecalis* compared to *E. coli* and *P. aeruginosa* was also observed in our previous work using Ag-exchanged zeolite prepared from fly ash.[26] Doubling the Cu-FAU concentration to 2 mg mL^{-1} and increasing the sampling time to 40 min indicated that Cu-FAU reduced the *E. faecalis* viable cells and had the potential to kill this microorganism as well, although to a less extent compared to the other ESKAPE microorganisms (Figure 19).
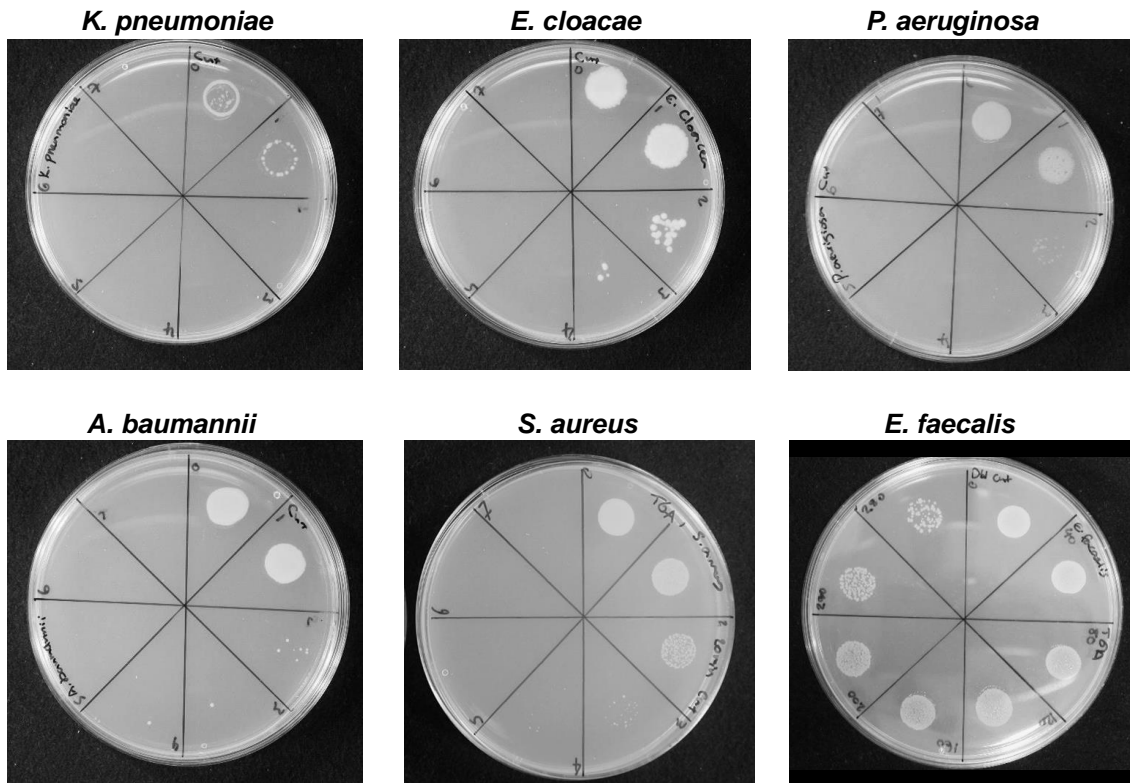
Figure 19. Spot inoculation of ESKAPE microorganisms following exposure to the Cu-FAU suspension. Each drawn segment on the plates above corresponds to 20 minutes sampling time (40 minutes for *E. faecalis*); total sampling time 0-140 minutes (0-280 minutes for *E. faecalis*). Microorganisms (clockwise): *K. pneumoniae*, *E. cloacae*, *P. aeruginosa*, *E. faecalis*, *S. aureus* and *A. baumannii*.
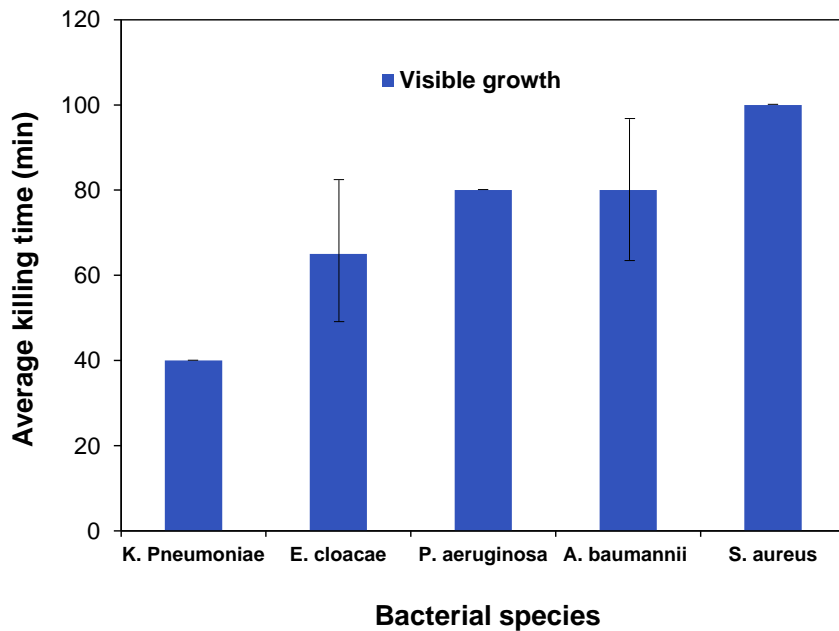
Figure 20. Summary of the average killing times determined in the semi-quantitative tests.

After establishing the potential of Cu-FAU colloidal suspensions to deactivate ESKAPE microorganisms, quantitative tests were designed to determine the survival of selected microorganisms on stainless steel coupons. The introduction of copper alloy surfaces in intensive care units has been shown to decrease rates of healthcare-acquired infections.[29] However, the replacement of surfaces is not always appropriate / possible and deactivation of fouled surfaces by simple spraying, which is applicable to all types of surfaces, seems a much more elegant approach. Stainless steel has been selected in this study as one of the most relevant surfaces in healthcare settings. Based on the semi-quantitative tests (Figure 19), three key ESKAPE microorganisms were selected to study the capacity of Cu-FAU to act as a surface decontamination agent, namely *K. pneumoniae* (shortest killing time), *P. aeruginosa* (middle killing time) and *S. aureus* (longest killing time amongst the microorganisms that died). In these experiments, bacterial cultures (50 µL) were inoculated and left to dry on stainless steel coupons. Coupons were then treated with 50 µL of Cu-FAU. At the appropriate sample time, 0, 5, 10, 20, 40 or 60 minutes, the coupons were dropped into a neutralizing buffer to halt the activity of Cu and the remaining viable cells on the surface were determined by the serial dilution method.[28] Complete kill was achieved within 20 minutes for *P. aeruginosa*, and within 10 minutes for the *K. pneumoniae* and *S. aureus* (Figure 21). Bacterial cells survived on the surfaces when treated with Na-FAU. These results indicate that Cu-FAU suspensions can be used for surface treatment to deactivate ESKAPE microorganisms.
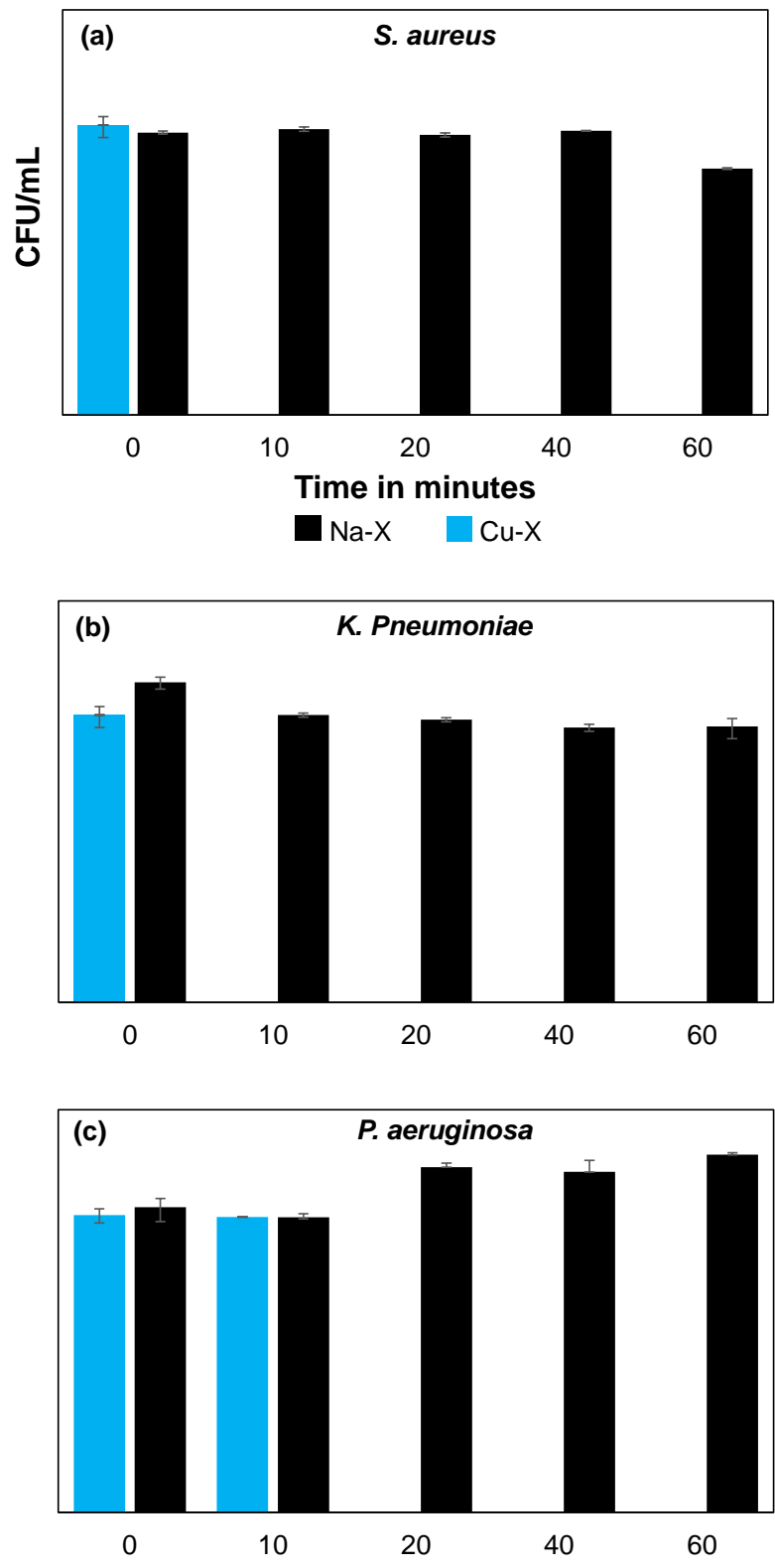
Figure 21. Survival of bacterial strains on stainless steel coupons: (a) S. aureus, (b) K. pneumoniae, and (c) P. aeruginosa.

4   Conclusions

Ultrasmall Cu-FAU zeolite crystals were prepared in the form of stable colloidal suspensions. The Cu-FAU zeolites showed activity against *E. coli* and all six ESKAPE microorganisms, as determined by a semi-quantitative drop test. The survival of three selected ESKAPE microorganisms on stainless-steel surfaces treated with Cu-FAU was studied quantitatively. None of the three microorganisms survived the Cu-FAU treatment. This result is significant considering the urgent need for new antimicrobial drugs, especially drugs that are effective against Gram-negative pathogens such as *Pseudomonas aeruginosa*, *Klebsiella pneumoniae* and *Acinetobacter baumannii*.[30] The use of Cu-FAU colloidal suspensions to inactivate ESKAPE pathogens on surfaces, particularly in healthcare settings, could lead to the significant reduction of bacterial infections, thus reducing the need for antibiotics treatment.

5 References

[1] H. W. Boucher, G. H. Talbot, J. S. Bradley, J. E. Edwards, D. Gilbert, L. B. Rice, M. Scheld, B. Spellberg, J. Bartlett, Clin. Infect. Dis. 48 (2009) 1-12.

[2] J. N. Pendleton, S. P. Gorman, B. F. Gilmore, Expert Rev. Anti Infect. Ther. 11 (2013) 297-308.

[3] J. O'Neill (Chair), The Review on Antimicrobial Resistance, Wellcome Trust, London, 2006.

[4] B. J. Schoeman, J. Sterte, J.-A. Otterstedt, J. Chem. Soc., Chem. Commun. (1993) 994-995.

[5] S. Mintova, M. Jaber and V. Valtchev, Chem. Soc. Rev. 44 (2015) 7207-7233.

[6] W. Schwieger, A. G. Machoke, T. Weissenberger, A. Inayat, T. Selvam, M. Klumpp, A. Inayat, Chem. Soc. Rev., 2016, 45, 3353.

[7] E.-P. Ng, D. Daniel Chateigner, T. Bein, V. Valtchev, S. Mintova, Science 335 (2012) 70-73.

[8] H. Awala, J.-P. Gilson, R. Retoux, P. Boullay, J.-M. Goupil, V. Valtchev, S. Mintova, Nat. Mater. 14 (2015) 447-451.

[9] P. Lalueza, M. Monzón, M. Arruebo, J. Santamaria, Chem. Commun. 47 (2011) 680-682.

[10] L. Ferreira, A. M. Fonseca, G. Botelho, C. Almeida-Aguiar, I. C. Neves, Microporous Mesoporous Mater. 160 (2012) 126-132.

[11] P. Saint-Cricq, Y. Kamimura, K. Itabashi, A. Sugawara-Narutaki, A. Shimojima, T. Okubo, Eur. J. Inorg. Chem. (2012) 3398-3402.

[12] C. Carolina, B. J. Carlos, B. M. L. Zapata, Z. J. Manuel, Microporous Mesoporous Mater. 188 (2014) 118-125.

[13] Y. Zhou, Y. Deng, P. He, F. Dong, Y. Xia, Y. He, RSC Adv. 4 (2014) 5283-5288.

[14] B. Dong, S. Belkhair, M. Zaarour, L. Fisher, J. Verran, L. Tosheva, R. Retoux, J.-P. Gilson, S. Mintova, Nanoscale 6 (2014) 10859-10864.

[15] S. A. Hanim, N. A. N. N. Malek, Z. Ibrahim, Appl. Surf. Sci. 360 (2016) 121-130.

[16] V. V. Singh, B. Jurado-Sánchez, S. Sattayasamitsathit, J. Orozco, J. Li, M. Galarnyk, Y. Fedorak, J. Wang, Adv. Funct. Mater. 25 (2015) 2147-2155.

[17] Y. Matsumura, K. Yoshikata, S. Kunisaki, T. Tsuchido, Appl. Environ. Microbiol. 69 (2003) 4278-4281.

[18] K. A. Rieger, H. J. Cho, H. F. Yeung, W. Fan, J. D. Schiffman, ACS Appl. Mater. Interfaces 8 (2016) 3032-3040.

[19] S. Belkhair, M. Kinninmonth, L. Fisher, B. Gasharova, C. M. Liauw, J. Verran, B. Mihailova, L. Tosheva, RSC Adv. 5 (2015) 40932-40939.

[20] M. M. Cowan, K. Z. Abshire, S. L. Houk, S. M. Evans, J. Ind. Microbiol. Biotechnol. 30 (2003) 102-106.

[21] C. Marambio-Jones, E. M. V. Hoek, J. Nanopart. Res. 12 (2012) 1531-1551.

[22] G. Grass, C. Rensing, M. Solioz, Appl. Env. Microbiol. 77 (2011) 1541-1547.

[23] M. Vincent, P. Hartemann, M. Engels-Deutsch, Int. J. Hyg. Environ. Health. 219 (2016) 585-591.

[24] R. Tekin, N. Bac, Microporous Mesoporous Mater. 234 (2016) 55-60.

[25] J. Behin, A. Shahryarifar, H. Kazemian, Chem. Eng. Technol. 39 (2016) 2389-2403.

[26] L. Tosheva, A. Brockbank, B. Mihailova, J. Sutula, J. Ludwig, H. Potgieter, J. Verran, J. Mater. Chem. 22 (2012) 16897-16905.

[27] C. Ning, X. Wang, L. Li, Y. Zhu, M. Li, P. Yu, L. Zhou, Z. Zhou, J. Chen, G. Tan, Y. Zhang, Y. Wang, C. Mao, Chem. Res. Tox. 28 (2015) 1815-1822.

[28] L. Fisher, S. Ostovapour, P. Kelly, K. A. Whitehead, K. Cooke, E. Storgårds, J. Verran, Biofouling 30 (2014) 911-919.

[29] C. D. Salgado, K. A. Sepkowitz, J. F. John, J. Robert Cantey, H. H. Attaway, K. D. Freeman, P. A. Sharpe, H. T. Michels, M. G. Schmidt, Infect. Control Hosp. Epidemiol. 34 (2013) 479-486.

[30] R. Tommasi, D. G. Brown, G. K. Walkup, J. I. Manchester, A. A. Miller, Nat. Rev. 14 (2015) 529-542.

Chapter 4- Nanosized zeolites as a theranostic tool to oxygenate and visualize aggressive brain tumours with magnetic resonance imaging

Abstract

Hypoxia is recognized as a major cause of resistance to radiotherapy in many types of solid tumours, including glioblastoma. Herein, we report a new approach based on the use of metal-containing micro-porous crystalline nanoparticles (nanosized zeolite) as a specific hyperoxic/hypercapnic gas carrier. First, the absence of acute and chronic toxicity of nanosized zeolites crystals in living animals (mice, rats and non-human primates) is confirmed. The nanosized zeolite particles act as a vasoactive agent for a targeted re-oxygenation of the tumour. Furthermore, thanks to the low amount of metals (either gadolinium or iron) introduced in the nanosized zeolite particles, they are used as a contrast agent for visualization of the tumour and tracking of the nanocrystals by magnetic resonance imaging (MRI). Our work thus provides the first proof of concept for the use of metal-containing nanosized zeolites as a theranostic tool for (i) diagnosis and (ii) vectorization of hyperoxic/hypercapnic gases in glioblastoma.

1 Introduction

Even with aggressive conventional therapies for the treatment of glioblastoma (GB), the most aggressive primary brain tumour[1] the median survival of patients remains around 15 months.[2] Hypoxia, a hallmark of many solid tumours, including GB,[3] is defined as the imbalance between oxygen supply and tissue consumption. This inadequate oxygen supply is caused by an inefficient gas transfer from the atypical tumour vascularization to the cancer cells, which exhibit a high metabolic rate associated to an elevated oxygen demand. It has been long recognized that hypoxia is a factor of poor prognosis for GB.[4]

Hypoxia triggers adaptive survival mechanisms in cancer cells, promoting tumour growth[5] and resistance to treatments, including radiotherapy (RT) and photodynamic therapy (PDT), two clinically approved anti-cancer treatment that generates cytotoxic reactive oxygen species (ROS) in the presence of molecular oxygen.[6] Hence, it would be of great interest to

develop a novel method to specifically increase oxygen level into the hypoxic tumour and image the tumour.

A number of approaches have been developed to reduce hypoxia in tumours including, oxygen or carbogen (a mixture composed of 5% CO_2 balanced with 95% O_2) breathing. However, the overall results were unsatisfactory in terms of sensitization to RT in brain tumours.[7,8] Using multiparametric magnetic resonance imaging (MRI) to simultaneously assess cerebral blood volume (CBV) and tissue oxygenation, we have recently demonstrated that carbogen increased the CBV and the oxygenation in the healthy brain at the expense of the tumour.[9]

Due to the abnormal architecture and structure of the tumour vasculature and the lack of a functional lymphatic system,[10] various nanoparticles (NP) of different chemical natures have been investigated as carriers of contrast agents and anti-cancer compounds owing to their ability to preferentially target tumours.[11,12] Moreover, several NP have also been developed to enhance tumour-specific RT efficacy and reduce collateral damage of healthy tissues. These include metal-containing NP taking advantage of the Auger effect,[13,14] NP that reduce the cancer cell's ability to repair itself from damage caused by RT,[15,16] NP that protect surrounding healthy tissue by reducing oxidative stress,[17] and in-situ oxygen generating NP.[18,19] However, few were designed to locally and specifically deliver gases (O_2 and CO_2) in the tumour. Even if micron-sized particles carrying approximately five times more oxygen that human red blood cells and liposomes designed to encapsulate hemoglobin for the delivery of oxygen in colorectal cancers were recently proposed, their use to alleviate hypoxia in brain tumours is not satisfactory because of their large diameter.[20,21]

Among nanoparticles, zeolites with their exceptional chemical selectivity, high sorption capacity and absence of toxicity,[22–26] are now increasingly considered for biomedical use[27,28] including cancer treatment.[29–31] Zeolites are crystalline, porous materials made of interconnected TO_4 tetrahedra, where T atoms are represented by Si and Al. They have regular framework structures composed of cages and pores of various size and shape.[32] Despite of the interest in the preparation of nanosized zeolites, only 24 out of the 239 structures known have so far been synthesized with nanosized dimensions and stabilized in colloidal suspensions.[33] The regular pores of the zeolites are able to adsorb and desorb different molecules, allowing them to act as molecular sieves and hosts for various gases including NO, CO_2 and O_2.[23,34] The tuneable chemical composition of these crystalline materials allows them to adapt to different chemical environments and thus to exhibit high stability in acidic and alkaline media. In addition to the unique properties of zeolites, the

introduction of different metal cations (Fe, Gd) within the nanosized zeolites can change their functioning, and thus considerably increase the interest of zeolite NP as a theranostic tool for imaging[35] and gases transport applications.[23] Therefore, it is interesting to explore nanosized zeolites as gas carriers to purposely target hypoxia in GB and as a contrast agent to image the tumour.

Herein, we present an original approach to specifically and efficiently deliver O_2 and/or CO_2 to tumours via metal-containing nanosized zeolite crystals with FAU-type structure to further improve oxygenation and/or blood volume. Gadolinium (Gd) and iron (Fe) have been incorporated into the FAU-type nanosized zeolite structure via ion exchange and stabilized in water suspensions in order to be delivered by intravenous injection and, thereafter, traced.

2   Materials and Methods

2.1 Preparation of nanosized faujasite X (Na-X) type zeolite

Stable suspension of discrete nanosized zeolite (Na-X) from colloidal precursor suspension under hydrothermal condition was prepared according to a recently published procedure.[36] The as-prepared precursor suspension for Na-X zeolite was aged at room temperature for 24 hours, followed by dehydration using freeze-drying method prior hydrothermal treatment at 50 °C for 26 h. After the hydrothermal treatment, the zeolite nanoparticles were purified by six step centrifuge (24,500 rpm, 45 min) and redispersed in double distilled water till pH of 7.

2.2   Ion exchange of nanosized faujasite X (Na-X) type zeolite

The purified zeolite suspensions (pH=7) were ion exchanged with gadolinium (III) nitrate hexahydrate $Gd(NO_3)_3.6H_2O$ and iron nitrate nonahydrate $Fe(NO_3)_3.9H_2O$.

25 mL of $Gd(NO_3)_3.6H_2O$ or $Fe(NO_3)_3.9H_2O$ (3 mM) were added to 5 mL Na-X suspension (2.5 wt%). The suspensions were then kept under stirring at room temperature for 1 h and then washed by double distilled water. This procedure was repeated three times to obtain finally the suspensions of ion-exchanged gadolinium (Gd-X) and iron (Fe-X) nanosized zeolites; pH=7

2.3 Powder X-ray diffraction (XRD) analysis

Powder samples were measured using a PANalytical X'Pert Pro diffractometer with CuKα monochromatized radiation (λ = 1.5418 Å). The samples were scanned in the range of 4-50 °2θ with a step size of 0.02 °.

2.4 Transmission electron microscopy (TEM)

The crystal size, morphology and crystallinity of samples were determined by a transmission electron microscopy (TEM) using a JEOL 2010 FEG and a FEI LaB6 TECNAI G2 30UT operated at 200 kV and 300 kV, respectively. Energy Dispersive Spectrometer (EDS) coupled with both microscopes was used to determine the chemical composition of the zeolite nanocrystals.

2.5 Dynamic light scattering (DLS) and zeta potential analysis

The hydrodynamic diameter of nanosized zeolite particles in water was determined using Malvern Zetasizer Nano. The analyzes were performed on samples after purification with a solid concentration of 1 wt %. Additionally, the surface charge of zeolite nanocrystals was determined by measuring the zeta potential value of the same suspensions.

2.6 N_2 sorption analysis

Nitrogen adsorption/desorption isotherms were measured using Micrometrics ASAP 2020 volumetric adsorption analyzer. Samples were degassed at 250 °C under vacuum overnight prior to the measurement. The external surface area and micropore volume were estimated by alpha-plot method using Silica-1000 (22.1 m^2 g -1 assumed) as a reference. The micropore and mesopore size distributions of solids were extracted from adsorption branch by the Nonlocal Density Functional Theory (NLDFT) and from the desorption branch using the Barret-Joyner-Halenda (BJH) algorithm, respectively.

2.7 In-situ adsorption of CO_2 and O_2 on nanosized zeolites

Powder samples of as prepared and ion-exchanged zeolites were pressed (~10^7 Pa) into self-supported disks (2 cm^2 area, 20 mg.cm^{-2}). Fourier-transform infrared (*FTIR*) spectra were

recorded using a Nicolet 6700 IR spectrometer equipped with a mercury cadmium telluride (MCT) detector and an extended KBr beam splitter. Spectra were recorded in the 400−5500 cm^{-1} range at 4 cm^{-1} with 128 scans. The *in situ* was evacuated or flooded with different gases and also heated up to 577 °C was used. The samples were activated at 225 °C for 2 h under vacuum. Various amounts of CO_2 (at 25 °C) or O_2 (at -196 °C) were introduced into the cell and kept in equilibrium for 5 minutes at the corresponding temperatures before recording each spectrum. All the spectra were normalized to the sample's mass and plotted as absorbance per gram over the wavelength.

2.8 Chemical analysis

The chemical composition of as prepared and ion-exchanged zeolites was determined by inductively coupled plasma (ICP) optical emission spectroscopy using a Varian ICP-OES 720-ES.

2.9 Release of oxygen in aqueous and hypoxic conditions

A hypoxia chamber (*IN VIVO*2 500, 3M) was used to obtain a stable and controlled gas composition of the atmosphere with a precision of 0.1% O_2 by adapting the amount of N_2. Phosphate buffered saline (PBS, Sigma-Aldrich) solution was equilibrated with the gas mixture contained in the hypoxia chamber for 1 h prior to the experiment. A closed reaction vessel containing 12 ml of equilibrated PBS at 37 °C was used, and a dissolved oxygen sensor (SevenGo (Duo) pro™ / OptiOx™, Mettler Toledo) was placed inside the hypoxia chamber. Prior to experiments, baseline was established by measuring the oxygen saturation in the system for 30 min. Nanosized zeolites were then added to the system (500 µl, 1 wt.%) and oxygen dissolved in the PBS solution was measured continuously for 1h. The oxygen release capacity of as prepared and ion-exchanged zeolites was compared to oxygen-saturated water (used as reference). The oxygen release capacity of Na-X nanosized zeolites was studied at various levels of oxygen in the atmosphere (21, 5, 1 and 0.1% of O_2).

2.10 Cell lines

A human glioblastoma cell line, U87-MG purchased from American Type Culture Collections (ATCC, Manassas, VA, USA) and HEK 293 cells (Human Embryonic Kidney

cells) were used. Cells were cultured in DMEM (Sigma-Aldrich, France). bEnd.3 mouse brain endothelial cells were purchased from ATCC (Manassas, VA, USA) and cultured in high glucose (4500 mg/l) DMEM (Sigma-Aldrich, France).

DMEM was supplemented with 10% foetal bovine serum (Eurobio, France), 2 mM glutamine (Sigma-Aldrich, France) and 100 U/ml penicillin/streptomycin (Sigma-Aldrich, France). Cells were maintained in culture at 37°C with 5% CO_2 and 95% humidity.

2.11 Primary culture of astrocytes

Cerebral cortices were isolated from neonatal (1 to 3-day-old) mice (Swiss, CURB, France) carefully stripped of the meninges and dissociated to generate a single-cell suspension. Cultures were allowed to grow in a humidified 5% CO_2 incubator at 37 °C to confluency (15-20 days) prior to use in DMEM supplemented with 10% foetal bovine serum (Eurobio, France), 10% horse serum (Eurobio, France), 2 mM glutamine (Sigma-Aldrich, France) and 100 U/ml penicillin/streptomycin (Sigma-Aldrich, France). At about 80% confluence, the growth medium was replaced by the same medium.

2.12 Primary cultures of cortical neurons/astrocytes

Cultures were prepared from E15–E16 mouse embryos (Swiss mice; CURB, France). Microdissection of cortices was followed by a dissociation of the tissue in a 37°C DMEM (Sigma-Aldrich, France). Cells grew on plates coated with poly-d-lysine (0.1 mg/ml) and laminin (0.02 mg/ml) in DMEM supplemented with 5% foetal bovine serum, 5% horse serum (Eurobio, France), and 2 mm glutamine (Sigma-Aldrich, France). Cells were maintained in a humidified 5% CO_2 atmosphere at 37°C. Neurons were used after 12 d *in vitro*.

2.13 Cells exposure to nanosized zeolites

Cells were exposed to zeolites (Na-X, Fe-X and Gd-X) for 48h. Zeolites were diluted in culture medium at a concentration of 1, 10, 50 or 100 µg/ml and added directly into the wells. Control tests (distilled water) in the wells with same volumes were performed.

The concentration range to test was determined using the following assumption: the average blood volume of a rat is ~64mL/kg. Given that 250-300mg animals were used in the

in vivo experiments, the rats had 16-19 ml of blood. 300 µl of a 1% wt. solution, which is 3 mg of material, equates to ~156-188 µg zeolite/mL of blood.

2.14 Cells viability

Cells were seeded in 24-wells plates to achieve 80% confluency for the control on the day of the analysis. Cell viability was assessed 48h following the exposure to zeolites with the WST-1 assay (Roche, France) according to manufacturer's instructions.

2.15 Injection in healthy animals

Intraperitoneal injections of 100 µl zeolite suspensions (1wt.% Na-X or Gd-X zeolites) and water as a control were performed in Swiss mice (Janvier laboratory, France) for 5 consecutive days. Animals were weighted every 24 hours for 30 days. At the end of the experiment, the spleen, the liver and the kidneys were removed and weighted.

300 µl of the CO_2-loaded Gd-X (1wt.%) or pure water as a control were intravenously injected in healthy Wistar rats (Charles-River laboratory, France). Then, blood samples were then collected every 5 minutes via an arterial catheter and the CO_2 partial pressure and the pH of the collected samples using a RapidLab 348 analyzer (Siemens, Germany) were measured.

300 µl zeolite suspension (1wt.% Fe-X) or water as a control were intravenously injected in healthy Wistar rats (Charles-River laboratory, France). 1 or 3 days later, the liver, the spleen, kidneys and the brain were fixed and then cryoprotected by immersion in a 30% sucrose solution (Sigma, France) for 48 h, before storage at −80 °C. The Fe-X zeolite crystals on 20-µm-thick slices using Prussian blue staining were detected. Slices were incubated with 2% potassium ferrocyanide (Perl's reagent, Sigma, France) in 2% HCl, washed and counterstained with eosin.

2.16 Detection of Gd-X zeolite nanocrystals with MRI

Experiments on tumour bearing rats were performed. After a scout view and a T2w-RARE8 scan, 300 µl Gd-X suspension (1wt.%) was administered intravenously; T1w-FLASH images (TR/TEeff= 500/10.32 ms; NEX=1; 10 slices; resolution = $0.15 \times 0.15 \times 1.5$ mm^3; acquisition time= 2 min) were obtained prior to and every 2 min following the injection.

2.17 Fractional cerebral blood volume maps.

For the imaging protocol, after a scout view and a T2w-RARE8 scan, fractional cerebral blood volume (fCBV) at equilibrium was measured as previously described.[9] Prior to the injection of the contrast agent, five T2*w (TR= 20,000 ms, NEX= 3, 50 contiguous slices, resolution = $0.3 \times 0.3 \times 0.3$ mm) and four T2w (TR= 20,000 ms, NEX= 3) images (echo planar imaging: EPI) with various echo times (TE for T2*w= 12, 15, 18, 21, and 24 ms and for T2w= 40, 60, 80, and 100 ms, respectively) were acquired. An intravenous administration of P904® (200 µmol.kg^{-1}, Guerbet Research) was performed, and T2*w images (TE= 12 ms) before and every 5 min for 1h after intravenous administration of 300 µl of gas loaded Gd-X (1wt.%) were acquired. Consequently, for each animal, fCBV maps were obtained under two conditions: baseline and after administration of gas loaded Gd-X zeolite. Image analysis with in-house developed macros based on the ImageJ software (http://rsb.info.nih.gov/ij/, 1997–2014) was performed as previously described.[9]

Following the injection, the T2* signal in the healthy and tumour tissue for all groups decreased. This was due to an elimination of the contrast agent used in the protocol for the quantitative measure, resulting in an artefactual decrease of the CBV. A comparison with the control group was performed and the data were normalized.

2.18 Oxygen saturation maps

Oxygen saturation (SatO$_2$) maps reflecting the percentage of hemoglobin binding sites occupied by oxygen in the bloodstream were computed as previously described.[9] Briefly, the SatO$_2$ maps as a function of the T2*w signal after correction of inhomogeneities of magnetic field (B0), blood volume fraction, and T2 effects were calculated (resulting SatO$_2$ values in a healthy brain tissue is around 70%. SatO$_2$ maps before and after administration of gas loaded Gd-X zeolite for each animal were generated.

3   Results and discussion

3.1 Properties of nanosized zeolites

The three zeolite sample (Na-X, Gd-X and Fe-X) with a large supercage (1.2 nm) has been described as gas carrier and drug delivery system earlier.[29,37] The main physicochemical properties of as synthesized (Na-X), gadolinium (Gd-X) and iron-containing (Fe-X) zeolite

nanocrystals with FAU-type framework structure are presented in Figure 22a-c, Figure 2 and Table 3 Table 4.

Powder X-ray diffraction (XRD) of the three zeolite samples show patterns with broadened peaks reflecting the small particle size. Typical Bragg peaks corresponding to FAU-type zeolite present in the Na-X sample (Figure 22a) are perfectly preserved after ion exchange treatment.

Incorporation of Gd or Fe into the zeolite did not induce any remarkable change in the crystals properties including size, shape, porosity and surface charge. The nanosized zeolites have an average size of 15-20 nm measured in water suspension (Figure 23) and surface charge of -43 to -45 mV (Figure 222b). The porosity of zeolite nanoparticles before and after ion exchange treatment was investigated by N2 sorption analysis (Figure 22c and Table 4). All the three samples exhibit similar features: Type I isotherm at low P/P0 characteristic for microporous materials and high adsorption uptake at P/P0 > 0.8 reflecting the high textural mesoporosity of closely packed zeolite nanoparticles with similar particle sizes.

The physisorbed O_2 and physi- and chemisorbed CO_2 were evaluated by in-situ IR spectroscopy following the introduction of controlled quantities of the desired gas into the zeolite samples. The CO_2 loading capacity of zeolites samples follows the trend Fe-X > Na-X > Gd-X. Despite the lower quadrupole moment of oxygen compared to CO_2 which renders it less efficient for adsorption on zeolites,[38] small amount of iron (1 wt. %, measured with ICP-AES, Table 3) introduced in the zeolite (Fe-X) substantially improved the O_2 adsorption capacity in comparison to the Na-X and Gd-X zeolite samples (Figure 22d).
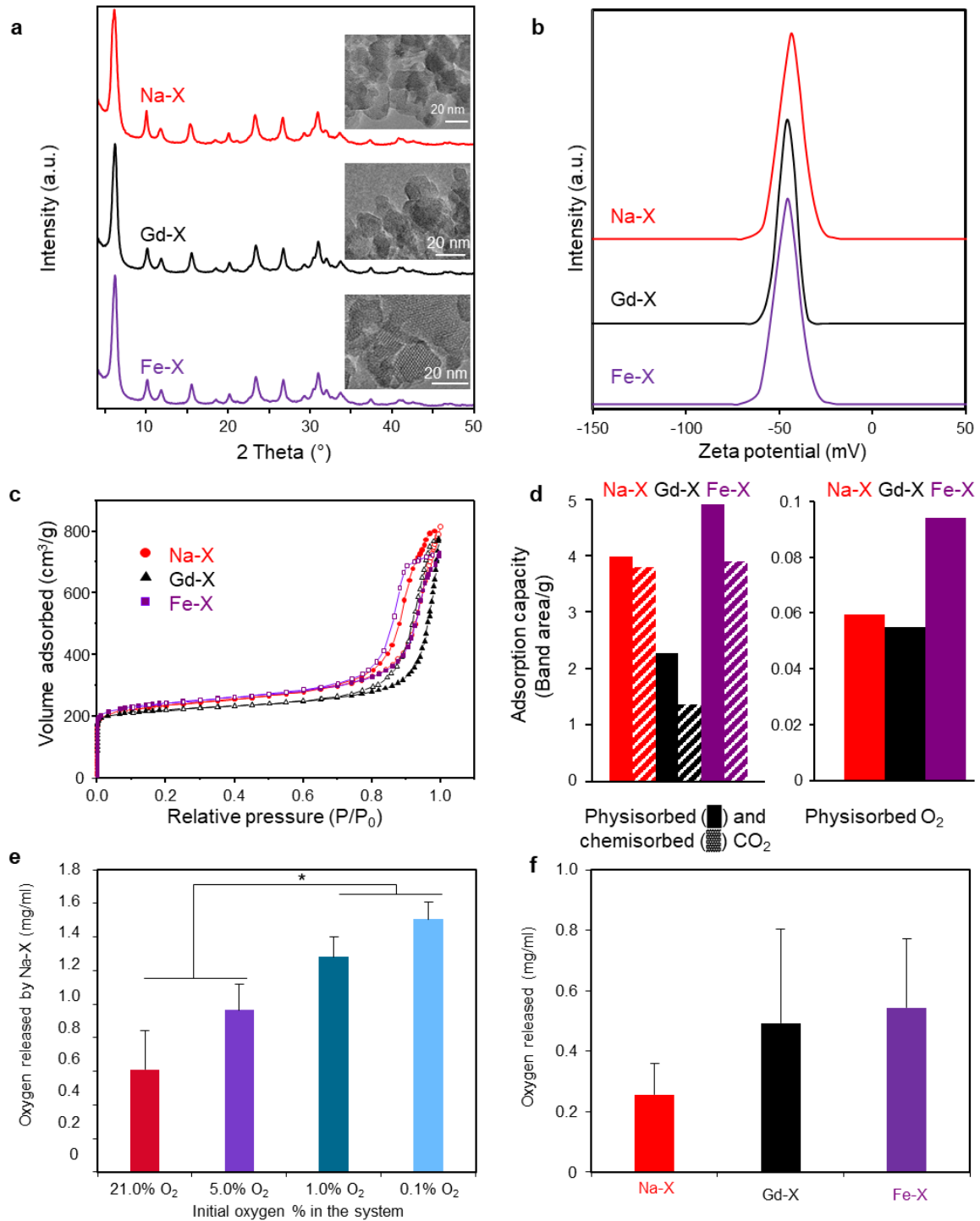
Figure 22. Main physicochemical properties of zeolite nanocrystals. a) XRD patterns (Inset: TEM images), b) zeta potential curves, c) nitrogen adsorption/desorption isotherms (full symbols refer to adsorption, open symbols refer to desorption) of nanosized Na-X, Gd-X, and Fe-X zeolite, d) physisorbed (full bars) and chemisorbed (shaded bars) CO_2 measured at 25 °C and physisorbed O_2 measured at -196 °C on nanosized Na-X, Gd-X, and Fe-X zeolites; Quantification of oxygen released from zeolites in a buffer solution (phosphate buffered saline, pH = 7.2, 37 °C) e) as a function of initial oxygen concentration of the solution and f) as a function of the charge balancing cation(*p<0.05; ANOVA). Mean ± s.d., n=3/condition.
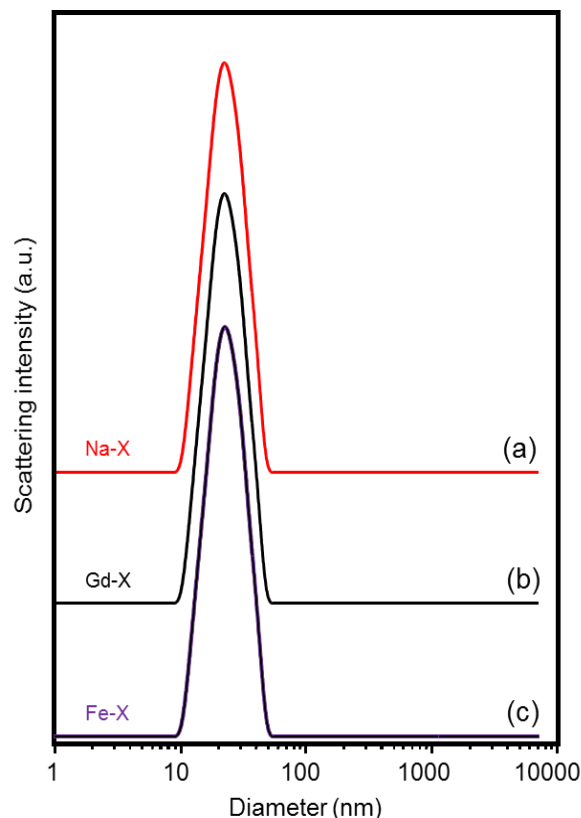
Figure 23. Dynamic Light Scattering (DLS) curves of a) as prepared (Na-X), b) gadolinium ion-exchanged (Gd-X) and c) iron ion-exchanged (Fe-X) zeolite samples.

Table 3. Summary of the main characteristics of nanosized FAU-X.

	Chemical composition (wt. %)					Size	Zeta potential	Half-life (blood)
	Si (wt. %)	Al (wt. %)	Na (wt. %)	Fe (wt. %)	Gd(wt. %)			
Na-X	18.10	14.59	13.41	0	0			
Gd-X	16.62	12.59	6.71	0	1.24	10-30 nm	-37.7 mV	12 min
Fe-X	17.6	14.35	11.96	1	0			

Table 4. BET specific surface area (S_{BET}), micropore volume (V_{mic}) and total pore volume (V_{total}) of as prepared (Na-X), gadolinium ion-exchanged (Gd-X) and iron ion-exchanged (Fe-X) zeolite samples.

	S_{BET} ($m^2.g^{-1}$)	V_{mic} ($cm^3.g^{-1}$)	V_{total} ($cm^3.g^{-1}$)
Na-X	777	0,29	1,26
Gd-X	738	0,27	1,25
Fe-X	798	0,28	1,15

The ability of nanosized zeolites to release their oxygen payload was investigated in aqueous solutions. Experiments were performed at various percentages of O_2 to mimic the oxygen gradients observed in the organism[39] and tumours.[40] The amount of O_2 released from the Na-X zeolites increased parallel to the decrease of the initial O_2 concentration in the

system. The release of O_2 from the zeolites was almost 56% more important at 0.1% O_2, mimicking severe hypoxia observed in some region of GB,[40] than at 5% of O_2, which corresponds to the O_2 percentage in the healthy brain (Figure 22e).[39] The O_2 release capacity of Na-X, Gd-X and Fe-X zeolite samples was then compared at 0.1% of O_2. To differentiate the quantity of oxygen provided by the zeolites from the oxygen provided by the dispersing solution (pure water), the values were deducted from the value of saturated water alone. Samples Na-X, Gd-X and Fe-X deliver to the system 0.26, 0.49 and 0.54 mg of oxygen per ml, respectively, as shown in Figure 22f. These results show that the Gd-X and Fe-X zeolites deliver more oxygen than the Na-X zeolite. Thus, Na-X, Gd-X and Fe-X zeolites transport 19, 37 and 41 mmol of O_2/g respectively, which is higher than the values recorded for HEMOXYCarrier®, a natural giant extracellular hemoglobin from polychaete annelids[41] and Polymer Hollow Microparticles (PHM)20. The HEMOXYCarrier® and PHM transport 0.0433 and 0.511 mmoles of O_2/g, respectively as reported. These results clearly show that the nanosized zeolites are appropriate gas carriers (CO_2 and/or O_2), and the type of the charge-balancing cation (Fe, Na or Gd) substantially modifies their gas affinity.

3.2 Assessment of potential toxicity of nanosized zeolites

Several studies have reported on the low toxicity of nanosized zeolites,[24,25,42] although possible adverse effects of zeolite nanocrystals have not been investigated, especially in the context of the brain. Moreover, the cations introduced in zeolites via post-synthesis treatment can have a great incidence on their toxic properties[22]. To verify that nanosized zeolites do not induce any *in vitro* cell damage, multiple cell types originating from various organs were exposed to zeolite suspensions (Na-X, Fe-X and Gd-X) with concentrations ranging from 1 µg/ml to 100 µg/ml for 48h (Figure 24a). Cell lines (mouse brain endothelial cells [bEnd.3], human glioma cells [U87-MG], and embryonic human kidney cells [HEK 293]) and primary culture (mouse astrocytes and neurons), theoretically more sensitive, were used. DLS measurements of the nanosized zeolites in the culture medium suggest no aggregation of the particles (data not shown).

No significant toxicity was observed for all cell lines and astrocytes (Figure 24a). Neurons appeared to be the most sensitive since the maximum loss in cell viability (65.8±2.1%) exposed to 100 µg/ml of Na-X was encountered (Figure 24a). The presence of gadolinium in sample Gd-X did not induce any further toxicity relative to the original Na-X or Fe-X zeolites

no matter the cell types and the concentrations used. These results show that a dramatic effect of nanosized zeolites on the cell viability is excluded.

To further analyze whether the nanosized zeolites are harmless on the cell cycle, we focused on cell lines, due to their high proliferative rates. The effect of nanosized zeolites (Na-X, Fe-X and Gd-X, 100 µg/ml) on the cell cycle of U87-MG and HEK 293 was assessed using flow cytometry after exposure for 14h and 48h; water was used as a control (Figure 24b). No difference in the cell distribution at different phases of cell cycle between the control group and cells exposed to nanosized zeolites was observed.

Some studies reported on a genotoxic effect of NP (30 nm) *in vitro* while showing no sign of cytotoxicity.[43] Consequently, a potential genotoxic effect of nanosized zeolites was investigated using an immunofluorescent labelling of γH2AX as a marker of DNA double strand breaks and a micronucleus formation assay as a marker of mitotic death. Both the U87-MG and HEK 293 cells were exposed to 100µg/ml zeolite suspensions for various times. The U87-MG cells showed almost no γH2AX positive cells for control conditions and after exposure to nanosized zeolites Na-X, Gd-X, and Fe-X. A slight decrease in the marker after 24h of experiment at all conditions was observed. HEK 293 cells exhibited a higher proportion of γH2AX positive cells compared to the U87-MG cells, and the percentage of γH2AX positive cells slightly increased after 24h and 72h. However, no change in the proportion of the γH2AX positive cells after exposure to the nanosized zeolites as compared to the control condition was detected (Figure 24c). These results are also supported by the micronuclei formation assay. In both the U87-MG and HEK 293 cells, the number of cells forming micronucleus was below 10%, which was not influenced by the experimental duration. Furthermore, no increase in the formation of micronuclei after exposure to the nanosized zeolites in comparison to the control sample was observed (Figure 244d). In terms of DNA damage, the results suggest that the Na-X, Fe-X and Gd-X nanosized zeolites do not have a genotoxic effect. Overall, the results clearly indicate an absence of cytotoxic and genotoxic effect of nanosized zeolite crystals in different cationic forms (Na-X, Fe-X and Gd-X) *in vitro* on a wide range of cell types.
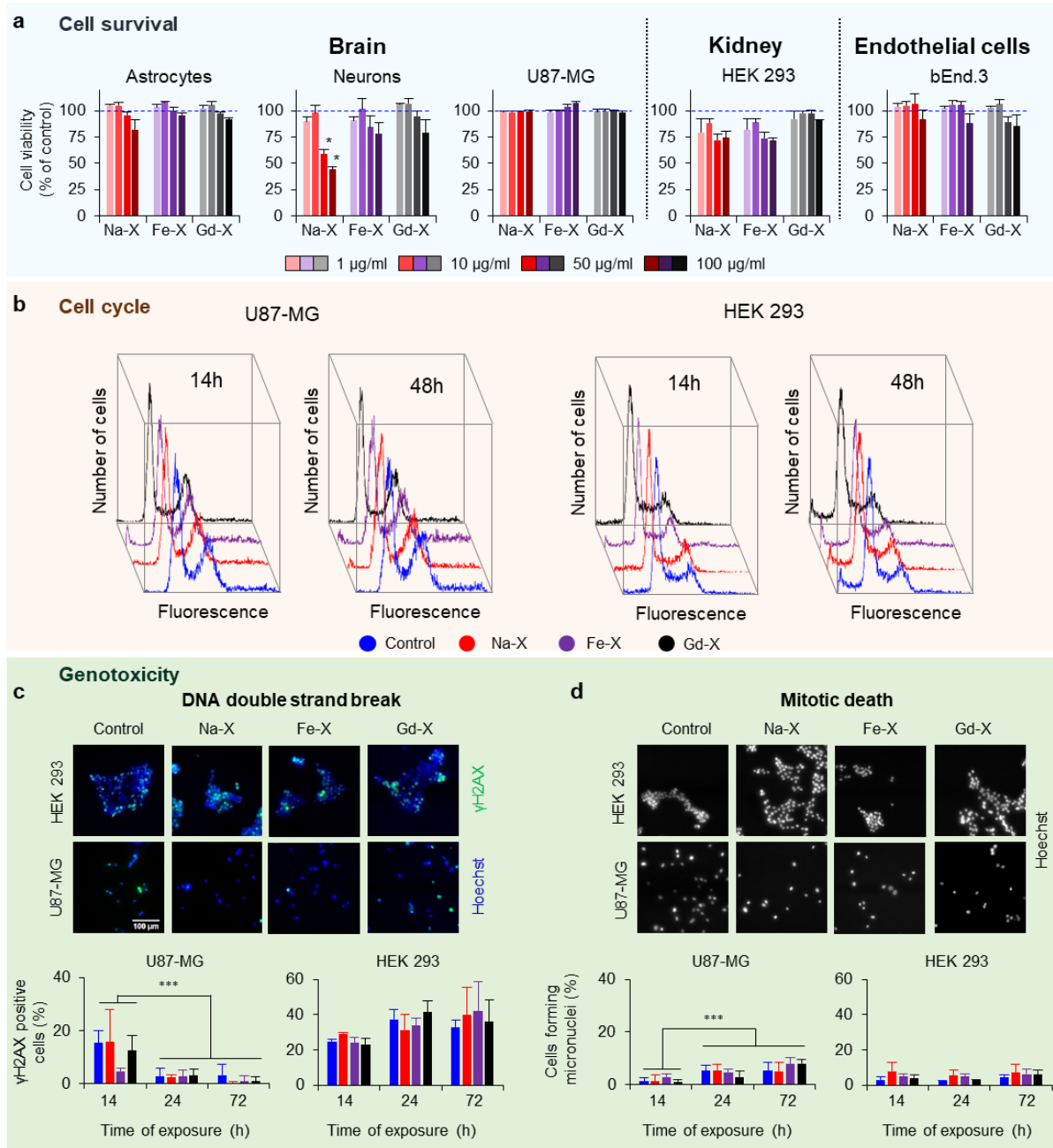
Figure 24. Nanosized zeolites show no sign of toxicity *in vitro*. a) Astrocytes, neurons, U87-MG, HEK 293 and bEnd.3 cells viability following a 48h exposure to nanosized zeolites with a concentration of 1, 10, 50 and 100 µg/ml. Mean ± s.d., n=3/condition; HSD Tuckey post-hoc test after a significant two-way ANOVA (*$p<0.05$ vs control, a significant dose effect vs control ($p<0.001$) is obtained for astrocytes (dose 100µg/ml), neurons (dose 50 and 100µg/ml), bEnd.3 (dose 100µg/ml) and HEK 293 cells (dose 100 µg/ml)); b) Cell cycle analysis by flow cytometry. Representative profiles from 3 independent experiments of U87-MG and HEK 293 cells distribution in the phases of cell cycle after 14 or 48h exposure to 100 µg/ml of Na-X, Fe-X, Gd-X or water as a control; c, d) Representative photographs of DNA double-strand breaks identified with γH2AX immunostaining (c) and micronuclei formation identified with Hoechst 33342 staining (d) on U87-MG and HEK 293 cells, 14h (c) and 72h (d) after exposure to 100 µg/ml of zeolites. Quantification after 14, 24 or 72h exposure to 100 µg/ml of zeolites. The proportion of γH2AX and micronuclei positive cells was measured relative to total cell number counted by Hoechst 33342 staining. Mean ± s.d., n=3 (3 independent experiments, 1 coverslip for each experiment, 5 representative fields per coverslip). HSD Tuckey post-hoc test after a significant two-way (*$p<0.001$; ANOVA).

3.3 Toxicity of nanosized zeolites in living animals

The potential adverse effects associated with a chronic injection of nanosized zeolites *in vivo* were studied. The nanosized zeolites (both Na-X and Gd-X) were injected into mice for five consecutive days, for a total dose of 5 mg per mouse (Figure 25a). The weight curves of the animals did not encounter a relevant change compared to controls (injection of water). Independently from the group considered, mice gained 7g (37% of their initial weight) during the time of the experiment. These results suggest no adverse effects of nanosized zeolites on rodents.

Although rodent models are helpful to understand the pathophysiology and test treatments of human diseases, more relevant animal models are needed to reflect the adverse responses seen in humans. In this respect, Chiarelli *et al.* recently demonstrated the importance of using both rodents and non-human primates for further evaluation of NP.[44]

To further confirm the low toxicity of the nanosized zeolites, the Gd-X suspension was injected intravenously (300 µl, 1% wt.) to non-human primates, and physiology was monitored especially for arterial pressure (AP). A slight decrease in arterial pressure was observed following the injection, from 63 mmHg to 42 mmHg, nevertheless, it was fully reversed in less than 2 min (Figure 25b). These results clearly demonstrate the absence of acute and chronic toxicity of zeolites nanocrystals applied to living animals.
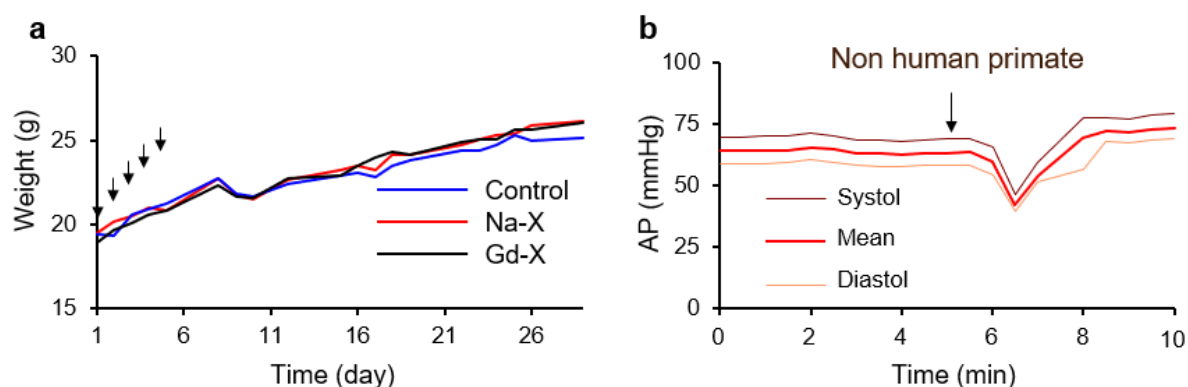
Figure 25. Assessment of toxicity of nanosized zeolites *in vivo*. a) Weight curves of mice following intraperitoneal injections of Na-X and Gd-X zeolites or water as a control during 5 consecutive days (represented with arrows). Mean, n=4 per group; b) Arterial pressure (AP) of a marmoset after i.v. injection of nanosized Gd-X zeolite carrying CO_2 (arrow indicates the time of injection). Representative example from three independent experiments.

3.4 In vivo detection of nanosized zeolites in rat bearing brain tumours

Taking advantage of the presence of Gd, we then assessed whether intravenously injected zeolites could have the ability to reach brain tumours. A previous study showed that nanosized zeolites are likely to extravasate and accumulate in the tumour tissue but do not cross the intact blood-brain barrier.[45] To verify this assumption, dynamic T1-weighted MRI was used to analyze the distribution of Gd-X zeolite nanocrystals in the brain after an i.v. injection. A hyper-signal appearing specifically inside the tumour was detected (Figure 26a and 26b). The difference between the T1-w images acquired before and after the injection confirms that the Gd-X zeolite nanocrystals efficiently reached the tumour and not the surrounding healthy tissue (Figure 26a). The maximum increase in the signal (3.67 ±3.04 %) was reached ≈100 sec after the injection (Figure 26b). The specific delivery of the Gd-X zeolite nanocrystals in the brain tumor was confirmed.

It is important to note that even if low concentrations of gadolinium are observed in the zeolite nanocrystals (1.24 wt.%, Table 3), it remains detectable by MRI. Indeed, the r1 parameter of the Gd-X nanosized zeolites (measured at 7 tesla and room temperature) was 74.2 mM^{-1}.s $^{-1}$, which is higher than Dotarem$^{®}$ (4.03 mM^{-1}.s^{-1}). This ~20-fold increase in r1 for the Gd-X zeolite as compared to standard Gd-based contrast agents has already been discussed by Csajbok *et al*. The structure of the zeolites allows water molecules to diffuse into its pores and cages, where Gd^{3+} ions are immobilized. Therefore, zeolites can be considered as a concentrated aqueous solution of Gd^{3+} that is exchanged by diffusion with the bulk water outside the zeolite.[35] This finding is important as it concerns the stability of gadolinium chelates complex currently in use, which is linked to suspected adverse effects in various tissues including the brain.[46] Gd-containing zeolites were already considered as MRI contrast agent and showed no leakage of Gd outside the framework.[35,47] Together, these findings indicate that T1-weighted MRI can efficiently be performed using Gd-X as contrast agent to visualize the tumour area.
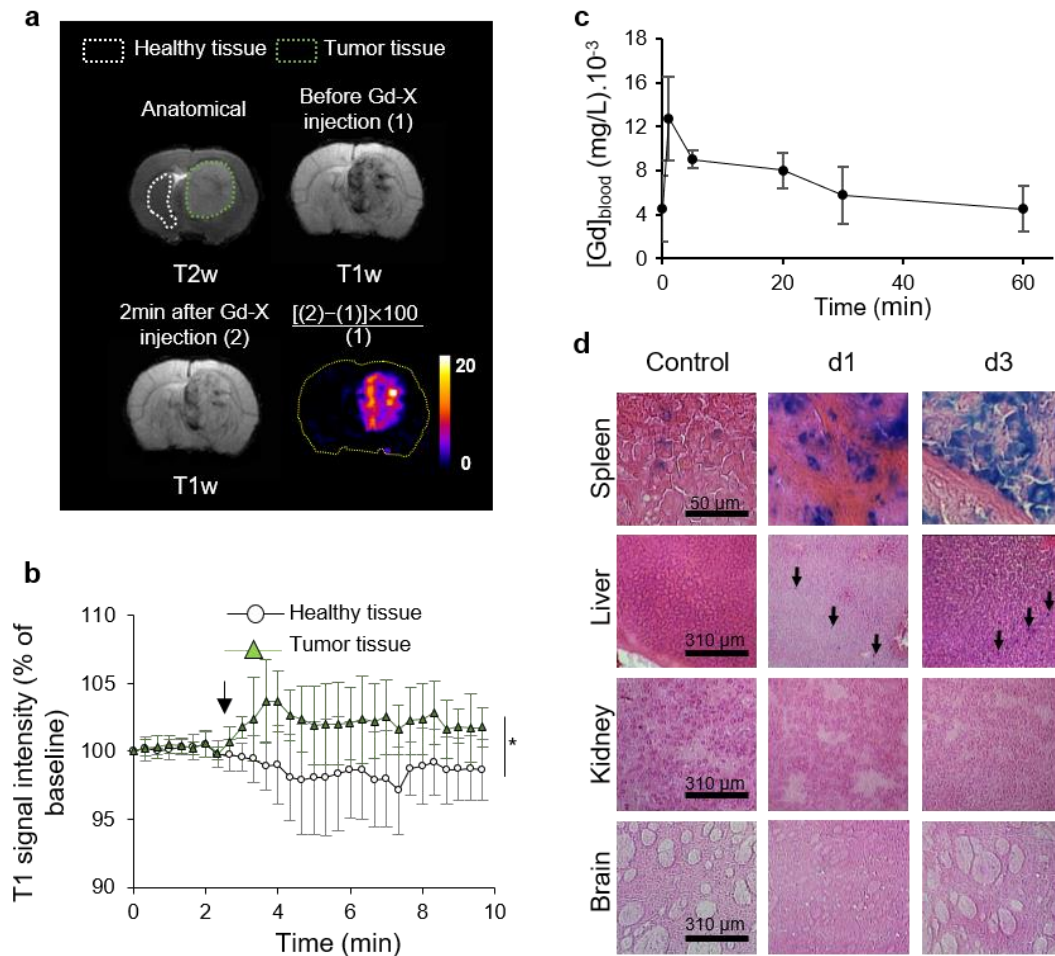
Figure 26. Bio-distribution of nanosized zeolites in rats. a) Representative T1-w images acquired before (1) or 2 min after (2) iv injection of Gd-X (300 µl, 1% wt.); T2w anatomic image (left) and a map of the differences between the two T1w images (right); b) Corresponding quantification of the normalized T1w signal intensity in the healthy and the tumor tissue. Baseline refers to measurement of T1w signal performed before injection and arrow indicates the time of injection. Mean ± s.d., n=5. (*p<0.0001; two-way ANOVA). See also the video in Supplementary Information; c) Quantitative measurement of gadolinium content in the blood versus time following i.v. injection of Gd-X (300 µl, 1% wt.). Mean ± s.d., n=4; d) Perl's staining after eosin counterstaining on spleen, liver, kidney and brain sections taken from a control rat, and 1 (d1) and 3 (d3) days from the injection of nanosized Fe-X zeolite. Blue spots indicate iron. Representative example from three independent experiments.

3.5 Bio-distribution of nanosized zeolites in healthy rats

After showing that nanosized zeolites could target the tumors, we were also aware that these nanoparticles could reach other organs after circulating into the bloodstream. First, Gd-X zeolite suspensions were intravenously injected in healthy rats, and blood samples were collected prior and after various times after the injection. The quantification of the Gd-X zeolite nanoparticles in the blood was performed through the characterization of gadolinium content with ICP-MS (Figure 26c). The blood half-life of Gd-X zeolite nanocrystals was calculated to be approximately 12 min.

To further characterize the bio-distribution, Fe-X zeolites were used; enabling detection in the tissues using Perl's staining. Histological analyzes revealed that once cleared from the blood, the Fe-X zeolites injected are accumulated preferentially in the spleen and the liver. In contrast, no accumulation of the Fe-X zeolite was detected in the healthy brain as expected,[45] and confirming our results with Gd-X, and the kidneys (Figure 26d). These results are consistent with published results, given the size and charge of the nanosized zeolites (Table 3).[48]

Based on these findings, we hypothesized that the nanosized zeolites specifically accumulated in the tumor tissue and not in the normal brain, which could be used to deliver hypercapnic/hyperoxic gases.

3.6 Nanosized zeolites as gas carriers to specifically target brain tumors

Multiparametric MRI in a human GB model was used to evaluate the functional benefits of nanosized zeolite particles as gas (CO_2 and O_2) carriers. Contrary to Gd-X zeolite, Fe-X zeolite could not be considered for the experimental setup due to interference with MR signal, particularly for the measure of both cerebral CBV and tissue saturation in oxygen ($SatO_2$), which lies on the use of another iron-based contrast agent (P904). On the other hand, Fe-X shows a superior activity in gas adsorption and release compared to the Gd-X zeolite and would be of interest for therapeutic application. Consequently, the Gd-X was applied to assess the potential theranostic application of zeolite nanoparticles as a gas carrier. The changes in cerebral blood volume (CBV) after an intravenous (i.v.) injection of the Gd-X zeolites loaded with CO_2 was quantified as readout of vasodilation and expressed as ΔCBV. Results revealed an increase in the CBV inside the tumor compared to the healthy tissue (Figure 27a, b), leading to a difference of 15% between the two tissues after 15 min from the injection

($\Delta\Delta$CBV). Water saturated with CO_2 was used as a control sample, and a difference of 5% of the CBV in the tumor compared to the healthy tissue was measured (Figure 27a, b). These results are at the opposite of those obtained in our previous study, where the breathing of pure carbogen led to an increase in the CBV and the oxygenation in the healthy brain but not in the tumor.[9] Upon replacing the pure CO_2 with carbogen (5% CO_2 and 95% O_2; used as hyperoxic/hypercapnic mixture) for targeting simultaneously the CBV and the tissue oxygenation, the difference of signal measured between the healthy and tumor tissues was 5.36% (Figure 27a, c).

The $SatO_2$, a method previously demonstrated to accurately reflect tissue hypoxia,[49] was quantified before and after injection of the Gd-X zeolite carrying CO_2 or carbogen and expressed as $\Delta SatO_2$. The possible re-oxygenation of the tumor relative to the healthy tissue ($\Delta\Delta SatO_2$) was measured (Figure 27a, b, c). The injection of Gd-X zeolite carrying CO_2 and carbogen resulted in a $\Delta\Delta SatO_2$ increase of 6.43% and 2.07%, respectively. An additional control was performed by injecting Gd-X zeolites (300 µl, 1 wt.%) without gas loading. No increase in CBV or $SatO_2$ was observed, supporting the idea that the changes are induced by the delivered gas and not by the presence of zeolite nanoparticles.

The lower effect observed with carbogen suggest that the primary effect is an increased perfusion via vasodilatory effects of CO_2 and not reoxygenation via oxygen delivery. However, the U87 GB model used is moderately hypoxic. Indeed, our previous studies showed that U87 tumors are devoid of any sign of hypoxia and exhibit an oxygen pressure level similar to the contralateral brain (~5% O_2)[50,51]. The results herein show that the delivery of oxygen by the zeolites is dependent on the oxygen pressure of the environment (Figure 22e). Therefore, the relatively high oxygen pressure in the tumor could prevent the zeolites from releasing their oxygen payload.

We finally assessed whether a small release of CO_2 could also occur in the systemic circulation by monitoring the arterial partial pressure of CO_2 ($PaCO_2$) after the i.v. injection of the Gd-X loaded with CO_2 (Figure 27d). The $PaCO_2$ increased by 4 mmHg reaching a peak after 10 min, consistent with the blood half-life of the nanosized zeolites (Figure 26c), paralleled by a slight acidification, i.e., the pH decreased from 7.53 to 7.36 (Figure 27e). Such a change was not measured in the experiment carried out with the control sample. This increase in the $PaCO_2$ could lead to a vasodilation. Consequently, dynamic BOLD-MRI was performed to track the changes in blood flow of large vessels, such as the venous sinus. The i.v. injection of nanosized zeolites carrying CO_2 resulted in the increase in the BOLD signal

up to $5.05 \pm 6.50\%$ as did inhalation of 5% CO_2. Injection of control sample or pure nanosized zeolites without CO_2 did not show any effect (Figure 27f).

Overall, the results show the ability of nanosized zeolites to carry CO_2 or carbogen resulting in functional effects on blood volume and oxygenation within the tumor tissue.
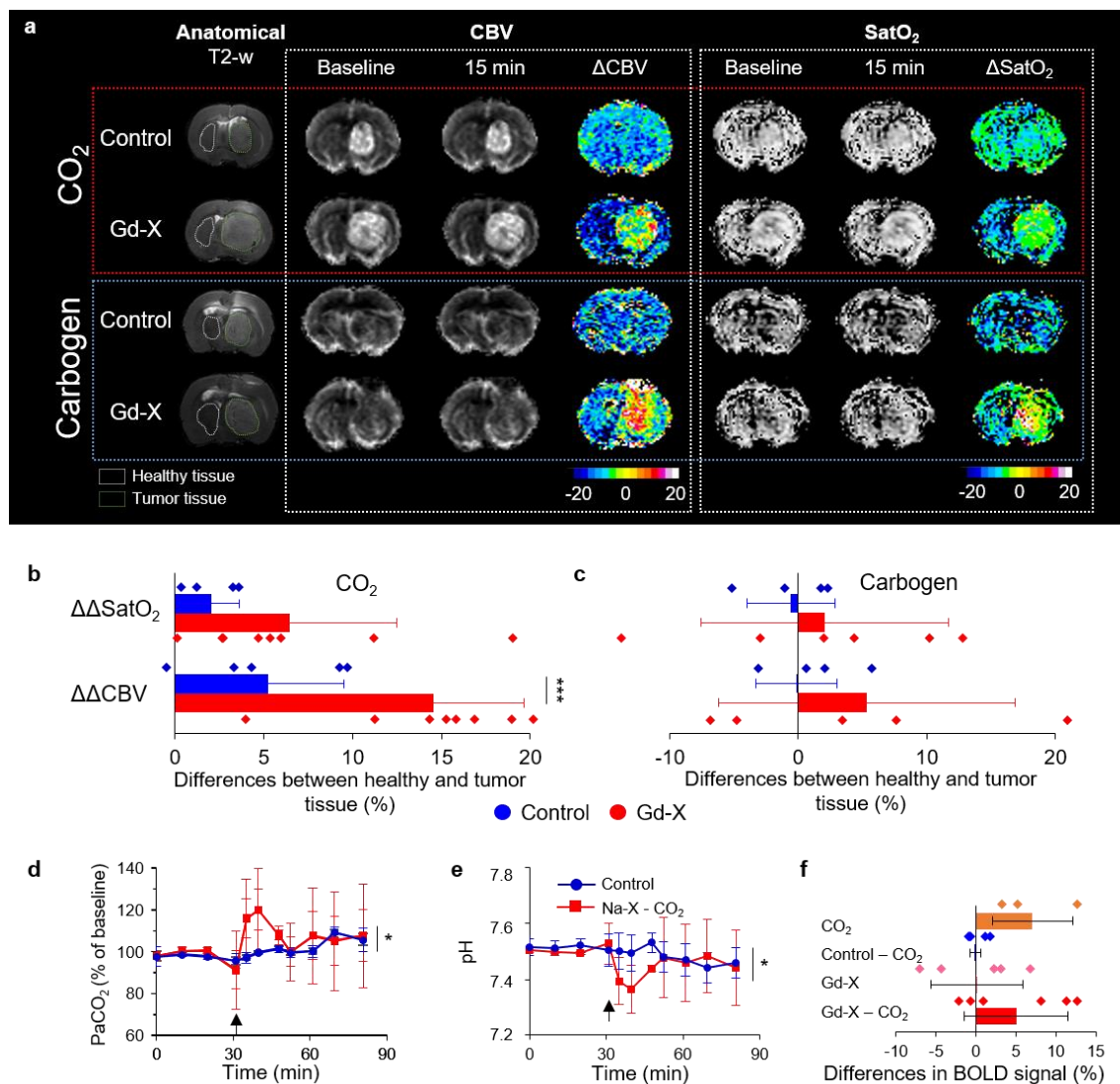

Figure 27. Nanosized zeolites carrying hyperoxic gases influence CBV and $SatO_2$ in the tumor. a) Representative T2-w anatomic images, CBV and $SatO_2$ maps obtained before and 15 min after i.v. injection of nanosized Gd-X zeolite (300 µl, 1% wt.) carrying CO_2 or carbogen and the corresponding differences between the two maps (ΔCBV and $\Delta SatO_2$, respectively). Control consisted of injection of H_2O saturated with CO_2 or carbogen; b) c) Quantification of the differences of ΔCBV and $\Delta SatO_2$ (%) between the healthy and the tumor tissue ($\Delta\Delta$CBV and $\Delta\Delta SatO_2$, respectively). Mean $\pm$ s.d. and dot-plot, n=5 for control group; n=8 for Gd-X with CO_2 group; n=5 for Gd-X with carbogen group (***p<0.001; ANOVA); d) Evolution of the arterial pressure of CO_2 ($PaCO_2$) expressed in percentage of baseline and e) pH in the blood of healthy Wistar rats following injection of Gd-X (300 µl, 1% wt.) carrying CO_2 or control. Baseline refers to measurement of $PaCO_2$ performed before injection and arrow indicates the time of injection. Mean $\pm$ s.d. and dot-plot, n=5 per group (*p<0.05; two-way ANOVA); f) Differences in Blood Oxygen Level Dependent (BOLD) signal measured in the venous sinus of healthy Wistar rats before and 3 min after an i.v. injection of Gd-X (300 µl, 1% wt.) carrying CO_2, or control or Gd-X without CO2 or breathing of 5% of CO_2. Mean $\pm$ s.d. and dot-plot, n=6 for Gd-X – CO_2 group; n=5 for Gd-X group; n=4 for control – CO_2 group; n=3 for inhalation of 5% CO_2 group.

4 Conclusions

The use of nanosized zeolite particles as a specific hyperoxic gas carrier to increase both the blood volume and the oxygen supply for re-oxygenation of glioblastoma tumors was studied. MRI was used to screen the resulting effect of the gases. The nanosized zeolites loaded with CO_2 or carbogen (95% O_2 and 5% CO_2) successfully increased the blood volume and oxygenation in the tumor tissue relative to the healthy tissue. Additionally, the low amount of Gd introduced in the zeolite nanoparticles allows tracking the specific accumulation of nanosized zeolite crystals in the tumor with MRI.

The results show that the quantity of oxygen released from the zeolites is more important as the external oxygen pressure is low. Interestingly, it can be assumed that in an organism, the zeolite would keep its oxygen payload until it reaches a hypoxic region, like in GB, where they would release the oxygen.

The limited toxicity of nanosized zeolites was confirmed by *in vitro* and *in vivo* experiments. Therefore, the great potential of nanosized zeolites as a theranostic tool is envisioned. Currently, nanoparticles containing gadolinium are undergoing a phase I clinical trial as a theranostic tool to increase the efficiency of radiotherapy.[14] This opens the door to the use of carbogen-loaded Gd-containing zeolite nanocrystal to the tumor site, as a carrier of (i) high-Z containing elements and (ii) re-oxygenating gases, which are known to increase the efficiency of radiotherapy. The results evidently demonstrate the development of original strategy (theranostic tool) using metal-modified nanosized zeolites to target specifically brain tumors.

5   References

[1]   D.N. Louis, A. Perry, G. Reifenberger, A. von Deimling, D. Figarella-Branger, W.K. Cavenee, H. Ohgaki, O.D. Wiestler, P. Kleihues, D.W. Ellison, Acta Neuropathol. 131 (2016) 803–820.

[2]   O.L. Chinot, W. Wick, W. Mason, R. Henriksson, F. Saran, R. Nishikawa, A.F. Carpentier, K. Hoang-Xuan, P. Kavan, D. Cernea, A.A. Brandes, M. Hilton, L. Abrey, T. Cloughesy, N. Engl. J. Med. 370 (2014) 709–722.

[3]   A. Chakhoyan, J.-S. Guillamo, S. Collet, F. Kauffmann, N. Delcroix, E. Lechapt-Zalcman, J.-M. Constans, E. Petit, E.T. MacKenzie, L. Barré, M. Bernaudin, O. Touzani, S. Valable, Sci. Rep. 7 (2017).

[4]   S.M. Evans, K.W. Jenkins, H.I. Chen, W.T. Jenkins, K.D. Judy, W.-T. Hwang, R.A. Lustig, A.R. Judkins, M.S. Grady, S.M. Hahn, C.J. Koch, Transl. Oncol. 3 (2010) 160–169.

[5]   K.L. Eales, K.E.R. Hollinshead, D.A. Tennant, Oncogenesis 5 (2016) e190.

[6]   W.R. Wilson, M.P. Hay, Nat. Rev. Cancer 11 (2011) 393–410.

[7]   J.H. Kaanders, J. Bussink, A.J. Van der Kogel, Lancet Oncol. 3 (2002) 728–737.

[8]   R.W.M. van der Maazen, H.O.M. Thijssen, J.H.A.M. Kaanders, A. de Koster, A. Keyser, M.J.J. Prick, J.A. Grotenhuis, P. Wesseling, A.J. van der Kogel, Radiother. Oncol. 35 (1995) 118–122.

[9]   A. Chakhoyan, A. Corroyer-Dulmont, M.M. Leblond, A. Gérault, J. Toutain, L. Chazaviel, D. Divoux, E. Petit, E.T. MacKenzie, F. Kauffmann, N. Delcroix, M. Bernaudin, O. Touzani, S. Valable, J. Cereb. Blood Flow Metab. 37 (2016) 2270–2282.

[10]   H. Maeda, H. Nakamura, J. Fang, Adv. Drug Deliv. Rev. 65 (2013) 71–79.

[11]   S.C. Baetke, T. Lammers, F. Kiessling, Br. J. Radiol. 88 (2015) 20150207.

[12]   N.Y. Hernández-Pedro, E. Rangel-López, R. Magaña-Maldonado, V.P. de la Cruz, A. Santamaría del Angel, B. Pineda, J. Sotelo, Biomed Res. Int. 2013 (2013).

[13]   Y. Dou, X. Li, W. Yang, Y. Guo, M. Wu, Y. Liu, X. Li, X. Zhang, J. Chang, ACS Appl. Mater. Interfaces 9 (2017) 1263–1272.

[14]   S. Kotb, A. Detappe, F. Lux, F. Appaix, E.L. Barbier, V.-L. Tran, M. Plissonneau, H. Gehan, F. Lefranc, C. Rodriguez-Lafrasse, C. Verry, R. Berbeco, O. Tillement, L. Sancey, Theranostics 6 (2016) 418–427.

[15]   A.R. King, C.D. Corso, E.M. Chen, E. Song, P. Bongiorni, Z. Chen, R.K. Sundaram, R.S. Bindra, W.M. Saltzman, Mol. Cancer Ther. 16 (2017) 1456–1469.

[16]   X. Tian, H. Lara, K.T. Wagner, S. Saripalli, S.N. Hyder, M. Foote, M. Sethi, E. Wang, J.M. Caster, L. Zhang, A.Z. Wang, Nanoscale 7 (2015) 20211–20219.

[17]   J. Xie, Y. Yong, X. Dong, J. Du, Z. Guo, L. Gong, S. Zhu, G. Tian, S. Yu, Z. Gu, Y. Zhao, ACS Appl. Mater. Interfaces 9 (2017) 14281–14291.

[18]   J. Chen, Q. Chen, C. Liang, Z. Yang, L. Zhang, X. Yi, Z. Dong, Y. Chao, Y. Chen, Z. Liu, Nanoscale 9 (2017) 14826–14835.

[19]   Y. Sheng, H. Nesbitt, B. Callan, M.A. Taylor, M. Love, A.P. McHale, J.F. Callan, J. Control. Release Off. J. Control. Release Soc. 264 (2017) 333–340.

[20] R.P. Seekell, A.T. Lock, Y. Peng, A.R. Cole, D.A. Perry, J.N. Kheir, B.D. Polizzotti, Proc. Natl. Acad. Sci. 113 (2016) 12380–12385.

[21] X. Guo, J. Qu, C. Zhu, W. Li, L. Luo, J. Yang, X. Yin, Q. Li, Y. Du, D. Chen, Y. Qiu, Y. Lou, J. You, Drug Deliv. 25 (2018) 585–599.

[22] C. Anfray, B. Dong, S. Komaty, S. Mintova, S. Valable, ACS Appl. Mater. Interfaces (2017).

[23] V. Georgieva, C. Anfray, R. Retoux, V. Valtchev, S. Valable, S. Mintova, Microporous Mesoporous Mater. 232 (2016) 256–263.

[24] S. Laurent, E.-P. Ng, C. Thirifays, L. Lakiss, G.-M. Goupil, S. Mintova, C. Burtea, E. Oveisi, C. Hébert, M. de Vries, M.M. Motazacker, F. Rezaee, M. Mahmoudi, Toxicol. Res. (Camb). 2 (2013) 270–279.

[25] L.C.J. Thomassen, D. Napierska, D. Dinsdale, N. Lievens, J. Jammaer, D. Lison, C.E.A. Kirschhock, P.H. Hoet, J.A. Martens, Nanotoxicology 6 (2012) 472–485.

[26] T. Kihara, Y. Zhang, Y. Hu, Q. Mao, Y. Tang, J. Miyake, J. Biosci. Bioeng. 111 (2011) 725–730.

[27] M.M. Tsotsalas, K. Kopka, G. Luppi, S. Wagner, M.P. Law, M. Schäfers, L. De Cola, ACS Nano 4 (2010) 342–348.

[28] M. Tsotsalas, M. Busby, E. Gianolio, S. Aime, L. De Cola, Chem. Mater. 20 (2008) 5888–5893.

[29] O. Martinho, N. Vilaça, P.J.G. Castro, R. Amorim, A.M. Fonseca, F. Baltazar, R.M. Reis, I.C. Neves, RSC Adv. 5 (2015) 28219–28227.

[30] L. Maggini, I. Cabrera, A. Ruiz-Carretero, E.A. Prasetyanto, E. Robinet, L. De Cola, Nanoscale 8 (2016) 7240–7247.

[31] R. Marega, E.A. Prasetyanto, C. Michiels, L. De Cola, D. Bonifazi, Small 12 (2016) 5431–5441.

[32] M. Zaarour, B. Dong, I. Naydenova, R. Retoux, S. Mintova, Microporous Mesoporous Mater. 189 (2014) 11–21.

[33] S. Mintova, M. Jaber, V. Valtchev, Chem. Soc. Rev. 44 (2015).

[34] D.G. Seifu, T.T. Isimjan, K. Mequanint, Acta Biomater. 7 (2011) 3670–3678.

[35] E. Csajbók, I. Bányai, L. Vander Elst, R.N. Muller, W. Zhou, J.A. Peters, Chemistry 11 (2005) 4799–4807.

[36] H. Awala, J.P. Gilson, R. Retoux, P. Boullay, J.M. Goupil, V. Valtchev, S. Mintova, Nat. Mater. 14 (2015).

[37] N. Vilaça, R. Amorim, A.F. Machado, P. Parpot, M.F.R. Pereira, M. Sardo, J. Rocha, A.M. Fonseca, I.C. Neves, F. Baltazar, Colloids Surfaces B Biointerfaces 112 (2013) 237–244.

[38] D. Bonenfant, M. Kharoune, P. Niquette, M. Mimeault, R. Hausler, Sci. Technol. Adv. Mater. 9 (2008).

[39] M.Y. Koh, G. Powis, Trends Biochem. Sci. 37 (2012) 364–372.

[40] H. Kempf, M. Bleicher, M. Meyer-Hermann, PLoS One 10 (2015) e0133357.

[41] T. Le Gall, V. Polard, M. Rousselot, A. Lotte, M. Raouane, P. Lehn, P. Opolon, E.

Leize, E. Deutsch, F. Zal, T. Montier, J. Biotechnol. 187 (2014) 1–9.

[42] K. Bhattacharya, P.C. Naha, I. Naydenova, S. Mintova, H.J. Byrne, Toxicol. Lett. 215 (2012) 151–160.

[43] N. Bayat, V.R. Lopes, J. Schölermann, L.D. Jensen, S. Cristobal, Biomaterials 63 (2015) 1–13.

[44] P.A. Chiarelli, R.A. Revia, Z.R. Stephen, K. Wang, M. Jeon, V. Nelson, F.M. Kievit, J. Sham, R.G. Ellenbogen, H.-P. Kiem, M. Zhang, ACS Nano 11 (2017) 9514–9524.

[45] A. Karageorgis, S. Dufort, L. Sancey, M. Henry, S. Hirsjärvi, C. Passirani, J.-P. Benoit, J. Gravier, I. Texier, O. Montigon, M. Benmerad, V. Siroux, E.L. Barbier, J.-L. Coll, Sci. Rep. 6 (2016).

[46] M. Rogosnitzky, S. Branch, BioMetals 29 (2016) 365–376.

[47] S.W. Young, F. Qing, D. Rubin, K.J. Balkus, J.S. Engel, J. Lang, W.C. Dow, J.D. Mutch, R.A. Miller, J. Magn. Reson. Imaging JMRI 5 (1995) 499–508.

[48] H. Kobayashi, R. Watanabe, P.L. Choyke, Theranostics 4 (2014) 81–89.

[49] T. Christen, B. Lemasson, N. Pannetier, R. Farion, C. Segebarth, C. Rémy, E.L. Barbier, NMR Biomed. 24 (2011) 393–403.

[50] S. Valable, A. Corroyer-Dulmont, A. Chakhoyan, L. Durand, J. Toutain, D. Divoux, L. Barré, E.T. MacKenzie, E. Petit, M. Bernaudin, O. Touzani, E.L. Barbier, J. Cereb. Blood Flow Metab. Off. J. Int. Soc. Cereb. Blood Flow Metab. (2016).

[51] A. Corroyer-Dulmont, E.A. Pérès, E. Petit, L. Durand, L. Marteau, J. Toutain, D. Divoux, S. Roussel, E.T. MacKenzie, L. Barré, M. Bernaudin, S. Valable, Biol. Chem. 394 (2013).

Chapter 5- Copper containing FAU nanozeolite as non-toxic nitric oxide and carbon dioxide gas carrier

Abstract

Nowadays, the growing interest to find the efficient nitric oxide (NO) and carbon dioxide (CO_2) gas carriers to prevent life treating conditions is a challenging matter. This is mainly due to the carrier material specificity and toxicity concerns. The gas adsorption properties of sodium- (Na-X) and copper-(Cu-X) containing FAU nanozeolite towards NO and CO_2 were studied. The materials were characterised using various characterisation techniques, namely XRD, TEM, ICP, DLS and *in-situ* FTIR. The as prepared Na-X showed better gas adsorption affinity towards carbon dioxide, whereas the ion-exchanged Cu-X was more efficient absorbent with regards to nitric oxide. In addition, the cytotoxicity tests disclosed that both nanozeolites show no toxicity making them suitable for further tests in biomedical field.

1 Introduction

The well-established activity of copper containing zeolites with nitric oxide (NO) and carbon dioxide (CO_2) have proved their functionality mainly as a de-NOx catalyst, where the zeolites are used to perform selective catalytic reduction of nitric oxide (NO)[1–3], as well as CO_2 adsorbent for gas separation in industrial and environmental processes.[4,5] Keeping that in mind, we will exploit other cases where zeolites can be employed to act as NO and CO_2 gas carriers for potential biomedical applications.

NO is an antibacterial, principal signalling molecule (generated within the body), that is involved in many biological processes, namely regulation of the blood flow, neurotransmission and immune response.[6–8] CO_2 is the essential moderator in human physiology, controlling blood circulation and pH. Besides, when inhaled in form of carbogen (mixture of O_2 95% and 5 % CO_2), it causes tissue oxygenation, which is important stage in tumour treatments.[9,10] The extrinsic delivery of such biologically active molecules is an interesting and challenging way of therapy that could potentially be an effective remedy for major illnesses. However, the broad range of effects generated in the body by these two gases raised an issue about its specificity and targeted delivery, which complicated the progress for their applications in biomedicine. Therefore, to overcome those uncertainties the development

of selective and most importantly non-toxic materials that can carry and release therapeutic gases is required.

Nowadays, there is a growing interest in finding suitable NO carriers to prevent life perilous conditions such as thrombosis (blood clot formation), at the surface of artificial blood vessels and medical devices. Currently, anticoagulants such as heparin are employed to fight thrombosis, however, the use of latter can cause an unexpected bleeding in other parts of the body, leading to loss of platelets and thus thrombocytopenia.[11] In case of carbogen administration, the inhalation via nasal cannula or facemask showed insufficiency on tissue reoxygenation in terms of progressive response to radio therapy.[12] As a result, a vast number of NO- and CO_2-carrying materials have been proposed, which are mainly based on synthetic polymers (PVC, PDMS) and fumed silica particles. For NO delivery purposes those materials have been functionalised with various amines, and upon reaction with NO, they form diazeniumdiolate ions. The latter, can hydrolyse in aqueous solution with suitable pH to release nitric oxide and thus act as a gas donor.[13–17] Over the years, it has been demonstrated that zeolites (inorganic, crystalline, porous materials) have high adsorption capacity towards NO and CO_2 [18–21]. This is due to their characteristics, namely, well-defined porous structure, high specific surface area and chemical/thermal stability.[22,23] Additionally, the chemical properties of zeolites, enable to control the gas adsorption capacity, which can be accomplished by tuning the zeolite composition, in terms of the type of metal ion present in the structure. The introduction of various cations (Fe^{3+}, Ce^{3+} Cu^{2+}, Gd^{3+}) in the zeolite is usually achieved via post-synthetic ion-exchange, to further functionalise the material for targeted application.[24,25] Other aspects influencing the gas sorption affinity are the zeolite physical features, such as size and framework type (more than 239), providing a great array of structures to choose from depending on desired use.

The zeolite toxicity plays a major role when it comes to biomedical applications. The modifications of zeolite crystal size, from micron to nanoscale, as well as development of template-free synthesis, yielded nanozeolites biocompatible become of important research field. The cytotoxicity of nanozeolites does not just depend on crystal size but also on particle agglomeration and stability in colloidal suspension. As a result of their low toxicity towards the most sensitive cells (astrocytes), nanocrystals have drawn particular attention of researches working in the field of biomedical science, especially for controlled drug,[26–28] and gas delivery purposes.[25,29,30] Moreover, it has recently been reported that the copper containing FAU nanozeolite (in form of stable suspension), can be used for direct sanitisation

of medical surfaces against ESKAPE bacteria and thus act as antimicrobial agent to prevent life threatening infections.[31]

Here, we report the preparation of sodium and copper containing FAU-type nanozeolite (zeolite X) with high sorption capacity towards NO and CO_2, which can be used as alternative way of gas delivery for biomedical applications. The sorption affinity of as prepared Na-containing FAU (Na-X) and Cu ion-exchanged zeolite (Cu-X) to NO and CO_2 was characterized by *in-situ* IR spectroscopy. Moreover, the cytotoxicity tests using a selection of cells, including, human tumour, kidney and most sensitive primary culture of astrocytes to assess biocompatibility of prepared nanozeolites were performed. We also demonstrated that Cu-X has greater adsorption capacity towards NO, whereas the as prepared Na-X has higher carbon dioxide sorption affinity, due to the presence of different cation. The high sorption capacity of non-toxic Cu-X, combined with antimicrobial properties, provide a platform for alternative therapies in biomedical field.

2   Experimental

2.1.   Preparation of Cu-FAU nanozeolite

The template-free, nanosized Na-X zeolite with FAU framework topology was synthesised as previously reported.[32] The aluminate solution consisted of 2.5 g of sodium hydroxide (NaOH, 97 %, Sima-Aldrich) which was dissolved in 3.0 g of dd H_2O, followed by gentle addition of 0.297 g aluminum powder (325 mesh, 99.5 %, Alfa Aesar). The mixture was stirred until a clear solution was obtained. The silicate solution was prepared by dissolving 1.1 g of NaOH in 1.0 g of double distilled H_2O (dd H_2O), followed by the addition of 10 g colloidal silica (Ludox-HS 30, 30 wt % SiO_2, Aldrich). The acquired white, turbid suspension was placed in the oven 100 °C for 5 min to obtain a clear suspension. The aluminate solution was added dropwise to the latter under ice and vigorous stirring. As a result, a clear suspension with the starting molar composition 9 Na_2O: 1.1 Al_2O_3: 10 SiO_2: 77 H_2O was produced, then aged at room temperature for 24 h, followed by dehydration (to adjust the H_2O content) and hydrothermal treatment at 50 °C for 26 h. The crystalline product were recovered by centrifugation (20000 rpm, 25 min) and purified by washing with dd H_2O until pH= 9.

The Cu-X was prepared by ion-exchange of 2.4 wt % Na-X suspension with 0.004 M copper nitrate (Cu $(NO_3)_2$.$9H_2O$) at room temperature for 1 h (zeolite to copper suspension

ratio 1:5). The sample was purified by centrifugation and redispersion in dd H$_2$O. The final pH of the Cu-X suspension was 7.

2.2. Characterisation

The stability and particle size distribution of Na-X and Cu-X zeolite suspensions (pH= 7) was determined by zeta potential and dynamic light scattering (DLS) respectively, using a Malvern Zetasizer Nano instrument. The crystal structure of the parent Na-X and the ion-exchanged zeolite Cu-X was determined by X-ray diffraction. The analyses were performed with a PANalytical X'Pert PRO-MPD diffractometer with Cu Kα radiation (λ = 1.5418 Å). The samples were scanned in the 2θ range of 4-50° with a step size of 0.016°. The size and morphology of zeolites were studied by scanning electron microscope (SEM, MIRA-LMH TESCAN) supplied with a field emission gun and a transmission electron microscopy (TEM, 200 kV JEOL 2010 FEG). The elemental analysis of the samples was performed by inductively coupled plasma-atomic emission spectroscopy (ICP-AES) using an OPTIMA 4300 DV (PerkineElmer) instrument. The elemental composition was determined by inductively coupled plasma-atomic emission spectroscopy (ICP-AES) using an OPTIMA 4300 DV (PerkinElmer) instrument.

The adsorption capacities of self-supported zeolites wafers (2 cm^2 area, 20 mg cm^2) towards NO and CO$_2$ were determined using Nicolet Magna 550-FTIR spectrometer (4 cm^{-1} optical resolution and 128 scans) equipped with MCT detector. Prior to the adsorption of gases each sample was activated at 300 °C for 4 hours in the presence of oxygen, under vacuum (10^{-6} Torr). The NO and CO$_2$ were adsorbed at room temperature using various amounts introduced in small volumes; 1-100 Torr for NO and 10-180 Torr for CO$_2$. All spectra were normalised to the sample weight.

2.3. Cytotoxicity tests: materials and methods

Cell lines: Human embryonic kidney (HEK 293) and human glioblastoma cells (U87-MG), were cultured in DMEM (Sigma-Aldrich, France) prior the toxicity tests. The cell lines listed above were purchased from ATCC (Manassas, VA, USA) and maintained in culture at 37°C with 5% CO$_2$ and 95% humidity.

DMEM was supplemented with 10% foetal bovine serum (Eurobio, France), 2 mM glutamine (Sigma-Aldrich, France) and 100 U/ml penicillin/streptomycin (Sigma-Aldrich, France).

Primary culture of astrocytes: Cerebral cortices (isolated from neonatal 1-3 days old mice, Swiss, CURB, France) were carefully stripped of the meninges and dissociated to generate a single-cell suspension. The cultures were left to grow in an incubator at 37 °C (humidified with 5% CO_2 to confluency up to 20 days) and supplemented with DMEM consisting of 10% foetal bovine serum (Eurobio, France), 10% horse serum (Eurobio, France), 2 mM glutamine (Sigma-Aldrich, France) and 100 U/ml penicillin/streptomycin (Sigma-Aldrich, France) prior use.

Cells exposure to nanosized zeolites: Before to cells exposure the Na-X and Cu-X nanozeolites were diluted in culture medium at concentrations: 1, 10, 50 or 100 µg/ml then added directly into the wells. Cells were exposed to nanozeolites for a period of 24, 48 and 72h. The control tests were performed with distilled water under exactly the same conditions.

Cells viability: Cells were seeded in 24-wells plates to obtain 80% of confluency on the day of analysis and measured in compliance with manufacturer's manual (WST-1 assay, Roche, France)

3   Results and discussion

3.1 Properties of prepared nanozeolites

The as synthesised Na-X nanosized zeolite sample is pure and highly crystalline. After ion-exchange with copper the framework structure of the sample Cu-X is completely preserved. The X-ray diffraction patterns of Na-X and Cu-X are alike in nature and typical for FAU-type zeolite. Figure 28a illustrates the Bragg peaks widening, which indicates the small size of zeolite crystals. The morphology of prepared samples was further assessed by TEM, which confirmed the nanosized particle size with mean diameter < 40 nm (Figure 28b and c). The homogeneous nanocrystals exhibit a typical octahedral morphology with fully crystalline and well-developed faces, which remained unchanged after copper introduction.
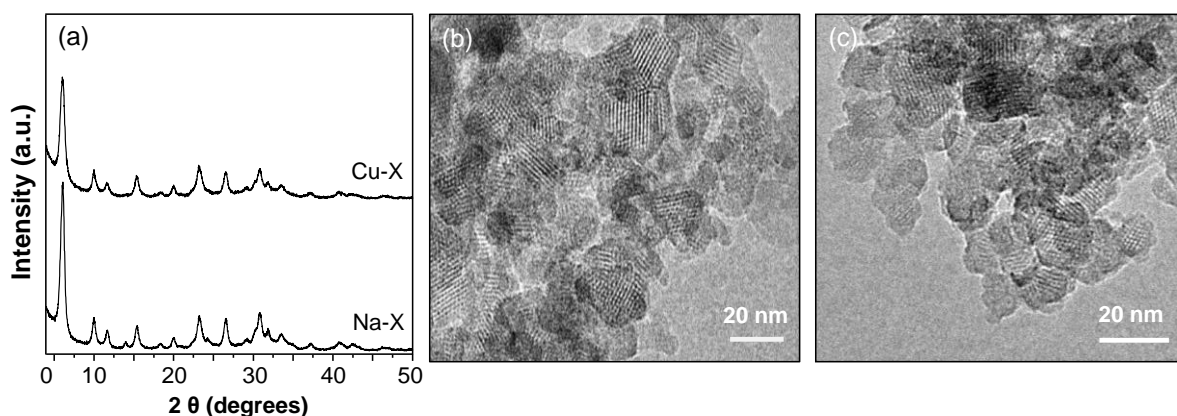
Figure 28. (a) XRD patterns of samples Na-X and Cu-X, and TEM images of (b) Na-X and (c) Cu-X.

The elemental composition of the samples is presented in Table 5. The ion-exchange process does not influence the Si/Al ratio, which was around 1.6 wt % for both samples. Consequently, 53 % of sodium was exchanged, leaving 5.11 wt % of copper present in the Cu-X sample.

The stability of colloidal zeolite suspensions is one of the prime factors considered for biomedical applications. The stability of Na-X and Cu-X samples is determined by evaluating the zeta potential values. This technique measures the surface charge of nanoparticles and it is influenced by pH/concentration of the zeolite suspension. Generally, the zeta potential limit value of ±30 mV is employed to determine the stability of nanozeolites in suspension. The zeta potential value are -43.1 mV to -42.4 mV for as synthesised Na-X and Cu-X nanozeolites, respectively, demonstrating the high colloidal stability of both zeolite suspensions (Figure 29a). In addition, DLS results show narrow, monomodal particle size distribution curves, similar for both samples (Figure 29b). This indicates that the ion-exchange does not influence the stability of zeolite nanocrystals.

Table 5. The elemental analysis of Na-X and Cu-X zeolites determined by ICP.

| Sample name	Na (wt. %)	Cu (wt. %)	Al (wt. %)	Si (wt. %)	Si/Al
Na-X	9.60	-	11.84	19.29	1.63
Cu-X	5.69	5.11	11.38	17.86	1.57
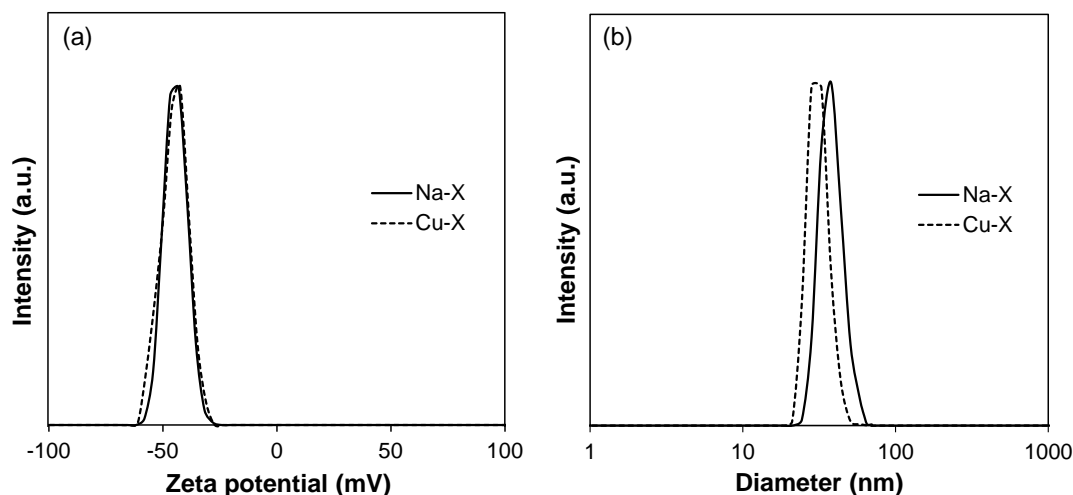
Figure 29. (a) Zeta potential and (b) DLS curves for Na-X and Cu-X zeolite suspensions.

3.2. In-situ FTIR measurements

In-situ IR spectroscopy was used to determine the sorption capacity of as prepared Na-X and Cu-X samples toward NO and CO_2.

The adsorption of nitric oxide on zeolite samples after activation was performed at room temperature. The IR spectra of NO adsorbed on Na-X and Cu-X in the region of 1652-1260 cm^{-1} are presented in Figure a,b. The spectra are similar with the exception of the bands at 1906 and 1883 cm^{-1} clearly observed in the Cu-X sample (Figure 30b).
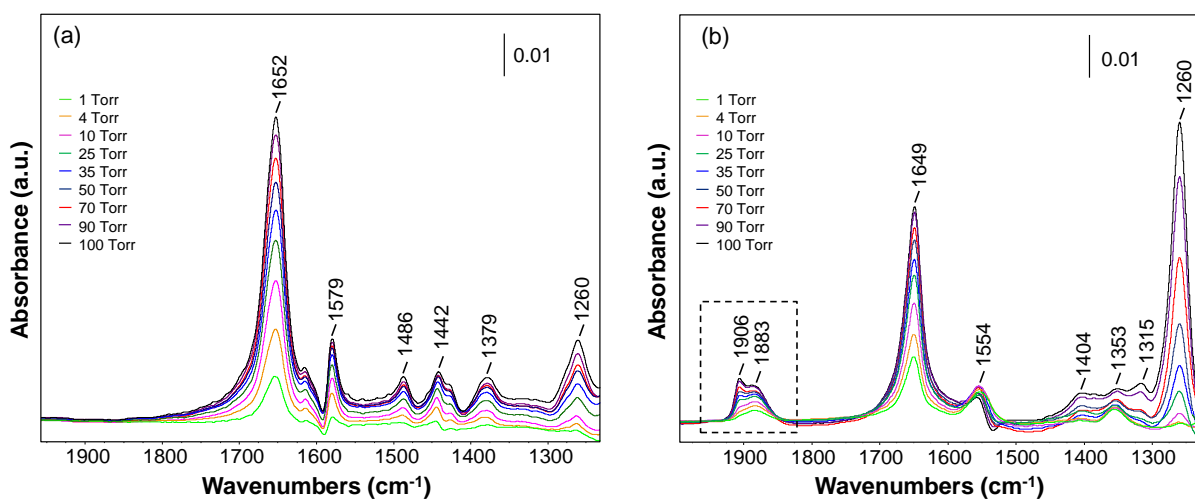

Figure 30. FTIR spectra evolution of NO adsorbed on (a) Na-X and (b) Cu-X nanozeolites at gas pressure varying from 1 to 100 Torr.

According to previous studies the bands positioned in the 1652-1260 cm^{-1} region correspond to surface species, in most cases nitrates, nitrites and nitro and/or nitrito

compounds (Table 6).[33–36] The bands at 1906 and 1883 cm^{-1} are attributed to nitrosyls, which are formed upon nitric oxide adsorption on two different Cu^{2+} sites, giving rise to formation of Cu^{2+}–NO species. No bands at 1900 cm^{-1} was observed for pure Na-X nanozeolite.

The adsorption capacity of both zeolites towards NO was evaluated by measuring the intensity of the IR bands at 100 Torr (Figure 31 left). The results indicated that copper-containing nanozeolite has greater NO capacity in comparison to the Na-X. This can be explained by the stronger interactions of NO with the copper.
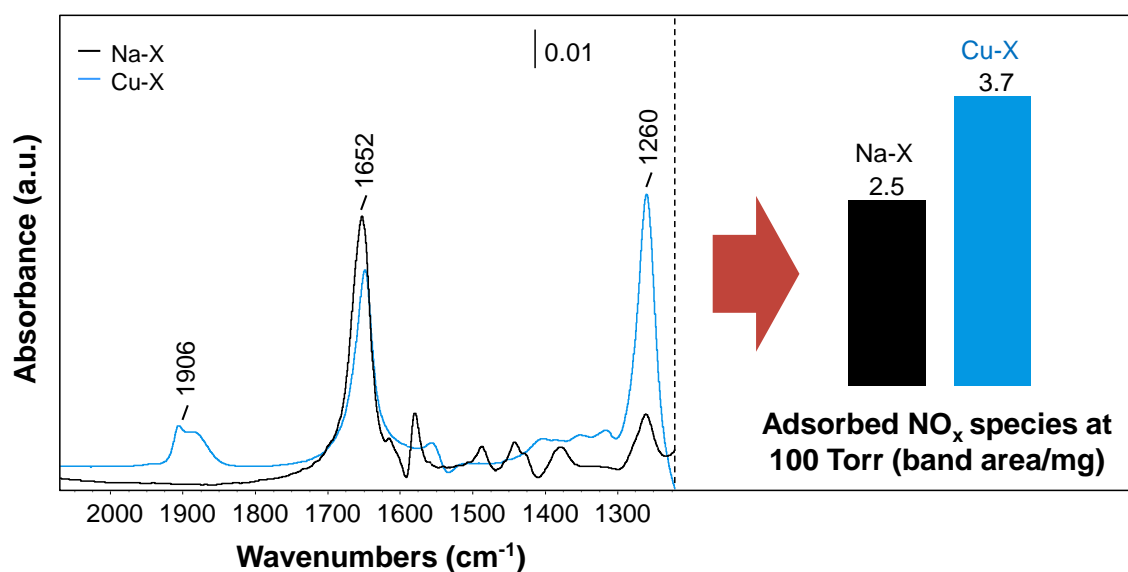

Figure 31. FTIR bands after NO adsorption on Na-X (black) and Cu-X (blue) at 100 Torr in the range 2075-1225 cm-1 (left), and sorption capacity measured by the area of the peaks in the 2075-1225 region cm-1(right).

Table 6. Assignment of the IR bands observed after NO adsorption on Na- and Cu-X.[35,36]

IR bands (cm$^{-1)}$	Structure	Notes
1906	NO on Cu^{2+}	on Cu^{2+} carrying extra lattice oxygen
1883	NO on Cu^{2+}	on isolated Cu^{2+} moved to accessible position
1652-1649	bridging nitrates	on Al sites
1579-1554	monodentate nitrates	on Si sites
1486	monodentate nitrate	-
1442	monodentate nitrito	-
1404	nitrate species	-
1379-1353	Nitro species	-
1315	Nitro/nitrate species	-
1260	Nitro species	on Na sites

The adsorption of carbon dioxide was carried out on the activated Na- and Cu-X zeolite samples at room temperature. Figure 32a,b presents the evolution of FTIR spectra for Na-X and Cu-X nanozeolites. Two regions of 2400-2300 cm^{-1} and 1800-1200 cm^{-1} were evaluated. These regions are characteristic for physisorbed and chemisorbed CO_2 species, respectively. Accordingly, a well pronounced adsorption bands at 2353 cm^{-1} and 2350 cm^{-1} are present for Na-X and Cu-X, which are ascribed to the asymmetric stretching mode of physically adsorbed carbon dioxide on the zeolite surface.[37]
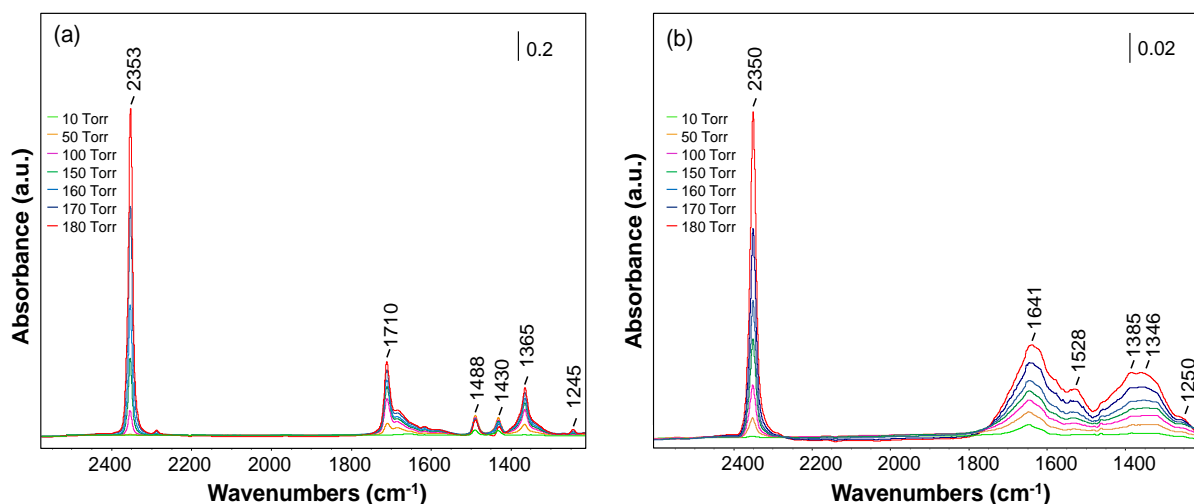

Figure 32. FTIR spectra evolution after carbon dioxide adsorption on (a) Na-X and (b) Cu-X nanosized zeolites at room temperature.
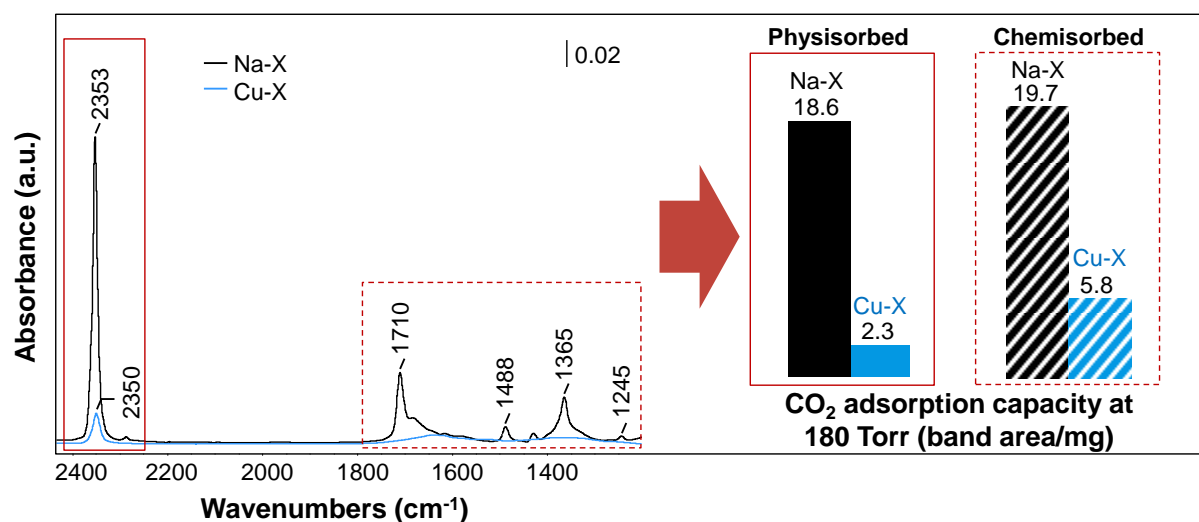

Figure 33. FTIR spectra after carbon dioxide adsorption at 180 Torr (left) and CO_2 adsorption capacity for Na- and Cu-X zeolite samples measured at 180 Torr (right).

The band intensity increases with increasing gas pressure, therefore the amount of physisorbed CO_2 was evaluated at constant pressure for both samples. The spectra of sodium and copper nanozeolites at 180 Torr are presented in Figure 33(left). The physisorbed CO_2 on the Na-X sample is eight times higher than on the Cu-X as showed in Figure 33(right).

The less pronounced bands in the 1800-1200 cm^{-1} region are typical for carbonates.[38] These carbonate species include notably stable mono-, uni- and bidentate carbonates, which are formed as a result of CO_2 interaction with the oxygen bridging aluminium or silicon atoms.[39] It was previously reported that the carbonate formation can limit carbon dioxide adsorption due to decrease of accessibility to zeolite surface.[40] In the copper containing sample the carbonate region is not very prominent, this made it difficult to distinguish between different types of carbonates present. The amount of chemisorbed CO_2 was measured at 180 Torr for Na-X and Cu-X, showing that sodium containing nanosized zeolite has three times greater adsorption capacity in contrast to the copper one (Figure 33). This demonstrates that by simple ion-exchange the properties of zeolite can be readily modified depending on the desired application.

3.3. Cytotoxicity tests of nanosized Na-X and Cu-X zeolites

In order to assess the biocompatibility of nanozeolites and thus prove their applicability in biomedicine, the toxicity measurements are performed. Different cell lines including human glioblastoma (U87-MG), human kidney (HEK 293) and mice astrocytes ware exposed to zeolite samples at different concentrations (1-100 µg/ml) for the period of 24-72 hours. As a result, no toxicity is observed for U87-MG cells which were subjected to both, Na-X and Cu-X nanosized zeolites (Figure 34). The only exception is a small decrease in cell viability after 72 hrs of exposure to high concentration of copper-containing nanozeolite.
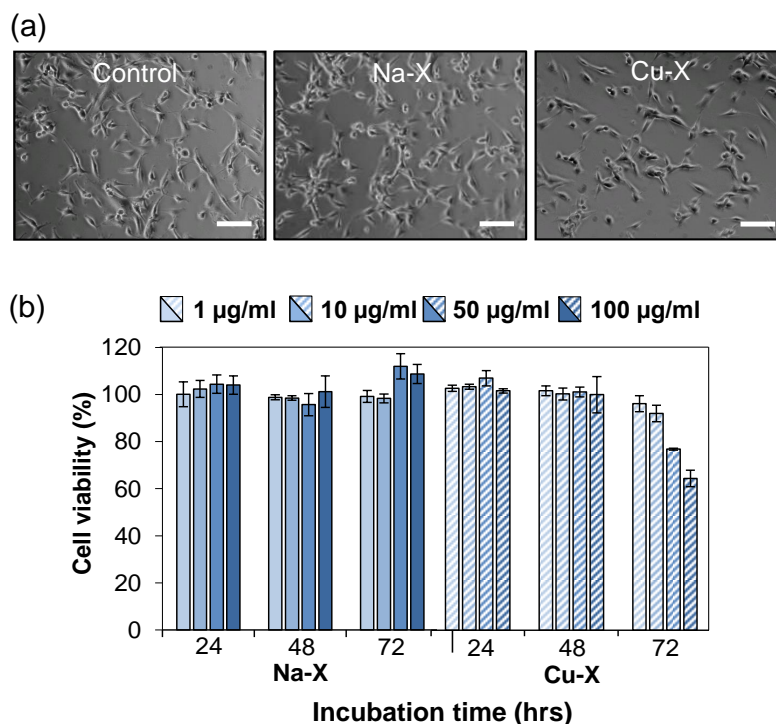
Figure 34. (a) Representative photographs of U87-MG cells after 24 hrs exposure to 10µg/ml of Na-X, Cu-X zeolites and control (H$_2$O), scale bar = 100µm. (b) Quantification of cell viability of human glioblastoma after 24, 48 and 72 hrs exposure to Na-X and Cu-X zeolites with four different concentrations. Cell viability was assessed using the WST-1 test. Mean SD. n = 3.

Human kidney cells display slightly higher sensitivity towards nanozeolites (Figure 35). In general, both zeolites are harmless to the HEK 293 cells when exposed to low concentrations, however, a 40 % decrease in cell viability was observed after 72 hrs at 100 µg/ml of Cu-X. Finally, the same trend follows for astrocytes cell lines, where no toxicity was observed after contact with zeolites at low concentrations, hence the cell viability decreased by ~43 % after exposure to 50-100 µg/ml of zeolites as presented in Figure 36.
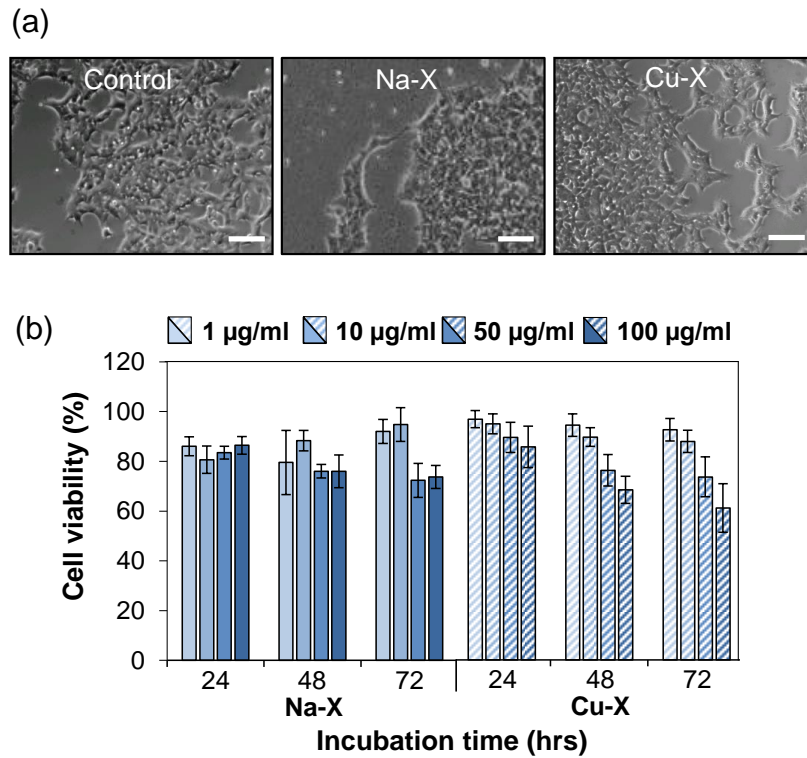
Figure 35. (a) Representative photographs of HEK 293 cells after 24 hrs exposure to 10μg/ml of Na-X, Cu-X zeolites and control (H$_2$O), scale bar = 100μm. (b) Quantification of cell viability of human glioblastoma after 24, 48 and 72 hrs exposure to Na-X and Cu-X zeolites with four different concentrations. Cell viability was assessed using the WST-1 test. Mean SD. n = 3.
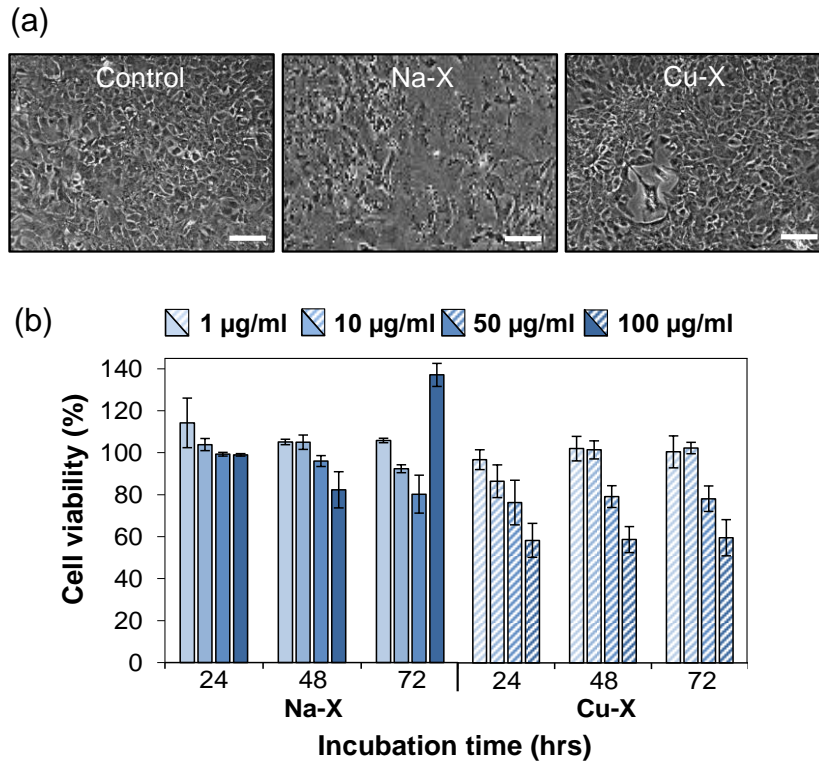

Figure 36. (a) Representative photographs of astrocytes after 24 hrs exposure to 10μg/ml of Na-X, Cu-X zeolites and control (H$_2$O), scale bar = 100μm. Quantification of cell viability of mice astrocytes after 24, 48 and 72 hrs exposure to Na-X and Cu-X zeolites with four different concentrations. Cell viability was assessed using the WST-1 test. Mean SD. n = 3.

4. Conclusions

The sodium- and copper-containing nanosized FAU zeolite crystals (Na-X and Cu-X) were prepared in the form of stable colloidal suspensions. The gas adsorption properties of both materials towards nitric oxide and carbon dioxide were evaluated; the materials are considered to be used for potential gas delivery systems in biomedicine. The copper ion-exchanged nanozeolites (Cu-X) show increased NO adsorption capacity by 36% in comparison to as prepared sodium form. On the other hand the Na-X shows better adsorption affinity towards CO_2. Both, Na- and Cu-X nanozeolites, show no cytotoxicity towards human glioblastoma, kidney and mice astrocytes, confirming their biocompatibility and thus ability to be further employed as gas carriers for biomedical applications.

5. References

[1] M. Iwamoto, S. Yokoo, K. Sakai, S. Kagawa, J. Chem. Soc. Faraday Trans. 1 Phys. Chem. Condens. Phases 77 (1981) 1629.

[2] P. Ciambelli, P. Corbo, F. Migliardini, Catal. Today 59 (2000) 279–286.

[3] G. Delahay, S. Kieger, N. Tanchoux, P. Trens, B. Coq, Appl. Catal. B Environ. 52 (2004) 251–257.

[4] C. Boruban, E. Nalbant Esenturk, J. Mater. Res. 32 (2017) 3669–3678.

[5] M.R. Hudson, W.L. Queen, J.A. Mason, D.W. Fickel, R.F. Lobo, C.M. Brown, J. Am. Chem. Soc. 134 (2012) 1970–1973.

[6] J. Bachmann, Pascale A., Luisi, Pier L., Lang, Nature 357 (1992) 57–59.

[7] V. Calabrese, C. Mancuso, M. Calvani, E. Rizzarelli, D.A. Butterfield, A.M. Giuffrida Stella, Nat. Rev. Neurosci. 8 (2007) 766–775.

[8] F.X. Guix, I. Uribesalgo, M. Coma, F.J. Muñoz, Prog. Neurobiol. 76 (2005) 126–152.

[9] A. Chakhoyan, A. Corroyer-Dulmont, M.M. Leblond, A. Gérault, J. Toutain, L. Chazaviel, D. Divoux, E. Petit, E.T. MacKenzie, F. Kauffmann, N. Delcroix, M. Bernaudin, O. Touzani, S. Valable, J. Cereb. Blood Flow Metab. 37 (2016) 2270–2282.

[10] J.H. Kaanders, J. Bussink, A.J. Van der Kogel, Lancet Oncol. 3 (2002) 728–737.

[11] Z. Cai, S. V. Yarovoi, Z. Zhu, L. Rauova, V. Hayes, T. Lebedeva, Q. Liu, M. Poncz, G. Arepally, D.B. Cines, M.I. Greene, Nat. Commun. 6 (2015) 1–10.

[12] R.W.M. van der Maazen, H.O.M. Thijssen, J.H.A.M. Kaanders, A. de Koster, A. Keyser, M.J.J. Prick, J.A. Grotenhuis, P. Wesseling, A.J. van der Kogel, Radiother. Oncol. 35 (1995) 118–122.

[13] R.S. Drago, B.R. Karstetter, J. Am. Chem. Soc. 83 (1961) 1819–1822.

[14] K.M. Davies, D.A. Wink, J.E. Saavedra, L.K. Keefer, J. Am. Chem. Soc. 123 (2001) 5473–5481.

[15] D.J. Smith, D. Chakravarthy, S. Pulfer, M.L. Simmons, J.A. Hrabie, M.L. Citro, J.E. Saavedra, K.M. Davies, T.C. Hutsell, D.L. Mooradian, S.R. Hanson, L.K. Keefer, (1996) 1148–1156.

[16] H. Zhang, G.M. Annich, J. Miskulin, K. Stankiewicz, K. Osterholzer, S.I. Merz, R.H.

Bartlett, M.E. Meyerhoff, J. Am. Chem. Soc. 125 (2003) 5015–5024.

[17]   H. Zhang, G.M. Annich, J. Miskulin, K. Osterholzer, S.I. Merz, R.H. Bartlett, M.E. Meyerhoff, Biomaterials 23 (2002) 1485–1494.

[18]   R.E. Morris, P.S. Wheatley, Angew. Chemie - Int. Ed. 47 (2008) 4966–4981.

[19]   P.S. Wheatley, A.R. Butler, M.S. Crane, A.G. Rossi, I.L. Megson, R.E. Morris, Stud. Surf. Sci. Catal. 158 B (2005) 2033–2040.

[20]   G. Maurin, R. Bell, B. Kuchta, T. Poyet, P. Llewellyn, Adsorption 11 (2005) 331–336.

[21]   L. Ohlin, P. Bazin, F. Thibault-Starzyk, J. Hedlund, M. Grahn, J. Phys. Chem. C 117 (2013) 16972–16982.

[22]   C. Martínez, A. Corma, Coord. Chem. Rev. 255 (2011) 1558–1580.

[23]   M. Zaarour, B. Dong, I. Naydenova, R. Retoux, S. Mintova, Microporous Mesoporous Mater. 189 (2014) 11–21.

[24]   V. Georgieva, C. Anfray, R. Retoux, V. Valtchev, S. Valable, S. Mintova, Microporous Mesoporous Mater. 232 (2016) 256–263.

[25]   S. Komaty, C. Anfray, M. Zaarour, H. Awala, V. Ruaux, S. Valable, S. Mintova, Molecules 23 (2018) 37.

[26]   R. Amorim, N. Vilaça, O. Martinho, R.M. Reis, M. Sardo, J. Rocha, A.M. Fonseca, F. Baltazar, I.C. Neves, J. Phys. Chem. C 116 (2012) 25642–25650.

[27]   D.G. Fatouros, D. Douroumis, V. Nikolakis, S. Ntais, A.M. Moschovi, V. Trivedi, B. Khima, M. Roldo, H. Nazar, P.A. Cox, J. Mater. Chem. 21 (2011) 7789.

[28]   N. Vilaça, A.F. Machado, F. Morais-Santos, R. Amorim, A. Patrícia Neto, E. Logodin, M.F.R. Pereira, M. Sardo, J. Rocha, P. Parpot, A.M. Fonseca, F. Baltazar, I.C. Neves, RSC Adv. 7 (2017) 13104–13111.

[29]   S.E. Russell, J.M. González Carballo, C. Orellana-Tavra, D. Fairen-Jimenez, R.E. Morris, Dalt. Trans. 46 (2017) 3915–3920.

[30]   P.S. Wheatley, A.R. Butler, M.S. Crane, S. Fox, B. Xiao, A.G. Rossi, I.L. Megson, R.E. Morris, J. Am. Chem. Soc. 128 (2006) 502–509.

[31]   J. Redfern, K. Goldyn, J. Verran, R. Retoux, L. Tosheva, S. Mintova, Microporous Mesoporous Mater. 253 (2017).

[32] H. Awala, J.P. Gilson, R. Retoux, P. Boullay, J.M. Goupil, V. Valtchev, S. Mintova, Nat. Mater. 14 (2015) 447–451.

[33] M. Iwamoto, H. Yahiro, Handb. Zeolite Sci. Technol. (2003).

[34] M. Shelef, Chem. Rev. 95 (1995) 209–225.

[35] T. Venkov, K. Hadjiivanov, D. Klissurski, Phys. Chem. Chem. Phys. 4 (2002) 2443–2448.

[36] K. Hadjiivanov, Catal. Rev. 42 (2000) 71–144.

[37] P. Galhotra, J.G. Navea, S.C. Larsen, V.H. Grassian, Energy Environ. Sci. 2 (2009) 401–409.

[38] J.W. Ward, H.W. Habgood, J. Phys. Chem. 70 (1966) 1178–1182.

[39] D. Bonenfant, M. Kharoune, P. Niquette, M. Mimeault, R. Hausler, Sci. Technol. Adv. Mater. 9 (2008).

[40] C.L. Angell, M. V Howell, J. Phys. Chem. 47 (1969) 3831–3836.

Chapter 6- General conclusion and outlook

1   Conclusions

The decreasing efficiency of conventional treatments such as antibiotics to fight infectious diseases caused by various types of bacteria is becoming a serious issue in regards to the number of deaths cases.[1] Moreover, development of new antibacterial drugs is laborious and expensive process and their extensive use leads to side effects. Consequently, the elaboration of new strategies to eliminate bacteria and thus prevent infectious diseases is of great demand. A second matter of concern regarding treatment resistance is connected to the effectiveness of radiotherapy in brain tumours. It has been reported that the resistance comes from oxygen deficiency in the tumour tissues, called hypoxia.[2] In the framework of present study we have explored the opportunity to use metal exchanged nanozeolites as antimicrobial agents and gas carriers. The faujasite-X is the chosen zeolite due to its tuneable properties, large pore volume as well as the high exchangeable cation capacity.

In this study, we report: (i) the effect of copper modified nanosized FAU-X zeolite on ESKAPE type bacteria, (ii) the metal containing nanozeolite as a tool for tissue oxygenation and visualisation using MRI, and lastly (iii) the use of faujasite nanozeolite as nitric oxide and carbon dioxide gas vector to prevent life threatening conditions.

In the case study described in Chapter 3 the use of Cu-FAU nanozeolite in form of stable suspension for direct sanitization of healthcare surfaces proved its efficiency as antimicrobial agent towards ESKAPE pathogens (Enterococcus species, Staphylococcus aureus, Klebsiella pneumoniae, Acinetobacter baumanii, Pseudomonas aeruginosa and Enterobacter species).

- Semi-quantitative tests using thioglycollate plates: ESKAPE pathogens were killed within 100 min when Cu-X suspension was applied. The *E. faecalis* proved to be the most resistant bacterium, therefore, in order to inhibit its growth the Cu-X concentration had to be doubled.

- The survival of microorganisms on stainless-steel coupons: A complete kill for three selected bacteria was achieved within 20 min for *P. aeruginosa*, and within 10 min for the *K. pneumoniae* and *S. aureus*. This confirmed that copper containing FAU-X nanozeolite is an effective antimicrobial agent.

- Sodium form of nanozeolite demonstrated no antibacterial activity.

In Chapter 4, the ability of nanozeolites to act as a gas carrier for tissue oxygenation in glioblastoma tumour was investigated.

- The metal containing nanozeolite showed no adverse toxic effects towards different cells, including human glioblastoma (U87-MG), kidney (HEK 293) and mice astrocytes. Proving their biocompability.

- The Gd-X nanozeolite loaded with CO_2 or carbogen (95% O_2 and 5% CO_2) increased both the blood volume and oxygen concentration in the tumour tissue which resulted in tissue re-oxygenation.

- Gd introduced in the zeolite act as a MRI contrast agent, allowing to track the specific accumulation of nanosized zeolite crystals in the tumour.

- The results confirmed the potentiality of metal containing nanozeolites to be used as a theranostic tool for development of novel strategies to fight brain tumours.

In the work presented in Chapter 5, the ability of copper containing FAU-X nanozeolite to adsorb nitric oxide (NO) and carbon dioxide (CO_2) along with the assessment of its toxicity towards cells was studied.

- The nanozeolite functionalised with copper increased the NO adsorption by 36 % in comparison to as prepared Na-X nanozeolite.

- The sodium form of faujasite demonstrated better adsorption capacity towards CO_2.

- The results indicated that by simple metal-exchange the gas adsorption properties of nanozeolites can be tuned, highlighting the significance of cation choice for desired application.

- Na- and Cu-X nanozeolite displayed non-toxic nature towards human glioblastoma (U87-MG), kidney (HEK 293) and mice astrocytes cells.

In summary, we have demonstrated the effective employment of metal-functionalised nanozeolites to act as antimicrobial agent and gas carrier in microbiology and biomedicine respectively. The results showed that by careful selection of zeolite extra framework cation the properties of material can be tuned, to make them competent for a chosen task. The high selectivity of nanozeolites along with non-toxicity opens a door for them to be tested in other biomedical applications, where the controlled substance delivery is considered. Nevertheless, further research is required to assess their full potential in this field.

2 Perspectives

Regardless to our research output, there are still fields within this work that demand further investigation. Moving forward, additional experiments are required to obtain in-depth knowledge about the performance of metal exchanged nanozeolites.

In presented research the important role of zeolite extra framework cation for both antimicrobial and gas adsorption properties was underlined. However, the specific cation location after ion exchange was not investigated. This could potentially improve our knowledge on how to particularly design a "perfect" material, taking into consideration all possible factors, such as the level of cation exchange to specific zeolite sites and its accessibility. The localisation of different cations could be studied using solid-state Nuclear Magnetic Resonance (NMR), Electron Paramagnetic Resonance (EPR) and Mössbauer spectroscopy.

In regards to microbiology, the further tests can include the incorporation of different cations into zeolite structure. The metals of interest will be the ones that already displayed antibacterial properties, namely Zn, Co, Zr, Ni.[3] It would be very beneficial to evaluate the potency of each metal against a wide array of microorganisms.

Considering the gas delivery applications, different types of zeolite framework could be tested to determine their adsorption capacity and specificity when exchanged with various cations. However, in order to use zeolites for biomedical applications, they have to be synthesised with the absence of organic templates, with sizes < 100 nm, which already limits the available zeolite types to eight.[4] Moreover, the exchange level of metals plays an important role, as over exchanged zeolites can block the accessibility to active sites, and thus restrict the adsorption.

This research project is on its way to make a great scientific impact. It is also significant for our society, as we are fighting a constant increase of treatment resistance. There are still a lot of possibilities to optimise zeolitic materials to find the most suited one for particular biomedical application. The further investigations have to be carried out to improve the knowledge and performance of zeolites in this area of science.

3 References

[1] R. Smith, J. Coast, Bmj 346 (2013) 1493–1493.

[2] A. Monteiro, R. Hill, G. Pilkington, P. Madureira, Cells 6 (2017) 45.

[3] M. Yasuyuki, K. Kunihiro, S. Kurissery, N. Kanavillil, Y. Sato, Y. Kikuchi, Biofouling 26 (2010) 851–858.

[4] S. Mintova, J. Grand, V. Valtchev, Comptes Rendus Chim. 19 (2016) 183–191.

Résumé

1 Introduction

L'utilisation de zéolithes dans des applications conventionnelles telles que la catalyse, l'échange d'ions et la séparation de gaz ont prouvé leur efficacité au fil des ans.[1–3] Les nanocristaux de zéolithes ont également été utilisés pour des applications plus avancées, notamment en biomédecine (capteurs, administration de médicaments et de gaz) et en microbiologie (agents antibactériens) grâce à leurs grandes surfaces spécifiques, leur non toxicité et leurs grandes stabilités chimiques / thermiques.[4] Cependant, le plein potentiel de l'utilisation de la nanozéolithes pour des applications prospectives concernant la science biomédicale n'a pas encore été complètement découvert.

La résistance aux traitements médicaux conventionnels, à savoir les antibiotiques et la radiothéraphie en microbiologie et en médecine, respectivement, est un sujet de préoccupation en termes de nombre croissant de décès causés par des maladies infectieuses et des cancers. De plus, les bactéries résistantes aux antibiotiques sont la principale cause d'infections graves, d'inflammations et d'intoxications alimentaires en milieu hospitalier. Au cours des trois dernières décennies, la résistance bactérienne a augmenté beaucoup plus rapidement que le nombre total de nouveaux antibiotiques approuvés, comme le montre la Figure 1.[5] De plus, l'utilisation intense d'antibiotiques n'est pas largement applicable en raison des effets secondaires. Par conséquent, le développement de nouvelles stratégies antimicrobiennes pour tuer les bactéries et prévenir un grand nombre de maladies présente un fort intérêt scientifique.
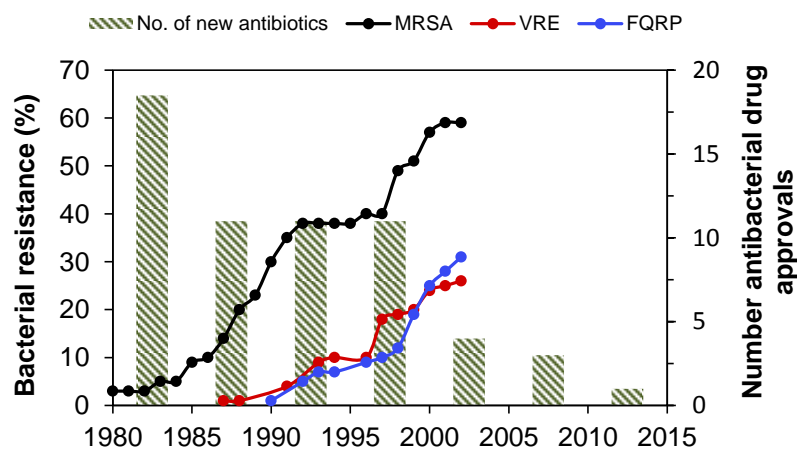

Figure 1. Nombre de nouveaux médicaments antibactériens autorisés par les demandes d'homologation et les taux de résistance pour trois types de bactéries: S. aureus résistant à la méthicilline (SARM), entérocoques résistants à la vancomycine et P. aeruginosa résistant aux fluoroquinolones (FQRP). Modifié de: Centres de contrôle et de prévention des maladies.[6]

Un autre problème important est le traitement des tumeurs cérébrales. Il a été reconnu que la principale cause de résistance aux traitements de radiothérapie des tumeurs, en particulier le glioblastome (tumeur cérébrale primaire), est causée par l'apport insuffisant d'oxygène à ses tissus, appelé hypoxie.[6] Auparavant, plusieurs voies ont été prises pour réduire l'hypoxie dans les tumeurs, à savoir la respiration par O_2 et carbogène. Les résultats de cette méthode étaient médiocres en termes de sélectivité et de réponse à la radiothérapie. En outre, la délivrance extrinsèque d'oxyde nitrique (NO) pour empêcher la formation de tissus sanguins à la surface des vaisseaux sanguins artificiels et des dispositifs médicaux est une question importante. De nos jours, l'héparine est utilisée comme anticoagulant pour prévenir la thrombose, mais son utilisation peut entraîner des saignements inattendus dans d'autres parties du corps, entraînant une perte de plaquettes.

Une solution possible pour prévenir les infections bactériennes, la résistance à la radiothérapie et la thrombose consiste à utiliser des nanozéolites à échange de métaux pour agir en tant qu'agents antimicrobiens et transporteurs de gaz. La taille des cristaux de zéolithes joue un rôle très important dans les études in vivo. Les zéolites à micronsure ont une structure de pores bien définie et une capacité de sorption élevée, mais elles ne sont pas stables dans les solutions, car elles ont tendance à s'agréger, ce qui influence leur activité et leur transport, entraînant des effets toxiques. En revanche, les nanozéolites de taille <100 nm possèdent toutes les propriétés texturales importantes et, surtout, sont stables dans les suspensions colloïdales. De plus, ils montrent l'absence de toxicité aiguë et chronique chez les animaux vivants, ce qui en fait des candidats parfaits pour une utilisation biomédicale

Bien que de nombreuses études aient été consacrées à l'étude de l'utilisation des zéolithes en microbiologie et en médecine, le potentiel de ces matériaux reste encore à développer, principalement en ce qui concerne leurs biocompatibilités et leurs sélectivités.

L'objectif de ce doctorat est de synthétiser et de modifier post-synthétiquement la nanozéolithes FAU-X sans agents structurants organiques pour des applications biomédicales. Les altérations post-synthèses impliquent principalement l'optimisation de la procédure d'échange d'ions pour l'introduction de différents cations et donc la fonctionnalisation pour l'application souhaitée. Les informations obtenues tout au long de cette étude permettront de comprendre l'effet de l'échange de cations dans la structure des zéolithes et ses propriétés liées aux applications recherchées.

2   Bibliographie

Les zéolithes sont par définition des aluminosilicates poreux cristallins constitués de quatre tétraèdres liés.[7] Les atomes cadres (TO$_4$) peuvent être substitués de manière isomorphe par d'autres éléments de taille et de valence appropriées (T = Ge, Ga, P, Ti, B, Fe…). Les atomes cadres s'organisent autour des espèces modèles, des cations de métaux alcalins avec leurs sphères d'hydratation ou des espèces organiques chargées positivement, pendant le processus de cristallisation, qui se déroule dans des conditions hydrothermales. Cette interconnexion spécifique forme une structure de réseau tridimensionnelle, résultant en un espace microporeux, des canaux et / ou des cavités, leur conférant des caractéristiques de tamis moléculaires. Il existe plus de 239 types de zéolithes synthétiques, tous répertoriés sur le site Web de l'International Zeolite Association (IZA).[8] Leur structure est définie par la topologie du cadre établie par la disposition des unités de construction primaires, secondaires et polyédriques.[9] Ces matériaux cristallins sont regroupés en trois types de catégories en fonction de la plus grande dimension des pores de l'ossature: (i) les zéolithes à petits pores, à 8 chaînons (8-MR) (RHO et CHA),[10] (ii) zéolithes à pores moyens, 10-MR (FER and TON)[11] et (iii) zéolithes à grands pores 12-MR (FAU, IWW).[12] Il y a peu de zéolithes à pores extra-larges (> 12-MR), mais la recherche de tels matériaux est très intense au cours de la dernière décennie.[13,14]

La base de données IZA contient des informations détaillées sur toutes les zéolithes synthétiques, à partir du type de structure, des dimensions, des conditions de synthèse, etc. Néanmoins, les propriétés finales d'une zéolithe sont contrôlées par une réaction spécifique. Le nombre d'atomes d'Al^{3+} dans la structure zéolithique est un paramètre important qui régit les propriétés principales des aluminosilicates. Si la matrice zéolithique est composée uniquement de cations Si^{4+}, la silicalite correspondante (SiO$_4$) dans la structure tétraédrique présente une charge neutre. Toute substitution de Si^{4+} par des atomes d'Al^{3+} se traduit par une charge cadre négative, qui doit être compensée par un contre-cation (Na$^+$, K$^+$, NH$_4^+$ ou H$^+$). Lors du changement du type de cation (situé dans les canaux de la structure et les cages), les propriétés physiques des zéolithes sont modifiées, ce qui influence leurs domaines d'applications. La teneur en Al^{3+} dans la structure contrôle également les propriétés hydrophiles des zéolithes, car sa charge négative qui attire les molécules d'eau polaires (H$_2$O). Par conséquent, les zéolithes à haute teneur en alumine sont considérées comme hydrophiles, tandis que celles à forte teneur en silice se révèlent hydrophobes. Par conséquent, l'acidité des

zéolithes augmente avec l'augmentation de la teneur en Al^{3+}. Sa force est influencée par la densité des sites acides et donc par le rapport Si/Al, qui est un point important compte tenu de l'utilisation de zéolithes en tant que catalyseurs acides solides.[15] Cependant, le degré de substitution Si^{4+} à Al^{3+} est limité à 50%, comme le stipule la règle de Löewenstein (règle d'évitement Al); deux espèces tétraédriques Al (O-Al-O) ne peuvent pas partager un atome O voisin en raison de la répulsion électrostatique de la charge négative, à la suite de quoi le O-Al-O doit être séparé par au moins un site O-Si-O.

La première zéolithe qui a ouvert la porte à des applications commerciales d'aluminosilicates a été utilisée dans les années 60 par Mobil Oil Corporation. Ils ont utilisé la zéolithe synthétique de type faujasite (FAU), X et Y, comme catalyseur du processus de craquage catalytique fluide (FCC).[16] De nos jours, la famille des zéolithes FAU et bien d'autres, à savoir MFI, Beta, FER, MOR et TON, sont utilisées dans divers procédés catalytiques et de séparation utilisés dans le raffinage du pétrole et la pétrochimie.[17] L'utilisation de zéolithes en tant que catalyseurs représente environ 27% du marché mondial des zéolithes, dont 95% sont utilisés comme catalyseurs FCC. La consommation mondiale totale de zéolithes est estimée à environ 350 000 tonnes par an, où l'Amérique du Nord est la principale consommatrice (Figure 2).[18]
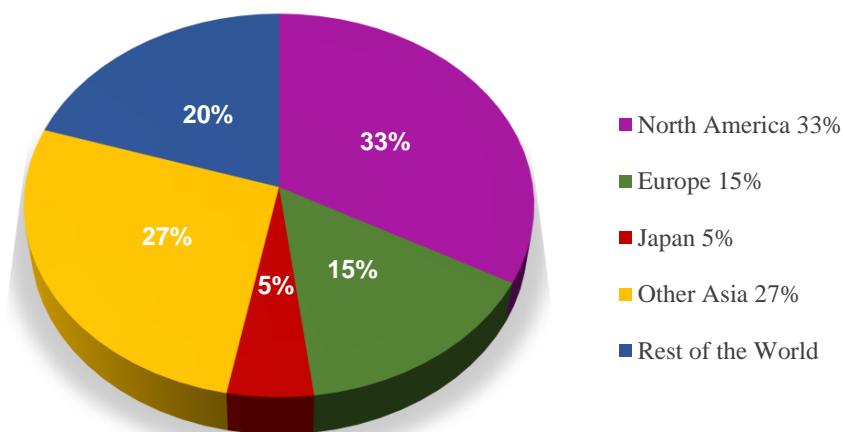

Figure 2: Consommation annuelle de zéolithes par zone. Modifié de [18]

L'attraction générale provoquée par les zéolithes dans les applications industrielles et environnementales peut être justifiée par leurs propriétés distinctives telles que: (i) une structure de pores bien définie, qui les rend sélectives, (ii) une stabilité thermique et chimique élevée, ce qui est important lors de conditions d'exploitation difficiles, (iii) forte acidité de

Brønsted (essentielle pour les transformations catalytiques) et (iv) capacité d'échange de cations, importante pour un usage environnemental, par exemple adoucissement de l'eau, traitement des eaux usées.[19,20] Par conséquent, toutes ces propriétés d'engagement des zéolithes ont largement utilisées dans le FCC mentionné précédemment, mais aussi dans l'isomérisation des paraffines, le traitement aromatique et la sorption/séparation des gaz.[21,22] En outre, les propriétés des zéolithes, à savoir la taille des cristaux, la porosité (zéolithes hiérarchiques micro-mésoporeuses) et l'accessibilité aux acides actifs peuvent être modifiées en utilisant diverses modifications post-synthétiques en fonction de l'application requise. L'examen général de toutes les modifications post-synthétiques possibles et de leurs résultats est bien présenté par Valtchev *et al*.[23]

Considérant toutes les transformations morphologiques importantes des zéolithes, où l'objectif principal est d'améliorer leurs propriétés et donc leurs activités a déjà été étudiée. Celui qui a attiré le plus d'attention était la réduction de la taille des cristaux de zéolithes à l'échelle nanométrique. Les principaux avantages des nanozéolithes sont la taille des cristaux variables, la surface externe élevée, l'accessibilité accrue aux micropores et la diminution des contraintes de diffusion (Figure 3).[24] Ces propriétés ont permis de tester les nanocristaux dans des réactions catalytiques ainsi que des membranes et des films dans la séparation et la détection des gaz.[25,26] De plus, la synthèse sans agents structurants organiques des aluminosilicates nanométriques, associés à leur ingénierie des cristaux et à leur biocompatibilité, a ouvert la voie à de nouvelles applications liées à la biologie et à la médecine, par exemple biosensing, administration de gaz / médicaments et antibactérien.[27–29]
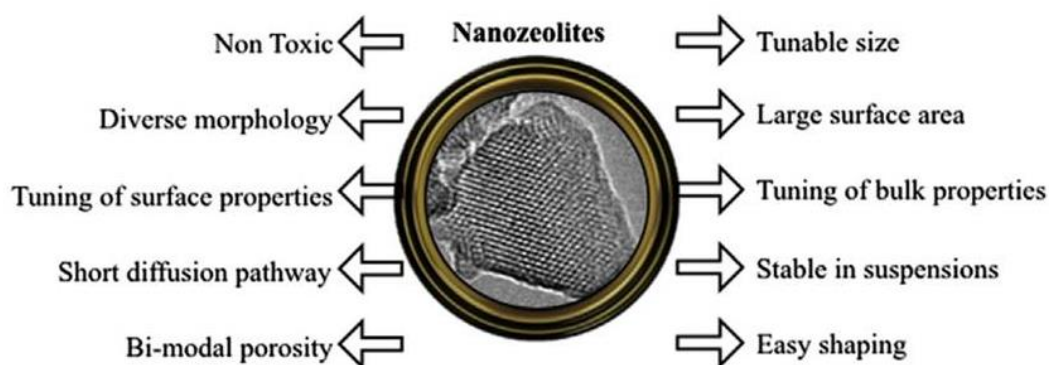

Figure 3: Propriétés avancées des nanozéolithes.[24]

3 Objectif et méthodologie

Le but de ce doctorat est de préparer et de modifier la zéolithe X nanométrique avec différents cations pour des applications biomédicales telles que la microbiologie et la distribution de gaz.

Il est essentiel de comprendre les propriétés physiques et chimiques du matériau zéolithique synthétisé afin de les fonctionnaliser pour certaines applications. Par conséquent, l'importance de choisir des techniques de caractérisation appropriées, hautement sensibles et précises est hautement reconnue. La boîte à outils des différentes méthodes de caractérisation a été utilisée car une technique solitaire n'est pas totalement représentative des zéolithes. Les méthodes de caractérisation consistent en:

- Diffraction RX → Cristallinité et pureté

- Dynamic light scattering → Distribution granulométrique

- Potentiel Zeta → Stabilité des particules

- Physisorption de gaz → Analyse texturale

- Analyse thermogravimétrique → Modifications physico-chimiques

- MEB → Morphologie

- Inductively coupled plasma atomic emission spectroscopy → Analyse chimique

- *In-situ* FTIR → Propriétés d'adsorption

- Magnetic Resonance Imaging → Réoxygénation tissulaire

4 Conclusion générale

L'efficacité décroissante des traitements conventionnels tels que les antibiotiques pour lutter contre les maladies infectieuses causées par divers types de bactéries devient un problème sérieux en ce qui concerne le nombre de cas de décès.[30] De plus, le développement de nouveaux médicaments antibactériens est un processus laborieux et coûteux et leur utilisation intensive entraîne des effets secondaires. Par conséquent, l'élaboration de nouvelles

stratégies pour éliminer les bactéries et prévenir ainsi les maladies infectieuses est très demandée. Un deuxième sujet de préoccupation concernant la résistance au traitement est lié à l'efficacité de la radiothérapie dans les tumeurs cérébrales. Il a été rapporté que la résistance provient d'un déficit en oxygène dans les tissus tumoraux, appelé hypoxie.[6] Dans le cadre de la présente étude, nous avons exploré la possibilité d'utiliser des nanozéolithes à échange de métaux en tant qu'agents antimicrobiens et transporteurs de gaz. La faujasite-X est la zéolithe choisie en raison de ses propriétés variables, de son grand volume de pores et de sa grande capacité de cations échangeables.

Dans cette étude, nous rapportons: (i) l'effet de la zéolithes FAU-X nanométrique modifiée au cuivre sur des bactéries de type ESKAPE, (ii) la nanozéolithe contenant du métal comme outil d'oxygénation et de visualisation tissulaire et enfin la nanozéolithe de type faujasite en tant que vecteur d'oxyde nitrique et de gaz carbogène pour prévenir des conditions mettant la vie en danger.

Dans l'étude de cas décrite au chapitre 3, l'utilisation de la nanozéolithe Cu-FAU sous forme de suspension stable pour la désinfection directe des surfaces de soins a prouvé son efficacité comme agent antimicrobien contre les agents pathogènes ESKAPE (espèces *Enterococcus, Staphylococcus aureus*, *Klebsiella pneumoniae*, *Pseudomonas aeruginosa* et les *espèces Enterobacter*).

• Tests semi-quantitatifs utilisant des plaques de thioglycolate: les agents pathogènes ESKAPE ont été tués dans les 100 minutes suivant l'application d'une suspension de Cu-X. E. faecalis s'est avéré être la bactérie la plus résistante. Par conséquent, pour inhiber sa croissance, la concentration en Cu-X doit être doublée.

• La survie des micro-organismes sur les coupons en acier inoxydable: Une destruction complète pour trois bactéries sélectionnées a été obtenue dans les 20 minutes pour P. aeruginosa et dans les 10 minutes pour K. pneumoniae et S. aureus. Cela a confirmé que le cuivre contenant la nanozéolithe FAU-X est un agent antimicrobien efficace.

• La forme sodique de la nanozéolithes n'a montré aucune activité antibactérienne.

Au chapitre 4, la capacité des nanozéolithes à agir comme vecteur de gaz pour l'oxygénation des tissus dans les tumeurs du glioblastome a été étudiée.

• La nanozéolithea contenant des métaux n'a montré aucun effet toxique nocif envers différentes cellules, y compris le glioblastome humain (U87-MG), les reins (HEK 293) et les astrocytes de souris, démontrant ainsi leur biocompatibilité.

• La nanozéolithe Gd-X chargée de CO_2 ou de carbogène (95% O_2 et 5% CO_2) a augmenté le volume sanguin et la concentration en oxygène dans le tissu tumoral, ce qui a entraîné une ré-oxygénation des tissus.

• Le Gd introduit dans la zéolithe agit comme un agent de contraste IRM, permettant de suivre l'accumulation spécifique de cristaux de zéolithes nanométriques dans la tumeur.

• Les résultats ont confirmé la possibilité d'utiliser des nanozéolithes contenant des métaux comme outil théranostique pour le développement de nouvelles stratégies de lutte contre les tumeurs cérébrales.

Dans les travaux présentés au chapitre 5, la capacité du cuivre contenu dans la nanozéolithe FAU-X à adsorber l'oxyde nitrique (NO) et le gaz carbonique (CO_2), ainsi que l'évaluation de sa toxicité vis-à-vis des cellules, a été étudiée.

• La nanozéolithes fonctionnalisée avec du cuivre augmente l'adsorption de NO de 36% par rapport à la nanozéolithes sous forme sodique.

• La forme sodique de la faujasite a démontré une meilleure capacité d'adsorption vis-à-vis du CO_2.

• Les résultats indiquent que les propriétés d'adsorption de gaz des nanozéolithes peuvent être ajustées par simple échange de métaux, soulignant l'importance du choix des cations pour l'application souhaitée.

• Les nanozéolithes Na- et Cu-X présentent un caractère non toxique envers les cellules de glioblastome humain (U87-MG), de rein (HEK 293) et d'astrocytes de souris.

En résumé, nous avons démontré l'utilisation efficace de nanozéolithes à fonction métallique pour agir respectivement comme agent antimicrobien et vecteur gazeux en microbiologie et en biomédecine. Les résultats ont montré que les propriétés du matériau peuvent être ajustées grâce à une sélection minutieuse du cation de la structure de la zéolithe afin de les rendre compétentes pour une tâche donnée. La grande sélectivité des nanozéolithes et leurs non-toxicités permettent de les tester dans d'autres applications biomédicales, où l'administration de substances contrôlées est envisagée. Néanmoins, des recherches supplémentaires sont nécessaires pour évaluer leur plein potentiel dans ce domaine.

5 Perspectives

Indépendamment de nos résultats de recherche, il y a encore des domaines dans ce travail qui exigent une enquête plus approfondie. À l'avenir, des expériences supplémentaires sont nécessaires pour obtenir des connaissances approfondies sur les performances des nanozéolithes à échange de métaux.

Dans les recherches présentées, le rôle important du cation dans la structure de la zéolithes dans les propriétés d'adsorption des antimicrobiens et des gaz a été souligné. Cependant, la localisation des cations n'a pas été étudiée. Cela pourrait être utilisé pour améliorer la compréhension de l'environnement et le rendre plus efficace. La localisation de différents cations pourrait être étudiée à l'aide de la résonance magnétique nucléaire à l'état solide (RMN), de la résonance paramagnétique électronique (RPE) et de la spectroscopie Mössbauer.

En ce qui concerne la microbiologie, les tests supplémentaires peuvent inclure l'incorporation de différents cations dans la structure de la zéolithe, Zn, Co, Zr, Ni.[31] Il serait très utile d'évaluer l'efficacité de chaque métal envers un large éventail de micro-organismes.

Compte tenu des applications de distribution de gaz, différents types de structures en zéolithes pourraient être testés pour déterminer leur capacité d'adsorption et leur spécificité lorsqu'ils sont échangés avec divers cations. Cependant, dans le cas des zéolithes pour des applications biomédicales, ils doivent être synthétisés en l'absence d'agents structurants organiques, avec des tailles <100 nm, qui sont à ce jour limitées à huit types de zéolithes.[24] En outre, l'échange de métaux joue un rôle important, tout en réduisant la disponibilité des sites actifs et en limitant ainsi l'adsorption.

Ce projet de recherche a un grand impact scientifique. C'est également important pour notre société, car nous luttons contre une augmentation constante de la résistance aux traitements. Il existe de nombreuses possibilités d'optimiser les matériaux zéolithiques pour trouver celui qui convient le mieux à une application biomédicale particulière. Les investigations complémentaires ont été menées pour améliorer les connaissances et les performances des zéolithes dans ce domaine scientifique.

6 Références

[1] A. Corma, J. Catal. 216 (2003) 298–312.

[2] M.W. Ackley, S.U. Rege, H. Saxena, Microporous Mesoporous Mater. 61 (2003) 25–42.

[3] S. Wang, Y. Peng, Chem. Eng. J. 156 (2010) 11–24.

[4] S. Mintova, J.P. Gilson, V. Valtchev, Nanoscale 5 (2013) 6693–6703.

[5] Cent. Dis. Control Prev. Antibiot. Resist. Threat. United States, 2013 (2013) 114.

[6] A. Monteiro, R. Hill, G. Pilkington, P. Madureira, Cells 6 (2017) 45.

[7] R.M. Barrer, Hydrothermal Chemistry of Zeolites, Academic Press, London, 1982.

[8] Int. Zeolite Assoc. Database Zeolite Struct. (n.d.).

[9] K. Byrappa, M. Yashimura, Handb. Hydrothermal Technol. (2013) 315–413.

[10] M. Dusselier, M.E. Davis, Chem. Rev. 118 (2018) 5265–5329.

[11] J.A.Z. Pieterse, S. Veefkind-Reyes, K. Seshan, J.A. Lercher, J. Phys. Chem. B 104 (2000) 5715–5723.

[12] A. Corma, M.J. Diaz-Cabañas, J. Martínez-Triguero, F. Rey, J. Rius, Nature 418 (2002) 514–517.

[13] J. Jiang, J. Yu, A. Corma, Angew. Chemie - Int. Ed. 49 (2010) 3120–3145.

[14] J. Jiang, Y. Yun, X. Zou, J.L. Jorda, A. Corma, Chem. Sci. 6 (2015) 480–485.

[15] A. Corma, Curr. Opin. Solid State Mater. Sci. 2 (1997) 63–75.

[16] A.G. Pelmenschikov, E.A. Paukshtis, M.O. Edisherashvili, G.M. Zhidomirov, J. Phys. Chem. 96 (1992) 7051–7055.

[17] A. Primo, H. Garcia, Chem. Soc. Rev. 43 (2014) 7548–7561.

[18] B. Yilmaz, U. Müller, Top. Catal. 52 (2009) 888–895.

[19] G. Busca, Microporous Mesoporous Mater. 254 (2017) 3–16.

[20] S. Wang, H. Li, S. Xie, S. Liu, L. Xu, Chemosphere 65 (2006) 82–87.

[21] N. Kosinov, J. Gascon, F. Kapteijn, E.J.M. Hensen, J. Memb. Sci. 499 (2016) 65–79.

[22] J.A. Martens, D. Verboekend, K. Thomas, G. Vanbutsele, J.P. Gilson, J. Pérez-Ramírez, ChemSusChem 6 (2013) 421–425.

[23] V. Valtchev, G. Majano, S. Mintova, J. Pérez-Ramírez, Chem. Soc. Rev. 42 (2013) 263–290.

[24] S. Mintova, J. Grand, V. Valtchev, Comptes Rendus Chim. 19 (2016) 183–191.

[25] D.J. Wales, J. Grand, V.P. Ting, R.D. Burke, K.J. Edler, C.R. Bowen, S. Mintova, A.D. Burrows, Chem. Soc. Rev. 44 (2015) 4290–4321.

[26] S. e. Gul, D. Cody, A. Kharchenko, S. Martin, S. Mintova, J. Cassidy, I. Naydenova, Microporous Mesoporous Mater. 261 (2018) 268–274.

[27] B. Ozansoy Kasap, S. V. Marchenko, O.O. Soldatkin, S. V. Dzyadevych, B. Akata Kurc, Nanoscale Res. Lett. 12 (2017).

[28] R. Amorim, N. Vilaça, O. Martinho, R.M. Reis, M. Sardo, J. Rocha, A.M. Fonseca, F. Baltazar, I.C. Neves, J. Phys. Chem. C 116 (2012) 25642–25650.

[29] S. Belkhair, M. Kinninmonth, L. Fisher, B. Gasharova, C.M. Liauw, J. Verran, B. Mihailova, L. Tosheva, RSC Adv. 5 (2015) 40932–40939.

[30] R. Smith, J. Coast, Bmj 346 (2013) 1493–1493.

[31] M. Yasuyuki, K. Kunihiro, S. Kurissery, N. Kanavillil, Y. Sato, Y. Kikuchi, Biofouling 26 (2010) 851–858.

Abstract

The properties of nanozeolites, namely, large surface area, hydrothermal stability and non-toxic nature, enable their utilization in forward-looking applications, including biomedicine (sensors, drug and gas delivery) and microbiology (antibacterial agents). Hence, a lot of research has been devoted to study the new biomedical applications using zeolitic materials, their full potential has still not been fully unveiled.

It is well recognised that growing resistance to already established treatments of tumors and bacterial infections using radiotherapy and antibiotics is a distressing matter. Therefore, the development of new therapeutic strategies towards above issues is of great demand.

The goal of this PhD research is to synthesise and post-synthetically modify nanosized zeolites for biomedical applications. This involves the ion-exchange of zeolite with various cations to find the most suitable one for desired applications in regards to antimicrobial treatment, tumour tissue reoxygenation and gas delivery.

In this study, we report: (i) the effect of copper modified nanosized FAU type zeolite on ESKAPE type bacteria (Chapter 3), (ii) the metal containing nanozeolite as a tool for tissue oxygenation and visualisation using MRI (Chapter 4), and lastly (iii) the use of FAU nanozeolite as nitric oxide and carbon dioxide gas vector to prevent life threatening conditions (Chapter 5).

Les propriétés des nanozéolithes, à savoir leur grande surface, leur stabilité hydrothermale et leur nature non toxique, permettent leur utilisation dans des applications prospectives, notamment la biomédecine (capteurs, administration de médicaments et de gaz) et la microbiologie (agents antibactériens). De nombreuses recherches ont été consacrées à l'étude de nouvelles applications biomédicales utilisant des matériaux zéolithiques, toutefois leur plein potentiel n'a toujours pas été pleinement dévoilé.

Il est bien connu que la résistance croissante aux traitements établis de tumeurs et d'infections bactériennes par radiothérapie et antibiotiques est un problème de première importance. Par conséquent, le développement de nouvelles stratégies thérapeutiques pour résoudre ces problèmes est très demandé.

L'objectif de cette recherche de doctorat est de synthétiser et de modifier post-synthétiquement des zéolithes nanométriques pour des applications biomédicales. Cela implique l'échange d'ions de zéolithe avec divers cations pour trouver celui qui convient le

mieux aux applications souhaitées : le traitement antimicrobien, la réoxygénation des tissus tumoraux et l'administration de gaz.

Dans cette étude, nous rapportons: (i) l'effet de la zéolithe FAU de type nanométrique modifiée au cuivre sur les bactéries de type ESKAPE (chapitre 3), (ii) l'utilisation de nanozéolithes contenant du métal comme outil d'oxygénation et de visualisation tissulaire (chapitre 4) et enfin (iii) l'utilisation de nanozéolithes FAU comme vecteur de l'oxyde nitrique et du dioxyde de carbone pour prévenir des maladies potentiellement létales (chapitre 5).